FINAL REPORT

Evaluation of Embankment Distress at Sander's Creed – SR20

Submitted by:

Michael C. McVay

and

Dinh Nugyen

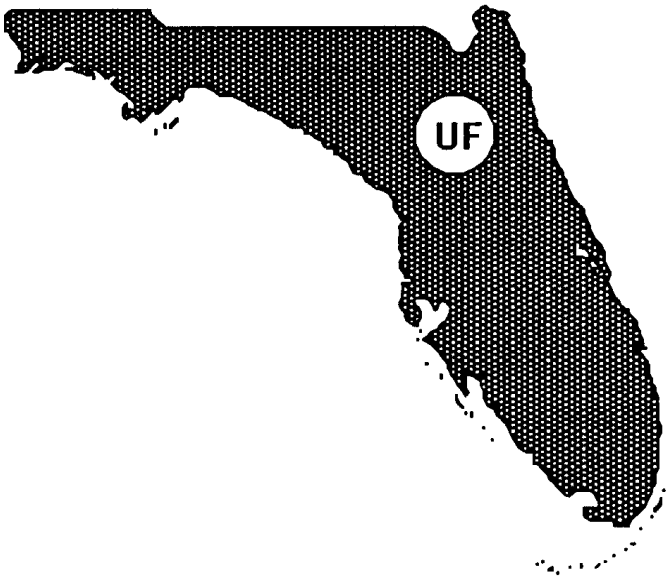

Submitted to: **Florida Department of Transportation**

Agency ID Nos. BC 354, RPWO# 17

UF Contract No. 4910-4504-734

May 2004

Technical Report Documentation Page

1. Report No.	2. Government Accession No.	3. Recipient's Catalog No.
Final Report		

4. Title and Subtitle	5. Report Date
Evaluation of Embankment Distress at Sander's Creek – SR20	May 2004
	6. Performing Organization Code: 4504-734

7. Author(s)	8. Performing Organization Report No.
Michael C. McVay and Dinh Nugyen	

9. Performing Organization Name and Address	10. Work Unit No. (TRAIS)
University of Florida, Dept. of Civil and Coastal Engineering, P.O. Box 116580 Gainesville, FL 32611-6580	11. Contract or Grant No.: BC 354 RPWO# 17

12. Sponsoring Agency Name and Address	13. Type of Report and Period Covered
FLORIDA DEPARTMENT OF TRANSPORTATION **605 Suwannee Street, MS 30** **Tallahassee, Florida 32399** **(850) 414-4615**	**FINAL REPORT** 12/27/99 – 2/28/04
	14. Sponsoring Agency Code

15. Supplementary Notes

PREPARED IN COOPERATION WITH THE USDOT AND FHWA

16. Abstract

The research focused on the settlement characteristic of insitu soils under embankments with various levels of organic content (OC) in the laboratory and field. Based on twenty-five laboratory oedometer tests, it was found that normally consolidated Florida soils with OC>25% exhibited significant secondary and tertiary creep response. All of the laboratory secondary and tertiary creep was predicted through Ladd's creep compression ratio, $C_{\alpha\varepsilon}$, normalized with respect to organic content and vertical effective stress. The laboratory tests also revealed that soils with organic contents varying from 25% to 50% did not exhibit downward creep upon unloading if surcharged to at least twice the current vertical effective stress. Soils with organic contents over 50%, however, did exhibit downward creep upon unloading, but at a greatly reduced rate (30% to 50%).

Field monitoring of a normally consolidated organic deposit under an existing embankment (SR20 in Florida Panhandle) exhibited significant settlement (secondary and tertiary creep), 18", after thirty years of monitoring. The latter was predicted very successfully from the laboratory consolidation and creep data.

In the case of field surcharging, the Turnpike's Toll Road 417 was monitored both short-term and long-term for settlements. The sensors identified that the field settlement due to surcharging was approximately 50% consolidation and 50% creep. Upon surcharge removal, the field exhibited heave with small amounts of downward creep (2 years after load removal). The site had deep deposits of organic soils with organic content varying from 25% to 75%.

A prediction program based on the Gibson-Lo's Theory using conventional laboratory data (Compression Index, permeability, Creep Compression Ratio, etc.) was developed. It was used successfully to predict both the SR20 and Toll Road 417 response and may be used to look at different design alternatives (surcharge levels, time, etc.).

17. Key Word	18. Distribution Statement
Organic soils, Settlements, Creep, Consolidation, 1-D Oedometer, Surcharging, Embankments	**NO RESTRICTION** **This report is available to the public through the NTIS, Springfield, VA 22161**

19. Security Classif. (of this report)	20. Security Classif. (of this page)	21. No. of Pages	22. Price
UNCLASSIFIED	**Unclassified**	176	

Final Report

Evaluation of Embankment Distress at Sander's Creek - SR20

ACKNOWLEDGEMENTS

The authors wish to acknowledge the State Material Office, specifically Dr. David Horhota, Ben Watson and Summer Hartley for performing all the laboratory Oedometer tests used in this research. Also the assistance of Wing Hueng for obtaining samples and field data at the Turnpike Toll Rd. 417 project is much appreciated.

DISCLAIMER

AThe opinions, findings and conclusions expressed in this publication are those of the authors and not necessarily those of the Florida Department of Transportation or the U.S. Department of Transportation.

Prepared in cooperation with the State of Florida Department of Transportation and the U.S. Department of Transportation."

SI* (MODERN METRIC) CONVERSION FACTORS

APPROXIMATE CONVERSIONS TO SI UNITS

Symbol	When You Know	Multiply By	To Find	Symbol
		LENGTH		
in	inches	25.4	millimeters	mm
ft	feet	0.305	meters	m
yd	yards	0.914	meters	m
mi	miles	1.61	kilometers	km
		AREA		
in^2	square inches	645.2	square millimeters	mm^2
ft^2	square feet	0.093	square meters	m^2
yd^2	square yards	0.836	square meters	m^2
ac	acres	0.405	hectares	ha
mi^2	square miles	2.59	square kilometres	km^2
		VOLUME		
fl oz	fluid ounces	29.57	milliliters	ml
gal	gallons	3.785	liters	l
ft^3	cubic feet	0.028	cubic meters	m^3
yd^3	cubic yards	0.765	cubic meters	m^3
NOTE: Volumes greater than 1000 l shall be shown in m^3.				
		MASS		
oz	ounces	28.35	grams	g
lb	pounds	0.454	kilograms	kg
T	short tons (2000 lb)	0.907	megagrams	Mg
		Temperature (exact)		
°F	Fahrenheit temperature	5(F-32)/9 or (F-32)/1.8	Celcius temperature	°C
		ILLUMINATION		
fc	foot-candles	10.76	lux	lx
fl	foot-Lamberts	3.426	candela/m^2	cd/m^2
		FORCE and PRESSURE or STRESS		
lbf	poundforce	4.45	newtons	N
psi	poundforce per square inch	6.89	kilopascals	kPa

APPROXIMATE CONVERSIONS FROM SI UNITS

Symbol	When You Know	Multiply By	To Find	Symbol
		LENGTH		
mm	millimeters	0.039	inches	in
m	meters	3.28	feet	ft
m	meters	1.09	yards	yd
km	kilometers	0.621	miles	mi
		AREA		
mm^2	square millimeters	0.0016	square inches	in^2
m^2	square meters	10.764	square feet	ft^2
m^2	square meters	1.195	square yards	yd^2
ha	hectares	2.47	acres	ac
km^2	square kilometers	0.386	square miles	mi^2
		VOLUME		
ml	milliliters	0.034	fluid ounces	fl oz
l	liters	0.264	gallons	gal
m^3	cubic meters	35.71	cubic feet	ft^3
m^3	cubic meters	1.307	cubic yards	yd^3
		MASS		
g	grams	0.035	ounces	oz
kg	kilograms	2.202	pounds	lb
Mg	megagrams	1.103	short tons (2000 lb)	T
		Temperature (exact)		
°C	Celcius temperature	1.8C + 32	Fahrenheit temperature	°F
		ILLUMINATION		
lx	lux	0.0929	foot-candles	fc
cd/m^2	candela/m^2	0.2919	foot-Lamberts	fl
		FORCE and PRESSURE or STRESS		
N	newtons	0.225	poundforce	lbf
kPa	kilopascals	0.145	poundforce per square inch	psi

* SI is the symbol for the International System of Units. Appropriate rounding should be made to comply with Section 4 of ASTM E380.

(Revised August 1992)

TABLE OF CONTENTS

LIST OF TABLES

TABLE **PAGE**

LIST OF FIGURES

FIGURES **PAGE**

CHAPTER 1

INTRODUCTION

1.1 BACKGROUND

Organic-rich soils are generally referred to as *Muck* and when they contain more than 75% organics, as *Peat.* The highly compressible nature of organic soil makes it one of the most undesirable foundation materials for highway construction. Besides its high compressibility, organic soil in its natural state has very low strength, which adds to its reputation as a poor foundation material.

Highway engineers try to avoid organic deposits whenever possible. Generally, local organic pockets and shallow deposits are excavated and replaced by a more desirable material, i.e., cohesionless soil. Unfortunately, there are situations when an organic deposit cannot be removed. For instance, if the deposit is of sufficient depth and extent it may not be economical to excavate and replace the organic soil. In such a situation, the highway engineer may have to use organic material as a foundation. When a highway alignment must pass over an organic deposit, the load caused by pavement and subgrade will cause some settlement to occur. For this reason, the highway pavement must be elevated above the deposit by means of an embankment. This embankment causes additional load on the soil resulting in more settlement. To minimize the settlement, several consolidation methods can be utilized. The most popular and widely used approach is *preloading* (i.e., surcharging, pre-compressing, pre-consolidating). This method relies on the principle that *over-consolidating* the soil will significantly reduce its deformability with respect to load and time. The main drawback of this approach is that it is time consuming and requires close monitoring of the field condition during construction. Other methods may

involve insitu improvements by using “thermal preconsolidation” as described by Edil and Fox (1994). Vacuum suction which induces negative pore water pressure to rapidly consolidate the soil mass has been mentioned in the literature. In some cases, reinforcing the soft soil with piles and geosynthetics has been used as in some sections of the Florida Turnpike.

Predicting and dealing with settlements has been a problem for highway designers and foundation engineers.

1.2 DISTRIBUTION

Organic soils are encountered at widely varying areas of the world. The glaciated areas of the northern hemisphere (Canada, the northern states of USA, northern Europe and Asia) have large areas where organic soils are encountered. It is encountered as part of *fluvial deposits* such as in San Joaquin Delta in California or along Mississippi River in Louisiana, USA or Po Valley in Italy. There are also *coastal* peat and organic soil deposits such as in Florida, USA or Adriatic coast of Italy. Additionally, such organic deposits are encountered in many parts of East Asia such as in Hokkaido as well as several other districts in Japan, in Kalimantan, as well as other islands of Indonesia, and in Sarawak and other states of Malaysia. Organic soils encountered in *tropical* areas have not been studied as intensely as the organic soils from the northern hemisphere (Edil, 2001).

1.2.1 United States

In the United States, the large organic deposits may be roughly assigned to two general regions – the *northern or glacial*, and the *Gulf and Atlantic* coast. Figure 1-1 shows the approximate distribution of organic deposits in the contiguous 48 states.

Figure 1-1. Frequency of Occurrence of High Organic Deposits.

After Soper and Osbon (1922) and Witczak (1972)

The northern organic region, which contains the most extensive deposits in the United States, includes Minnesota, Wisconsin, Michigan, eastern South Dakota, the northern part of Iowa, Illinois, Indiana, Pennsylvania, New York, New Jersey, and the New England states. This region is characterized by numerous ponds, marshes, and lakes formed by glacial action during *Pleistocene* time and by relatively low temperature and high humidity during the growing season. Most of the organic soils originated in basins. Probably the largest organic deposit in this country is in northern Minnesota. It covers nearly 10,000 square kilometers (Soper and Osbon, 1922).

The Atlantic coastal region embraces the southern and eastern part of Delaware, Maryland, Virginia, the Carolinas, Georgia and all of Florida. The nearness of the Ocean causes heavy rainfall and high relative humidity in this region, and the deposits occur in drowned valleys and lagoons, which were formed by the gradual emergence of the *Coastal Plain* and by wave action on the flat, imperfectly drained areas farther inland.

Organic soils also occur in a belt of land adjoining the Gulf coast which includes parts of Alabama, Mississippi, Louisiana, and Texas. In the west, organic soil is found in the valleys of Sacramento, San Joaquin Rivers of California, and in the basins of several lakes and rivers in Oregon and Washington. It also occurs to a limited extent along the Mississippi river.

1.2.2 Florida

Of the total area of organic soils in North America, an area of two millions acres is in a single deposit known as the *Everglade* (Thomas, 1965). Geologically, the state of Florida can be divided into three regions: Panhandle in the North, Central Highlands and Coastal Lowlands in the south.

The Florida panhandle belongs to the belt of land adjoining the Gulf coast which is rich in peat deposits.

Peninsular Florida may be divided into two major geomorphic provinces: the Central Highlands and the Coastal Lowlands. The Central Highlands region consists of rolling topography which forms a ridge running down the center of the peninsular and offsets slightly to the west. The Coastal Lowlands, which includes all of south Florida, rim the peninsular extending far south of the Central Highlands. This region consists of plains representing marine terraces which have occasionally been modified by erosion.

The Coastal lowlands of South Florida have been subdivided into several physiographic provinces. These are the Everglades, the Big Cypress Swamp, The Mangrove, and Coastal Glades, the Sandy Flatlands and the Atlantic Coastal Ridge. The Sandy Flatlands is located immediately to the west of the Atlantic Coastal Ridge, and is bordered on the west and south by the Everglades province. It consists of southward sloping topography which is underlain by sedimentary deposits of sand and limestone. In this western region of the Broward County, the Everglades province fingers eastward into Sandy Flatlands province. Surficial soils that generally characterize the Everglade province are peats and organic silts (Kaderabek et al., 1987).

In this research, organic soil samples from all of the three aforementioned areas were studied. Of interest were the consolidation and creep settlements of organic soils during both the preload and its subsequent removal.

1.3 RESEARCH SCOPE

The ever growing demand for space to accommodate new construction and the expansion of existing facilities has forced the construction industry to build upon soft ground, including the area of extensive organic deposits. Well aware of the trend, FDOT has funded the Geotechnical Group of University of Florida to investigate the construction of embankments over organic deposit. The outcome of this research is the development of a model to determine deformation of organic soils due to surcharge and after surcharge removal. The latter is to avoid other costly methods of construction over organic soils like soil replacement or piling.

One of the most common use methods for construction over organic soils is preloading. This method requires the understanding of organic soil behavior under *loading/unloading* conditions in which time play a significant role in the total amount of settlement during construction and life span of the structures. This method is the main subject of this research.

Three highway constructions projects are surveyed in this research. They are:

P-1: Sanders Creek Bridge and embankment for State Road 20 (SR-20) in Okaloosa County, Florida (Panhandle Region). The embankment was built in 1974 directly over peat without any soil improvement program. This project demonstrates the consequence of large post consolidation settlement.

P-2: Toll 417/Seminole Expressway Project is located near Sanford, Florida (Central Highlands). This project involved the pre-compression (in 2001) of two new ramps over peat by using surcharge technique.

P-3: State Road 15/700 in Palm Beach County, Florida (Coastal Lowlands). The roadway embankment was widened by adding two lanes to the existing road. To minimize the settlement, preloading was utilized in conjunction with an extensive site-monitoring program.

Research Activities Include:

Sampling of undisturbed soil samples for laboratory tests: In cases of P-1, the soil samples were recovered after roadway construction. The samples of P-2 and P-3 were recovered prior to the consolidation.

Site instrumentation: In cases of P-2 and P-3, the sites were extensively monitored with piezometers, inclinometers, settlement sensors and settlement plates. The field data has been collected since the beginning of construction and will continue on as long as necessary. In P-1, the settlement was recovered from maintenance records.

Laboratory testing: The undisturbed samples recovered from the three test sites were subjected to 1-D consolidation tests, constant rate of strain (CRS) consolidation tests, and permeability tests in order to establish an extensive understanding of the deformation characteristics

of peat with respect to loading/unloading conditions as well as to change in time. Laboratory testing also helps identify/classify the common types of organic soils, which are often encountered in Florida. The relationship between some soil physical properties to its deformability is also part of this task.

Develop a computational model: Based on the results and correlations observed from laboratory testing, a computational model was proposed. The model must be able to predict the deformation of soil samples with respect to change of load and time. This computational tool provides engineers with a prediction tool for embankment deformation. Time effect is a very important issue since it controls both the magnitude and duration of surcharge. Understanding the time effect helps to answer the questions: How much surcharge is enough? How long it should be maintained? And how much settlement would the embankment experience during construction as well as after it? Properly answering these questions would significantly contribute to a successful design.

Using the field data to validate the computational model: This part involves actually using the laboratory test results to reproduce the field settlement curves with respect to change in load and time. Necessary adjustments or improvements will be added to the model so it can provide a realistic response of peat at field conditions.

1.4 REPORT ORGANIZATION

Chapter 2 presents a literature review on classification of organic soils, consolidation theories and the principle of preloading with special attention to the potential methods. Chapter 3 covers physical properties of organic soils. Chapter 4 discusses the results of 1-D oedometer tests, which will explore the factors that control deformability. Chapter 5 is the focal point of this research in which contains the development of the computational model for compression.

Chapter 6 describes the field conditions of the three construction projects. This chapter also outlines the instrumentation program to monitor the field behavior. Field data is used to verify the computer program developed in Chapter 5. Chapter 7 presents conclusions and recommendations for future research. Several appendices and a complete bibliography follow Chapter 7.

CHAPTER 2

LITERATURE REVIEW

The first part of the chapter reviews the classification system of organic soils proposed by ASTM. Next, the behavior of organic soils is outlined, focusing on the deformability of peat with respect to change of *load* and *time*. A review of consolidation of cohesive soils is presented followed by a focus on organic soils. Different consolidation theories are explored. Those suitable to describe the settlements of organic soils are examined in detail. The second part of the chapter covers the principle of *preloading*, its pros and cons and field applications employing instrumentation.

2.1 CLASSIFICATION SYSTEM FOR ORGANIC SOILS

The American Society for Testing and Materials (ASTM) is currently working on a standard classification system that would apply to all interested disciplines. The activity is within Committee D18 (Soils and Rocks), and specifically Subcommittee D18.18 (Peats and Organic Soils). The proposed classification would be based on the following properties with the subheadings used as descriptors. Standards are from ASTM (1981).

Fiber Content (ASTM D1997):

- Fibric: peat with greater than 66.6% fibers.
- Hemic: peat with between 33.3% and 66.6% fibers.
- Sapric: peat with less than 33.3% fibers.

Ash Content (ASTM D2974):

- Low ash: peat with less than 5% ash.
- Medium ash: peat with between 5% and 15% ash.
- High ash: peat with between 15% and 25% ash.

Acidity (ASTM D2976):

- Highly acidic: peat with pH less than 4.5.
- Moderately acidic: peat with pH between 4.5 and 5.5.
- Slightly acidic: peat with pH between 5.5 and 7.0.
- Basic: peat with a pH greater than 7.0.

Absorbency (ASTM D2980):

- Highly absorbent: peat with a WHC (Water Holding Capacity) greater than 1500%.
- Moderately absorbent: peat with a WHC between 800% and 1500%.
- Slightly absorbent: peat with a WHC between 300% and 800%.
- Nonabsorbent: peat with a WHC less than 300%.

Botanical Composition: (Floristic Designation): Name dominant plants in the fibers.

Disagreements as to the behavior of "peat," as evident from a review of the literature, generally can be shown to arise from a lack of proper definition of the material concerned. The term peat has been incorrectly used to described organic silts and clays with mineral contents as high as 90% (Jeffries, 1936). It is important from the geotechnical point of view, to distinguish between peats and organic soils, so the described behavior can be related to the proper material. The ASTM Subcommittee D18.18, in an attempt to distinguish peat from organic soils has proposed the following organic soil classification to be used as a standard definition (Table 2-1):

1. Peat has less than 25% inorganic materials as defined by ASTM D2974.
2. Muck has between 25% and 75% inorganic material.
3. Organic silt or clay has greater than 75% inorganic material (25% or less organics)

Peat is distinguished from phytogenic material of higher rank (i.e., lignite coal) by its lower BTU value on an "as-received", water-saturated basis (ASTM D388).

Table 2-1. Grouping of Organic Materials (Tentative ASTM Standard).

Ash Content (%)	Material Description
0 to 25	**PEAT**
25 to 50	Peaty muck
50 to 75	**MUCK**
50 to 75	Silty or clayed muck
> 75	**ORGANIC SILT or CLAY**
75 to 90	Highly organic silt or clay
90 to 100	Slightly organic silt or clay

2.2 THEORIES OF CONSOLIDATION

The theory of consolidation occupies a unique place in the history of geotechnical engineering. The development of the theory of consolidation (Terzaghi, 1921, 1923, 1924) was the catalyst which firmly established the study of earth and rock as an engineering material as a major sub-discipline of civil engineering, known initially as *Soil Mechanics*, and currently recognized as *Geomechanics,* or more broadly as *Geotechnical Engineering*.

The theory of consolidation is a mathematical expression that portrays the deformation of a porous media accompanied by a flow of water, which fills the pores of the medium. The porous media consists of solid particles arranged in a *skeleton*. The spaces between the particles (*pores*) are filled with water (*pore-water*).

When the medium is subjected to a compressive force the skeleton will compact and the pore-water will be forced out of the compacting medium in a diffusive manner. This is the process of consolidation. The complimentary process is *swelling* in which the skeleton expands and pore-water infuses into the skeleton.

The *mechanical* theory of consolidation relates to a process motivated by mechanical force, *i.e., stress*. Other theories are *thermo-osmotic* consolidation in which thermal energies are involved, *electro-osmotic* consolidation, which makes use of electrical energy, *etc.* (Mitchell, 1991, 1993).

Hydraulic or *primary* consolidation refers to a process in which the volume fraction (void ratio or porosity) is a single-valued function of effective stress alone. *Secular* consolidation refers to a process in which the skeleton exhibits intrinsic time effects (*creep*).

A *finite* strain theory of consolidation is one in which no restrictions are placed on the magnitude of deformation of a point in the medium. An *infinitesimal* (small) strain theory assumes that the deformation of a consolidating medium is in some sense small.

The *constitutive* assumptions relate compressibility and permeability with the change in stress or time. A *linear* theory assumes that the compressibility and permeability are constants. The conventional theory is based upon linear properties and infinitesimal deformations.

The theories of consolidation depend on three groups of equations:

- The equilibrium equations.
- The conservation of mass equations.
- And the principle of effective stress.

We will examine the assumptions applied to these equations that distinguish one theory from the others.

2.2.1 Primary Consolidation

Terzaghi (1921, 1923, and 1924) was the first to describe and formulate the primary consolidation process for cohesive materials (clays) based on the three aforementioned groups of

equations. Terzaghi's theory is applicable to one-dimensional consolidation with the following assumptions:

1. Compression and flow are one-dimensional.
2. Soil is saturated and homogenous.
3. Solid and water are incompressible.
4. Darcy's law is valid.
5. Coefficients of compressibility and permeability are constant within the range of applied stress.
6. Total applied load is constant during the consolidation process.
7. Small strains.
8. Linear relationship between stress and strain.

The governing equation for one-dimensional consolidation is:

$$C_v \frac{\partial^2 u}{\partial z^2} = \frac{\partial u}{\partial t} \tag{2.1}$$

Where:

C_v = $\frac{K(1+e_0)}{a_v \gamma_w}$ - Coefficient of consolidation.

K = Hydraulic conductivity.

e_0 = Initial void ratio.

a_v = Coefficient of compressibility.

γ_w = Unit weight of pore-water.

z = Time-independent space coordinate (initial coordinate).

u = Excess pore-water pressure.

t = Time.

As shown in Equation 2.1, in order to solve for pore-water pressure, the composite parameter, coefficient of consolidation, is the only soil parameter needed. Two curve-fitting methods, Casagrande's (1938) logarithm of time and Taylor's (1948) square root of time method, are often used to determine C_v directly from laboratory deformation-time data.

Equation 2.1 is a standard *parabolic heat transfer* PDE. Therefore, after the initial and boundary conditions are specified, a closed-form solution can be obtained through separation of variables (Holtz and Kovacs, 1981):

$$u = \Delta\sigma \sum_{N=0}^{\infty} \left[\frac{2}{M} \sin\left(M \frac{Z}{H} \right) e^{-M^2 T_v} \right] \tag{2.2}$$

Where:

$\Delta\sigma$ = Stress increment.

$M = (2N+1)\frac{\pi}{2}$

$T_v = \frac{C_v t}{H^2}$ - Dimensionless time factor.

$Z = \frac{Z}{H}$ - Dimensionless geometry parameter

H = The longest drainage distance.

This widely used solution is in reasonable agreement with laboratory test results for a wide range of soils. However, considerable variations between the predicted and observed settlements in the field have been reported for some clays and organic soils. The reasons for the departure from Terzaghi's theory are often due to apparent failure to satisfy the assumptions of the theory, such as constant permeability, linear void ratio-effective stress relationship and small strain in the field (McNabb, 1960; Schiffman and Gibson, 1964; McVay, *et al.*, 1986). Experimental evidence indicates that the coefficient of permeability decreases with decreasing void

ratio and that a nonlinear relationship between void ratio and effective stress exists as represented by a straight line in a semi-log plot. It is obvious that the error resulting from these over-simplified assumptions will be minimized if the strain is small.

Many researchers have tried to modify the Terzaghi's formulation with some more realistic assumptions. Richart (1957) removed the small strain assumption. Schiffman and Gibson (1964) took the variable permeability and compressibility into account. Davis and Raymond (1965) derived an equation based on the assumptions that the void ratio is linear with the logarithm of effective stress and the decrease in permeability during which the consolidation process is proportional to the decrease in compressibility, that is, coefficient of consolidation remains constant. Gibson, England and Hussey (1967) derived an equation which allows finite strain with variable permeability and compressibility. The finite strain equation governing one-dimensional consolidation is expressed as:

$$\frac{\partial}{\partial z}\left(\frac{K(e)}{\gamma_w}\frac{\partial \sigma'}{\partial e}\frac{\partial e}{\partial z}\right) = -\frac{1}{1+e_0}\frac{\partial e}{\partial t} \tag{2.3}$$

Where:

σ' = Effective stress.

e = Current void ratio.

e_0 = Initial void ratio.

K(e) = Hydraulic conductivity which is a function of e.

z = Convective coordinate – time dependent space coordinate.

It is pointed out that the classic Terzaghi's equation is actually a special case of Equation 2.3 (Schiffman, 1980).

2.2.2 Secondary Compression

The earlier modified methods, however, did not really eliminate the discrepancies between observed and predicted data. The reason lies in the oversimplified assumption that settlement is totally controlled by the expulsion of pore-water pressure and ceases when the excess pore-water pressure diminishes. Secular creep theories of consolidation need to be considered.

Buisman, as early as 1936, had observed that soil compression did not stop at the end of excess pore-water dissipation. Other researchers confirmed this phenomenon (Barden, 1969; Mesri, 1973; Edil and Dhowian, 1979). Soil compression that occurs at constant effective stress is called *secondary* compression (Leonards, 1977). The amount of secondary compression is relatively small for inorganic soils but is quite significant for organic soils and may constitute more than 50% of the total settlement (Edil and Dhowian, 1979). The exact mechanism of secondary compression is *not* fully understood. Following are several mechanisms that have been proposed.

Terzaghi (1941) and Taylor (1942) attributed secondary compression to the *readjustment* of grains delayed by the gradual transfer of stress from film to grain bond. The basic assumption for this mechanism is that when a soil element is loaded, the total stress is shared by pressure in the free pore-water, the plastic resistance in the highly viscous *absorbed water* (film bond) and the solid to solid contacts between soil particles (grain bonds). During secondary compression, since the excess pore-water pressure is negligible, the total stress is share by film and grain bonds. The pressure from the film is gradually transferred to the grain bond, and this transferring process is associated with very slow viscous flow. When the equilibrium state is reached, grain bonds support the applied load only.

Tan (1958) believed that the secondary compression is due to the jumping of bonds formed by soil particles. Soil particles form a network, which can be described as a "card house" with water in the voids, and contacts between solids are treated as mechanical linkages. When the soil element is loaded, the links are broken in certain locations, but due to the attractive forces, they can be formed again in another stronger and more stable structural arrangement. Breaking and reforming bonds may occur at the same time at different locations. The process of breaking and reforming of bonds is called "jumping bonds."

Another theory for secondary compression was proposed by Adams (1965) and De Jong (1968) specifically for peat. They recognized that there were two levels of structure (*macro* and *micro*) in a peat element and that the consolidation resulted from the expulsion of water from both the macro and micro pores. The primary consolidation is due to the dissipation of *macro-pore* water pressure, but the secondary compression is attributed to the expelling of water from the *micro-pore*. Because the permeability of the micro-pores is much lower than that of the macro-pores, the process takes much longer to finish.

It is important to know that different definitions have been given to describe the rate of secondary compression. The most popular are:

$$C_{\alpha} = \frac{\Delta e}{\Delta \log(t)} \tag{2.4}$$

and

$$C_{c\alpha} = \frac{C_{\alpha}}{1+e_p} = \frac{\Delta \varepsilon_{ver}}{\Delta \log(t)} \tag{2.5}$$

The first is called the *secondary compression index* (Mesri and Godlewski, 1977). The second is *secondary compression ratio* (Ladd, 1977). The second is the expression of the first normalized with respect to void ratio, which converts it to strain.

Buisman (1936) suggested that C_α is a *constant* which means the settlement curve is a straight line for secondary compression on a semi-logarithm time graph. Since then, many tests have been devoted to study the influence of other factors on C_α. Some of those factors are: specimen thickness, load increment ratio, time duration, *etc*. Unfortunately, because the mechanism of secondary compression is not fully understood and the study of C_α often requires long-term testing, disagreements regarding factors affecting C_α are abundant in literature. Newland and Alley (1960) showed that C_α was not affected by the specimen thickness nor load increment ratio. Similar results were also observed by Raymond and Wahls (1976) for clays and by Barden (1969) for peats. In contrast, Leonards and Ramiah (1959) and Lo (1961) indicated that C_α is not a constant. For peats, Harahan (1954) showed the effect of sample thickness on C_α. Mesri and Godlewski (1977) concluded that C_α may increase, decrease or remain constant with time depending on the slope of the e-log(σ') curve. In terms of temperature, C_α has been reported as constant by Mesri (1973); however, Gray (1936), Buisman (1936) and Lo (1961) have opposite conclusions.

2.3 PEAT CONSOLIDATION

2.3.1 Consolidation of Peat

Mesri (1997) has identified creep compression of peats more significant than that of other geotechnical material:

- Peat deposits exist at very high natural water contents and void ratios. Peat deposits accumulate at high void ratios because plant matters that constitute peat particles are light and hold a considerable amount of water. Because of high insitu void ratios, peat deposits display high values of compression index, C_c and because C_α is directly related to C_c then peat deposits display high C_α.

- Among all geotechnical materials, peats have the highest value of C_α/C_c. Mesri recommended the C_α/C_c for peats is 0.06±0.01.
- Duration for primary consolidation for peats is relatively short due to the high initial permeability.

During the consolidation process, the permeability of peat decreases drastically due to large void ratio change. Peat consolidation is complicated by the extraordinary large change of void ratio and permeability (Berry and Poskitt, 1972). Consolidation tests on peats by Thompson and Palmer (1951) indicated that the secondary compression rate is not constant with time. Furthermore, within the time of engineering interest, compression of peats has no end. For instance, settlement of a peat layer in the field after 91 years has been reported by Van de Burght (1936).

Based on a series of long-term laboratory consolidation tests on peat, Dhowian and Edil (1980) reported that the strain-logarithm of time curve consists of four components (Figure 2-1):

- An *instantaneous* strain ε_i, which takes place immediately after the application of a pressure increment, and the result of shear deformation;
- A *primary* strain component ε_p, which occurs at relatively high rate and continues for a short period of time to t_a due to expulsion of water;
- A *secondary* strain component ε_s, which results from a linear increase of strain with the logarithm of time for a number of log cycles of time until a time t_k, after which the time rate of compression increases significantly giving rise to a tertiary strain component;
- The *tertiary* strain component ε_p, which continues indefinitely until the whole compression process ceases.

The instantaneous strain component, ε_i, is the result of instant load increment that almost only occurs in laboratory condition; so it is difficult to observe this phenomenon in the field. The end of primary (EOP), t_p, in a large number of laboratory consolidation tests, is hard to detect due to the smooth transition between primary and secondary compression.

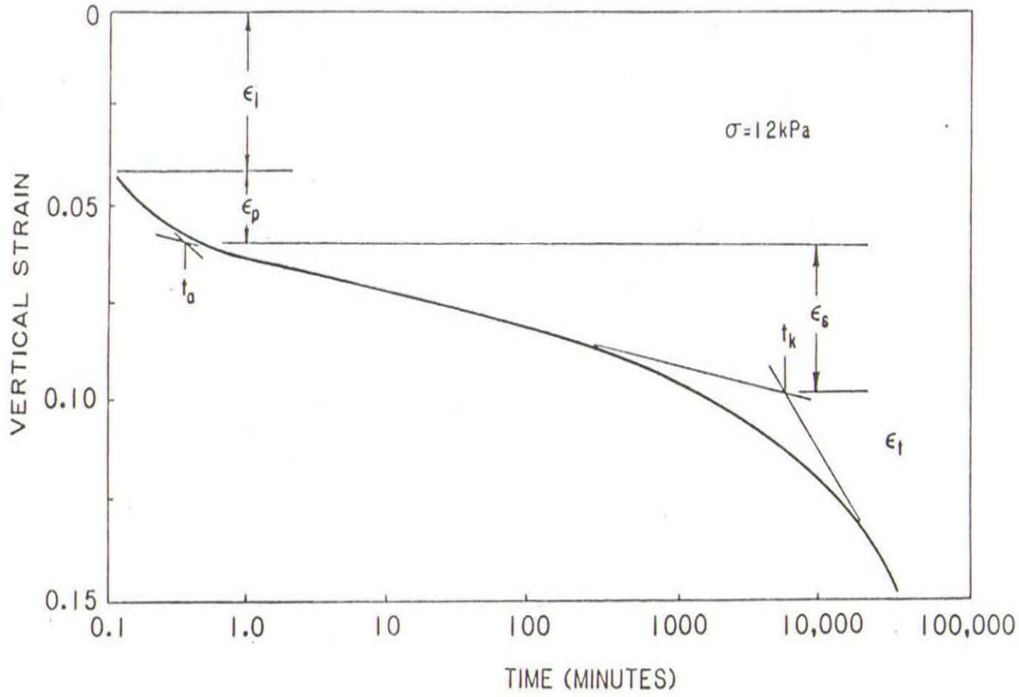

Figure 2-1. Laboratory Strain - Time Curve for Peat.

Instead of representing consolidation on logarithm of time, square root of time can be used in conjunct with Taylor's method to determine t_a. Also, the transition point t_k, for higher load increments, may be hard to locate.

Initially, the existence of tertiary compression was questioned, did it really exist in the field or was it a laboratory effect? This question was answered by Candler and Chartres (1988) who reported the existence of tertiary compression under three trial embankments underlain by peaty soils. Katona (1984) provided a mechanistic insight of the transition between secondary and tertiary compressions.

There is confusion over the terminology used in the literature. Some researchers address the whole process after *primary* consolidation as *secondary* regardless of the change in strain rate with respect to logarithm of time. This report will distinguish between *secondary* and *tertiary* compressions. In most of the contexts, the term secondary *compression* is used interchangeably

with the term secondary *consolidation*. *Creep*, as defined for one-dimensional compression of soils, is the continuing compression of soil skeleton under constant effective stress. So creep is the generic term that covers both the secondary and tertiary stages.

2.3.2 Theories Including Secondary Consolidation

It is well known that consolidation is a continuous process. The separation of total strain into primary compression and secondary compression brings out an interesting issue. Ladd et al. (1977) reviewed two hypotheses regarding soil consolidation. Hypothesis A assumes that creep occurs only *after* End of Primary (EOP) consolidation, which implies that at EOP every sample would have the same void ratio regardless of its thickness. On the other hand, hypothesis B states that intrinsic time effect occurs *during* the dissipation of pore water pressure. This leads to the difference in void ratio at the EOP since thicker sample need more time to expel pore water. Figure 2-2 illustrates both Hypotheses A and B. Lee and Brawner (1963) supported hypothesis A with laboratory and field data. This later was reconfirmed by Mesri and Choi (1985). However, Samson and LaRochelle (1972) showed that the EOP void ratio in the field was smaller than that in the laboratory sample which supported hypothesis B. Kabbaj; et al. (1988) also showed field evidence that supported B. So far, no conclusive statement can be made about the validity of either A or B. Fortunately, for peat because the primary consolidation process usually is a quick, the intrinsic effect, if it takes place during that period, can be ignored.

A significant amount of research has been done in order to correctly address and simulate creep phenomenon for geomaterials. Due to the vast amount of research literature, it is not possible to list all of those findings. This section is an attempt to review a few of them, which are considered to be related to this project.

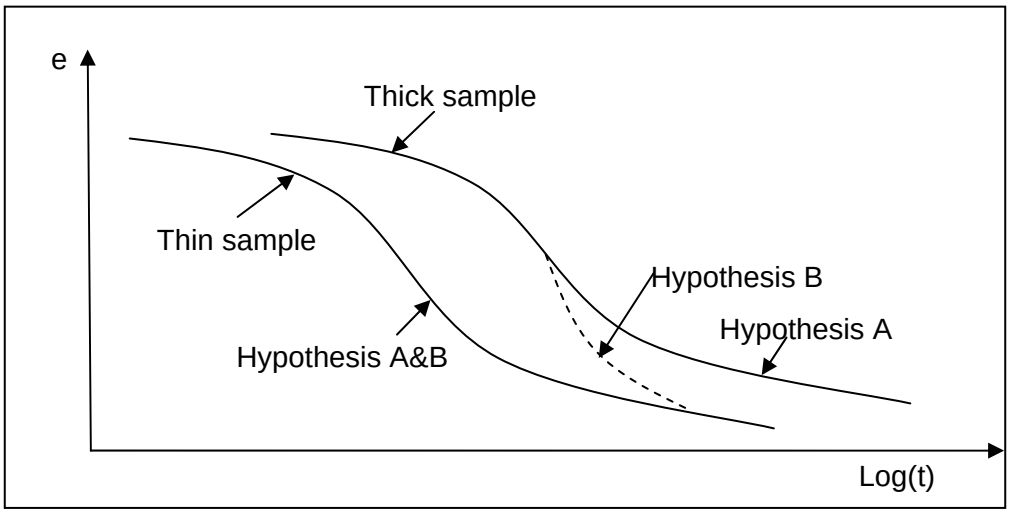

Figure 2-2. Hypothesis A and B.

As early as 1936, Buisman observed the creep phenomenon at constant stress and described it as *straight* line on the void ratio – logarithm of time curve. This is the first attempt to capture the creep behavior for soils. Although simple, this approach still is widely used with reasonable accuracy for inorganic soils. The most significant modification on Terzaghi's conventional theory is to incorporate the intrinsic time effects into the consolidation theory. The rate of secondary compression can be calculated directly from the void ratio – time data.

There are models that can be used to simulate the creep process for geomaterials, as well as ones that have been developed specifically for peat. For instance, Berry and Poskitt (1972) proposed a peat consolidation model based on the concept of *micro* and *macro* pores in which macro pore water is responsible for the primary consolidation while the highly viscous micro pore water induces intrinsic time effect to the process - creep. A schematic sketch of this model is illustrated in Figure 2-3.

The most recent research on modeling peat consolidation has been the work of Litus-Lan (1992) and Fox (1992) at the University of Wisconsin-Madison.

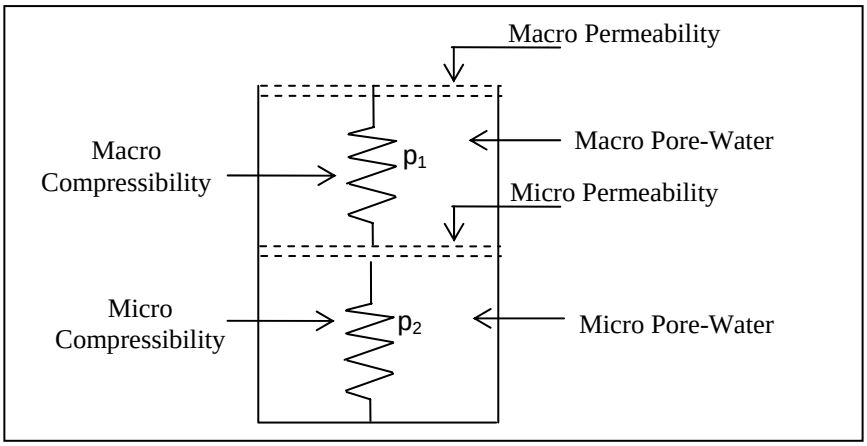

Figure 2-3. Berry and Poskitt Model.

2.4 METHOD OF SURCHARGING

It is well known that *overly-consolidated* soils are much stiffer and stronger than *normally-consolidated* soils. Surcharging, essentially, with unloading is the process of over-consolidating the soft ground. Surcharging is an *insitu* method of ground improvement to reduce compressibility and increase strength. Surcharging is done by applying load to compress a weak or soft soil layer. The load is sustained until a certain degree of compression is reached; it is then removed and construction of the superstructures (i.e., roadway embankments, buildings, *etc.)* are started. The application of the load is usually in the form of *dead weights* like: embankments, water tanks or grain silos. Laboratory and field monitoring suggest that surcharging reduces the magnitude of both primary and creep settlements. Surcharging has been applied successfully in all types of soils (Johnson, 1970).

If the soil is saturated or nearly saturated, the compression under load is usually accomplished by consolidation. Consolidating requires time which is the main drawback of surcharging. Other risks involved are the buildup of pore-water pressure, loss of effective stresses and strength at the early stage of loading which can lead to stability failures. To alleviate

drainage issues, wick-drain may be employed to quickly dissipate excess pore-water pressure, and accelerate consolidation, preventing slope failure. In general, surcharging is an economical choice if it is designed and constructed correctly. It is very beneficial to utilize surcharging if the project under consideration is widespread like roadway alignments or reclamation activities. More on the design and construction of a surcharging project is covered in Chapter 6.

2.4.1 Surcharge Loading to Compensate for Primary Consolidation

When using the degree of consolidation as the criterion for surcharge load removal, i.e., Figures 2-4 and 2-5, it is apparent that the required degree of consolidation, U_{f+s}, when the load is removed is:

$$U_{f+s}\Delta H_{f+s} = \Delta H_f \tag{2.6}$$

or

$$U_{f+s} = \frac{\Delta H_f}{\Delta H_{f+s}} \tag{2.7}$$

If the compressible layer is normally consolidated, then:

$$\Delta H_f = \frac{H}{1+e_0} C_c \log\left(\frac{p_0 + p_f}{p_0}\right) \tag{2.8}$$

$$\Delta H_{f+s} = \frac{H}{1+e_0} C_c \log\left(\frac{p_0 + p_f + p_s}{p_0}\right) \tag{2.9}$$

In which:

H = Layer thickness.

e_0 = Initial void ratio.

C_c = Compression index.

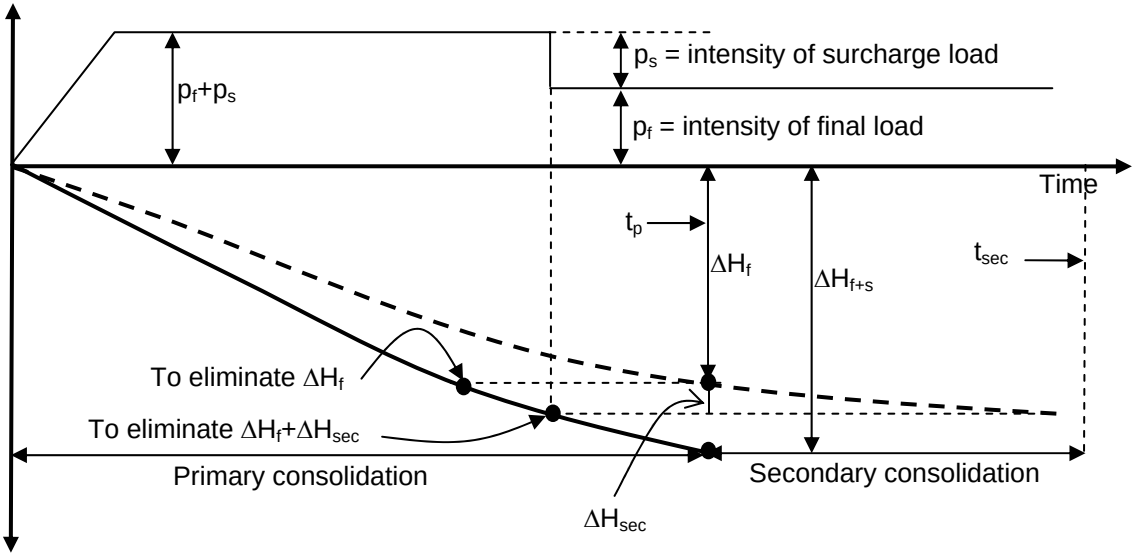

Settlement under p_f

Settlement under p_f+p_s

p_0 = Existing overburden stress.

ΔH_f = Settlement due to primary consolidation under p_f.

ΔH_{sec} = Settlement due to secondary consolidation under p_f.

ΔH_{f+s} = Settlement due to complete primary consolidation under p_f+p_s.

$U_{f+s} = \frac{\Delta H_f}{\Delta H_{f+s}}$ or $\frac{\Delta H_f + \Delta H_{sec}}{\Delta H_{f+s}}$ - Percent consolidation under p_f+p_s required to eliminate primary or primary + secondary under p_f.

t_p = time required for completion of primary consolidation under either p_f or $p_f + p_s$.

t_{sec} = time to completion of specific amount of secondary compression – take t_{sec}/t_p =10

Figure 2-4. Surcharge Design for Primary Consolidation Compensation.

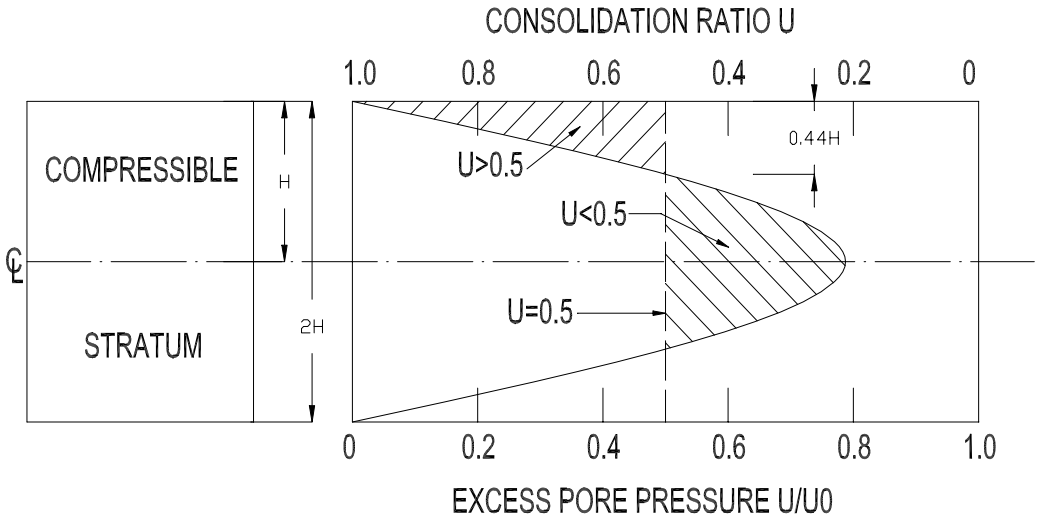

Figure 2-5. Surcharge Design for Primary Consolidation Compensation.

Therefore, the required degree of consolidation at the midpoint of the compressible layer at the time of surcharge load removal is:

$$U_{f+s} = \frac{\log\left(1+\frac{p_f}{p_0}\right)}{\log\left(1+\frac{p_f}{p_0}\left(1+\frac{p_s}{p_f}\right)\right)} \tag{2.10}$$

Figure 2-6 provides the relationship between surcharge effort and the degree of consolidation for the surcharge duration.

2.4.2 Surcharge Loading to Partially Compensate for Secondary Consolidation

This design approach is based on the concept proposed by Taylor (1942). By considering primary consolidation and secondary consolidation as separate phases, the simple Figure 2-7 constructed by Taylor, shows the design concepts involved. Taylor proposed, in effect, that secondary compression under various constant effective stresses would result in a constant time lines of the general nature.

From Figure 2-8, the design process can be described as follow:

$$H_{sr} = \Delta H_f + \Delta H_{sc} \tag{2.11}$$

in which ΔH_{sc} is the amount of secondary compression to be eliminated, or compensated for, during surcharge loading. Also:

$$\Delta H_{f+s} = \Delta H_f + \Delta H_{sc} + \Delta H_{sec} \tag{2.12}$$

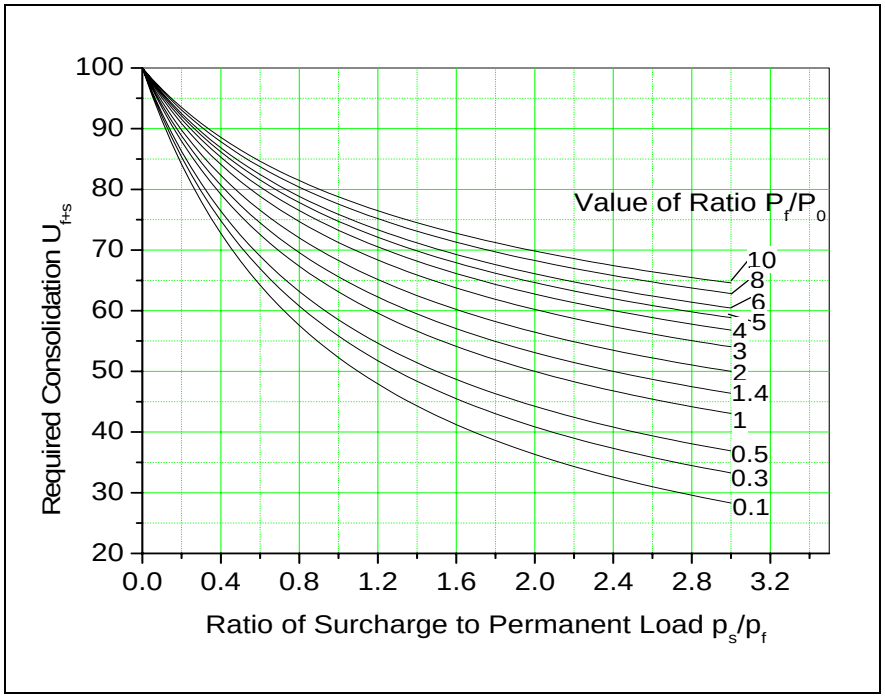

Figure 2-6. Design Chart for Primary Consolidation Compensation.

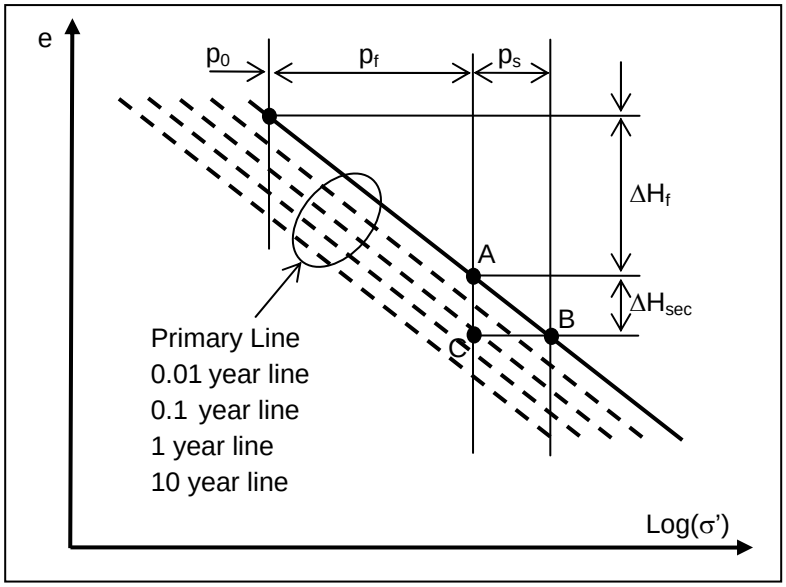

Figure 2-7. Taylor's Concept.

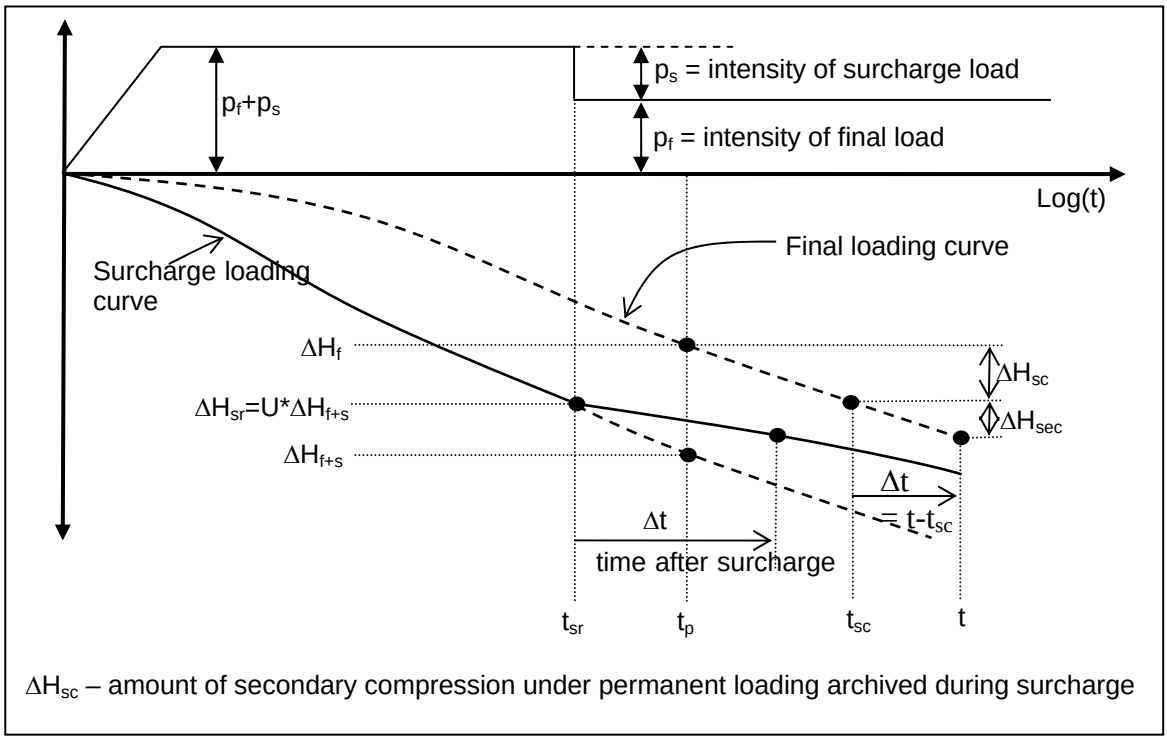

Figure 2-8. Surcharge Design for Secondary Consolidation Compensation.

Therefore, the degree of consolidation at the time of surcharge removal is:

$$U_{f+s} = \frac{1}{\Delta H_{f+s}}\left(\Delta H_f + \Delta H_{sc}\right) \tag{2.13}$$

or

$$U_{f+s} = \frac{1}{\Delta H_{f+s}}\left(\Delta H_f + C_\alpha \left(H - \Delta H_f\right)\log\frac{t_{sc}}{t_p}\right) \tag{2.14}$$

If the soil is normally consolidated, then U_{f+s} becomes:

$$U_{f+s} = \frac{\left(1 - C_\alpha \log\frac{t_{sc}}{t_p}\right)\log\left(1+\frac{p_f}{p_0}\right) + \frac{C_\alpha}{C_c}\left(1+e_0\right)\log\frac{t_{sc}}{t_p}}{\log\left[1+\frac{p_s}{p_0}\left(1+\frac{p_s}{p_f}\right)\right]} \tag{2.15}$$

Secondary compression after surcharge removal can be estimated by:

$$\Delta H_{sec} = C_\alpha H_p \log\left(1+\frac{\Delta t}{t_{sc}}\right) \quad (2.16)$$

Where:

ΔH_{sec} = Secondary compression after surcharge removal.

H_p = Total thickness after surcharge removal.

Δt = Time since surcharge removal.

2.4.3 Effect of Surcharging to the Secondary Compression Index

Mesri and Feng (1991) described the surcharging process using Figure 2-9 and 2-10. The surcharge effort is expressed in terms of total surcharge ratio:

$$R_s = \frac{\sigma_{vs}}{\sigma'_{vf}} - 1 \quad (2.17)$$

And the surcharging time ratio:

$$R_t = \frac{t_s}{t_{ps}} \quad (2.18)$$

Which:

$$\sigma_{vs} = \sigma'_{vf} + \Delta\sigma_{vs} \quad (2.19)$$

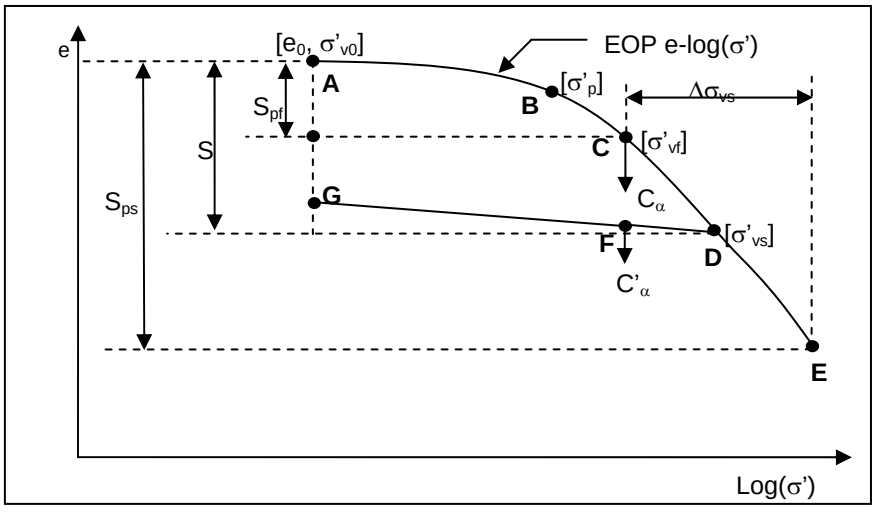

Figure 2-9. Definition of Surcharging Pressure and Settlement.

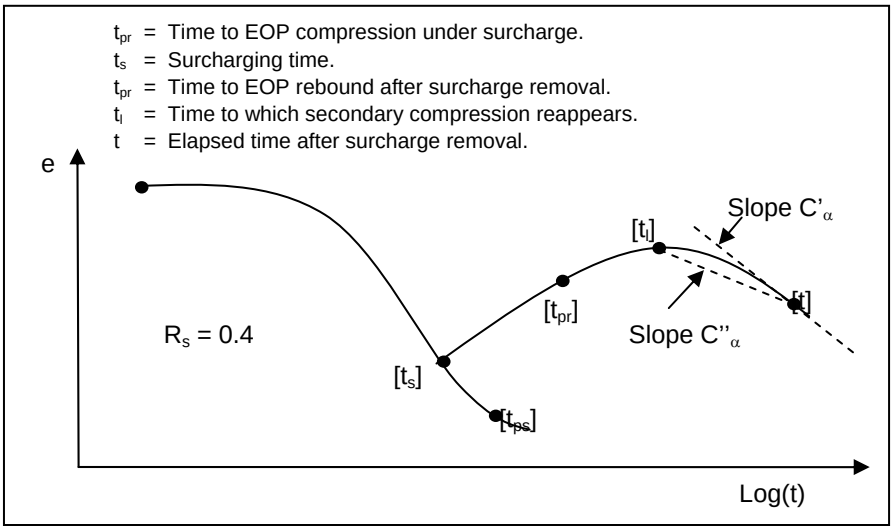

Figure 2-10. Definition of Elapsed Times Using on Surcharge Design.

σ'_{vf} = is the final vertical effective stress after the surcharge removal.

$\Delta\sigma_{vs}$ = is the total surcharge pressure.

t_s = is the surcharging time.

t_{ps} = is the time to EOP under surcharge.

Alternatively, surcharging effort can be expressed in terms of effective surcharge ratio:

$$R'_s = \frac{\sigma'_{vs}}{\sigma'_{vf}} - 1 \qquad (2.20)$$

Where: σ'_{vs} = is the maximum vertical effective stress reached before the surcharge removal.

In case $R_t = \frac{t_s}{t_{ps}} = 1$ then $R_s = R'_s$. If $R_t = \frac{t_s}{t_{ps}} \leq 1$ then $R_s \leq R'_s$. Note, surcharging may be ineffective whenever at any depth of soil $\sigma'_{vs} \leq \sigma'_{vf}$ - negative R'_s likewise it is generally uneconomical if $t_s \geq t_{ps}$.

The effectiveness of surcharging in reducing long-term settlement is evaluated by the ratio C'_α / C_α - the smaller the better.

Based on the above reasoning, Mesri and Feng (1991) were able to produce the correlation in Figure 2-11.

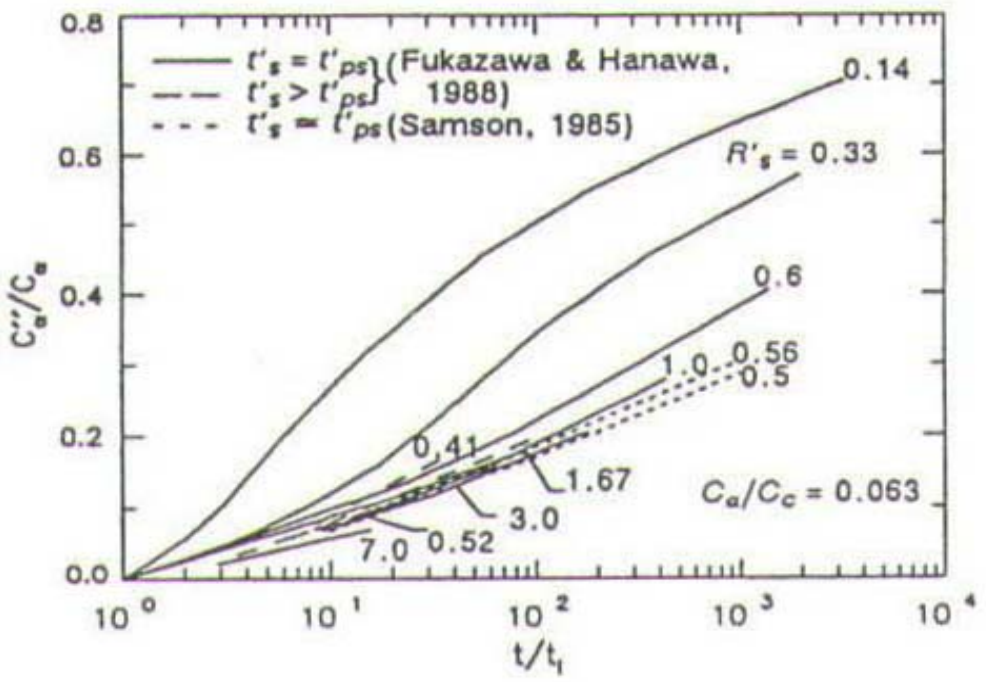

Figure 2-11. Effectiveness of Surcharging.

CHAPTER 3

CLASSIFICATION OF ORGANIC SOILS AND PROPERTIES

A discussion of the classification of organic soils as proposed by ASTM is presented. Also physical properties as related to organic soil classification are given.

3.1 ORGANIC SOILS CLASSIFICATION

The organic soils (Chapter 1) used in this project can be classified based on the proposed ASTM standard (Chapter 2). Such a classification is based largely on organic content and visual descriptions of the samples. Table 3-1 summarizes the laboratory soil properties that were used to classify the materials. The first group of nine samples is considered *Organic Silt* because of the low organic content, OC, less than 25%. This group has the visual appearance of an amorphous material with high degree of humification.

The next group contains of six samples with OC in the range from 25% to 75%, which can be called *Muck*. The visual description includes some *fibrous* organic material in the process of humification covered by *amorphous-granular* particles.

The last group of six samples is *Peat* with OC greater than 75%. This type of soil contains mostly fibrous material at the early process of humification.

Organic materials are well known for their high variability in soil properties, especially in organic contents. Samples from one Shelby tube may have their OC range from *Organic Silt* to *Peat* (SP-16), so in the field it is hard to describe soil layering system based on OC. But in general, the high OC – light weight - less humidified fibrous peat is near surface and the heavier – more humidified – low OC - amorphous-granular material is at greater depth. Chapter 6 describes in detail the soil layering systems encountered in the field.

Table 3-1. Organic Soil Samples.

Site Location	No.	Sample ID	Depth (ft)	Moisture Content (%)	Organic Content (%)	Specific Gravity	Void Ratio	PH level
Turnpike	1	SP16(2)-1	24.0-26.0	25.02	4.8	2.55	0.73	8
Turnpike	2	SP16(2)-2	24.0-26.0	39.85	6.45	2.54	1.04	N/A
Turnpike	3	SP17(2)-1	18.0-20.0	70.4	9.8	1.88	1.16	8.5
Turnpike	4	SP20(1)-1	23.0-25.0	50.87	12.64	2.06	0.94	N/A
Turnpike	5	SP6(2)-1	28.0-30.0	80.5	14.7	2.4	1.78	8.6
Turnpike	6	SP16(3)-1	34.0-36.0	91.69	18.93	1.9	1.67	N/A
Turnpike	7	SP22(2)-1	33.0-35.0	118.9	22.3	2.29	2.78	N/A
Turnpike	8	SP6(3)-2	38.0-40.0	105.25	22.7	2.2	2.58	N/A
Turnpike	9	SP6(3)-1	38.0-40.0	105.5	24.7	2.21	2.18	N/A
Turnpike	10	SP22(2)-3	33.0-35.0	105.29	27.8	1.97	2.42	N/A
Turnpike	11	SP22(2)-2	33.0-35.0	160.27	29.4	2.13	3.32	N/A
Turnpike	12	SP20(3)-1	43.5-45.5	183.15	34.5	2.1	3.98	9
Turnpike	13	SR20(16)	N/A	233.68	44.7	1.774	4.13	N/A
Turnpike	14	SP22(3)-1	48.0-50.0	145	47.1	1.43	1.95	N/A
Turnpike	15	SR20(15)	N/A	300	67.6	1.551	5.2	N/A
SR-20	16	SP16(1)-C	14.0-16.0	420.07	80.1	1.32	5.51	6.7
SR-20	17	SP22(1)-1	18.0-20.0	562.35	81.9	1.22	6.93	8.3
SR-20	18	SP16(1)-S	14.0-16.0	445.11	82.5	1.28	5.94	7.1
SR-20	19	SP22(1)-2	33.0-35.0	474	82.5	1.1	5.35	8.8
SR-20	20	SP17(1)-1	18.0-20.0	582	85.6	1.28	7.7	8.5
SR-20	21	SP17(1)-2	18.0-20.0	582	91.5	1.39	8.68	N/A

3.2 PHYSICAL PROPERTIES

Organic soil is a mixture of fragmented organic material derived from vegetation which has accumulated in wet areas such as swamps, marshes, or bogs. It may consist mainly of fibers (fibrous peat), or may tend to be more granular (amorphous-granular peat). Many engineers do not consider peat a soil due to its high organic content. This may be justified when one observes the behavior and characteristics of peat as opposed to a mineral soil. In this section, some physical properties of high OC soils which are of interest to the engineer will be reviewed.

3.2.1 Fiber Content

The amount of fiber material presence has an influence on the mechanical and physical properties of organic soils. The fiber content is determined by a wet sieving procedure. Peat has the highest fiber content in all organic soils. Amorphous-granular peats tend to behave similarly to mineral soils, whereas this behavior deviates more and more as the fiber content increases. The effect of fibrosity on peat characteristics is shown in Table 3-2.

Table 3-2. Relative Values of Various Peat Properties for Predominant Types. (MacFarlane, 1969).

Predominant structural characteristics	**Peat Properties**						
	Water content	**Natural permeability**	**Natural void ratio**	**Natural unit weight**	**Shear strength**	**Tensile strength**	**Compres-sibility**
Amorphous-granular	3*	3	2	1	3	3	2
Fine-fibrous (woody and non-woody)	1	2	1	3	2	2	1
Coarse-fibrous (woody)	2	1	3	2	1	1	3

*Each column differentiates coarse fibrous to amorphous effects as 1-strong influence, 2-moderate and 3-less significant influence.

3.2.2 Water Content

Organic soils have a high water holding capacity. Peat with a small amount of mineral contamination (pure peat), generally has a water content varying from 750% to 1500% (Feustel and Byers, 1930). Fibrous peat normally has higher water content than amorphous granular peat. This is because the fibers have an open cellular structure, which allows water retention within these organic "solids." The water content is determined for peat in the same manner as for mineral soils. The amount of water in organic material is directly correlated to its OC as shown in Figure 3-1.

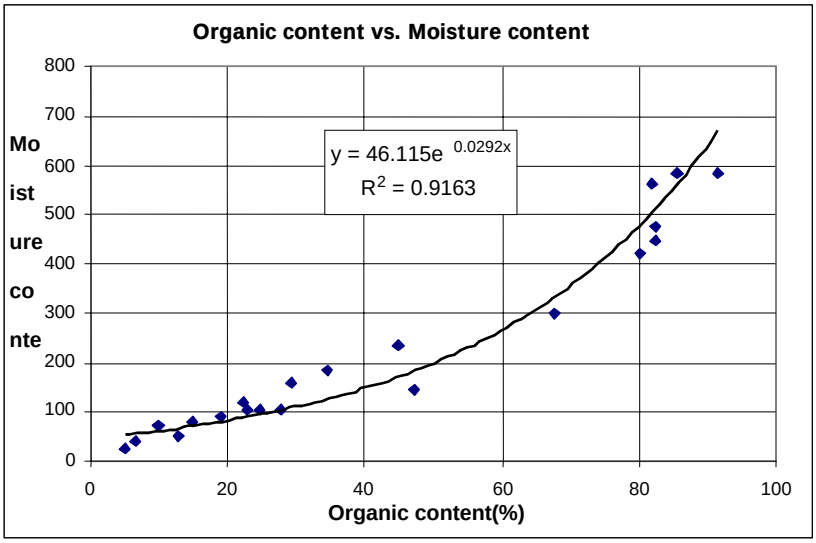

Figure 3-1. Water Content vs. Organic Content.

3.2.3 Ash Content

The ash content is the amount of non-organic material, expressed as percentage of dry weight, remaining after an organic sample has been fired at 450 degrees Fahrenheit. This firing procedure burns off the organic matter, which is generally combustible carbonaceous matter. The remaining ash represents the mineral constituent. Pure peats may have ash content as low as 2%. On the other extreme, peat by definition may not have more than 25% non-organic material (Goodman and Lee, 1962).

3.2.4 Organic Content

The organic content has a considerable effect on the physical and mechanical properties of organic soil. In general the greater the organic content the greater the water content, void ratio, and compressibility. The approximate organic content is found by subtracting the ash content from 100%. This is only approximate because since during the firing process, more than just the organics are burned off. According to Jackson (1958) this method can produce an error of 5% to 15%. MacFarlane and Allen (1964) presented a more accurate method to determine the organics content. This method involves treating the sample with chromic acid in hot sulphuric acid. Next, the excess chromic acid that remains after oxidation of the carbon is quantitatively determined by titrating against a standard ferrous ammonium sulphate solution. The ash content method is generally preferred for engineering purposes. Figure 3-2 shows the organic content grouped into Low, Medium and High subgroups. The organic contents were determined by the standard Loss on Ignition procedure.

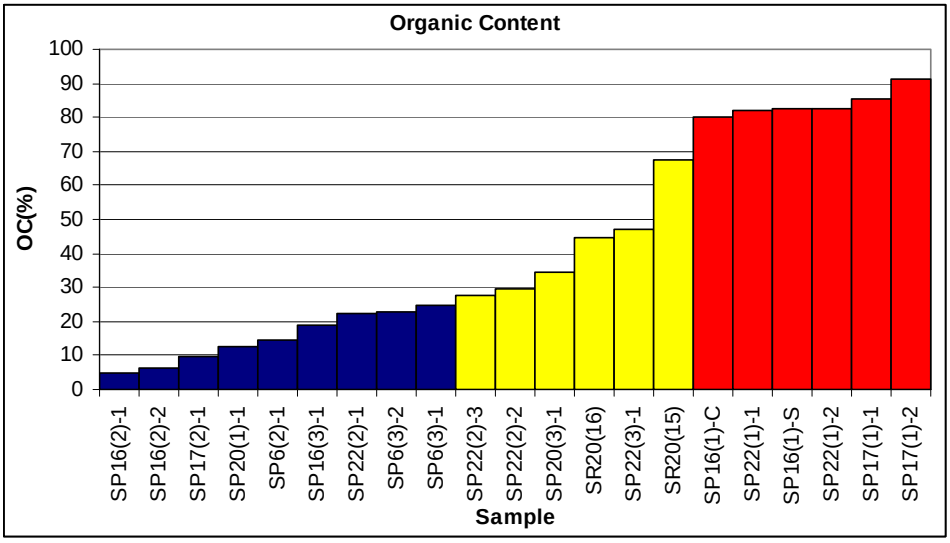

Figure 3-2. Organic Content.

3.2.5 Void Ratio

The void ratio of organic soil is generally high; with fibrous peats having greater void ratios than that of amorphous-granular peats. Extreme ranges in void ratio for amorphous to granular peat have been reported from 2 to 25, with 5 to 15 being a more usual range (Hanrahan, 1954). The void ratio corresponds to high water content, high permeability and high compressibility. In our study the natural void ratio ranges from 1 to 9 and a direct correlation between void ratio and OC can be established as shown in Figure 3-3.

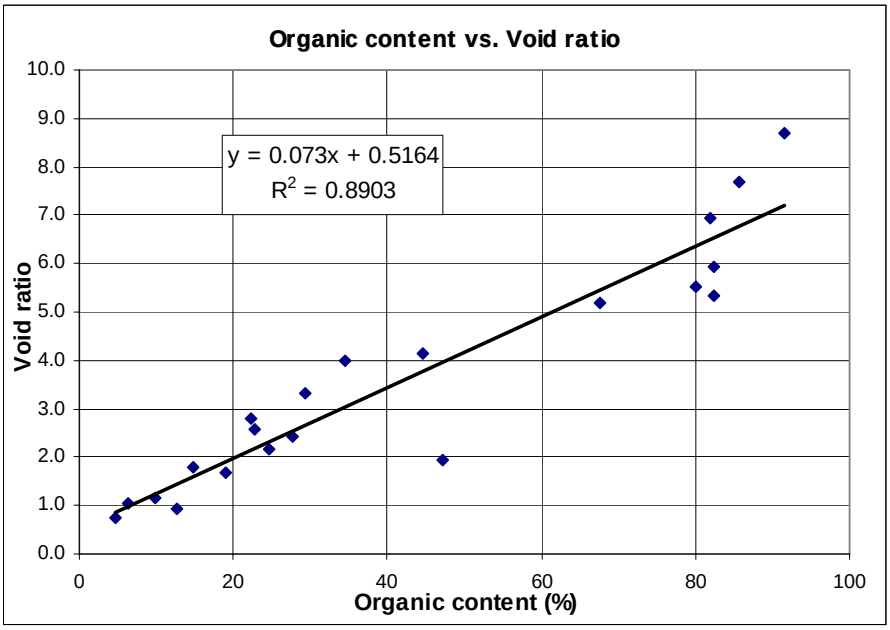

Figure 3-3. Void Ratio vs. Organic Content.

3.2.6 Density of Solids

The density of solids depends on the amount of mineral matter present. Values of density of solids vary from 1.1 to 2.5 g/cm^3. Most peats are in the range from 1.4 to 1.8 g/cm^3 (Wyld, 1956). Figure 3-4 shows the relationship between solid density and OC.

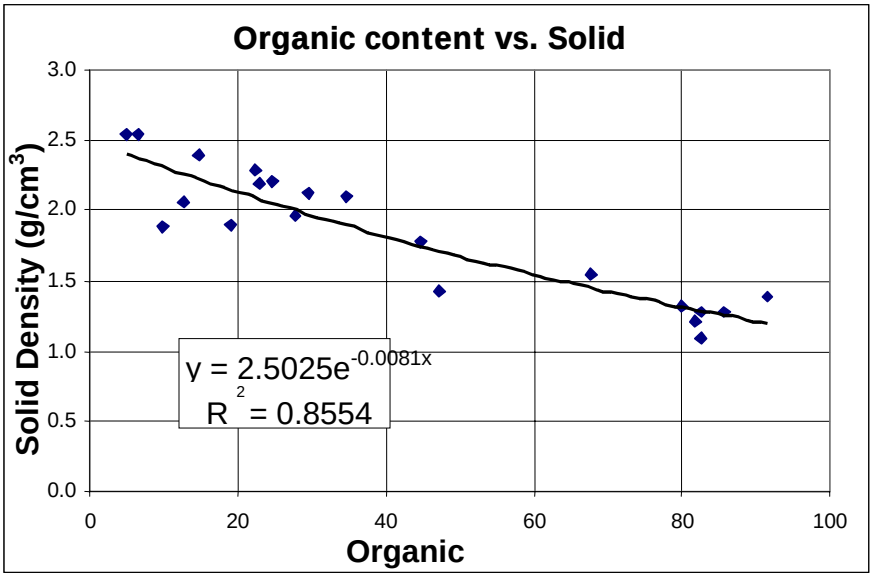

Figure 3-4. Solid Density vs. Organic Content.

3.2.7 Density

The natural density is dependent on the composition of the deposit and the water content. The density of pure peat is generally close to that of water. The density increases as more mineral soil becomes intermixed with the organic matter. MacFarlane (1969) reports natural densities have been observed to range from 0.4 g/cm^3 (25 pcf) for a moss peat to 1.2 g/cm^3 (75 pcf) for an amorphous-granular peat. Dry densities range from 0.082 g/cm^3 (5 pcf) to 0.32 g/cm^3 (20 pcf), the latter value representing considerable mineral soil contamination. Data on soil density collected from this research is shown in Figure 3-5.

3.2.8 Atterberg Limits

The consistency limits are difficult if not impossible to obtain on most peats. The fibrous nature of many peats renders the Atterberg limits tests practically useless. The liquid and plastic limits can be determined on highly decomposed and amorphous-granular peats, but the use of this information is questionable. When dealing with peats, determination of the Atterberg limits in general is neither beneficial nor recommended.

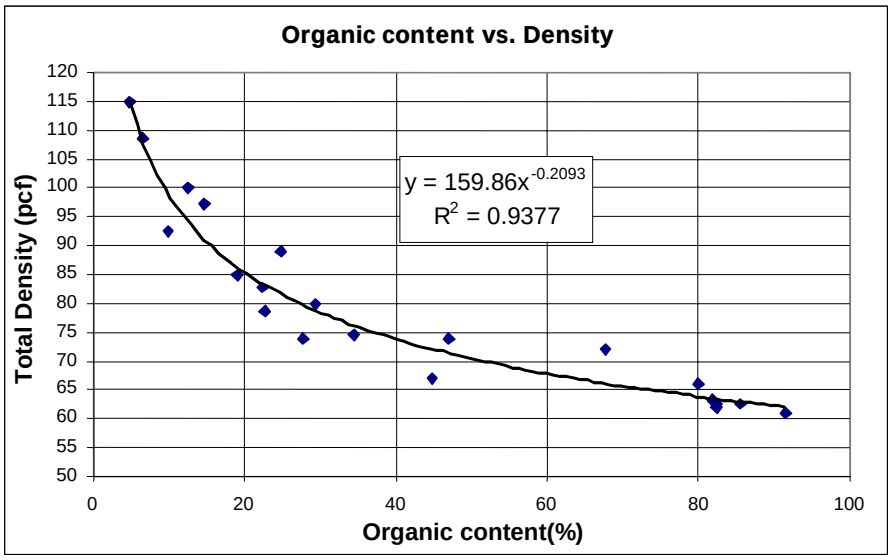

Figure 3-5. Soil Density vs. Organic Content.

3.2.9 Permeability

The permeability of organic soils varies widely, depending on:

- The amount of mineral matter.
- The degree of consolidation.
- The extent of decomposition.

Amorphous-granular soils tend to be less permeable than fibrous soils. The fibrous organic soils provide many interconnected flow channels through which water can easily flow. These channels tend to have a horizontal orientation, causing permeability in the horizontal direction to be higher than that in the vertical direction. At a given void ratio, the horizontal permeability is about 300 times larger than the vertical permeability (Dhowian and Edil, 1980). As soil is compressed, the decrease in void ratio results in large decreases in permeability. Hanrahan (1954) applied a load of 56 kG/cm^2 (8psi) on a sample of partly humified peat with a natural void ratio of 12 and initial permeability of 4 x 10^{-4} cm/s. After two days, the void ratio

was reduced to 6.75 and the permeability to 2 x 10^{-6} cm/s. After 7 months under the same load, the void ratio was reduced to 4.5 and the permeability to 8 x 10^{-9} cm/s. The final permeability corresponded to 1/50,000 of the initial permeability value.

Most naturally occurring peats have relatively high initial permeability (1 x 10^{-3} cm/s to 1 x 10^{-5} cm/s, Wyld, 1956). It should be noted that many peat types are, in fact, relatively impermeable. This is evident by the fact that peat has been used for the impermeable core of rock dams in Norway (Tveiten 1956, Silburn 1972). This extreme range in void ratios makes it difficult to assess the mechanical behavior of organic soil. Figure 3-6 shows the relationship between void ratio and permeability that was used for this research. It was back computed from Coefficient of Consolidation (Cv) and Compressibility (Cc) laboratory data.

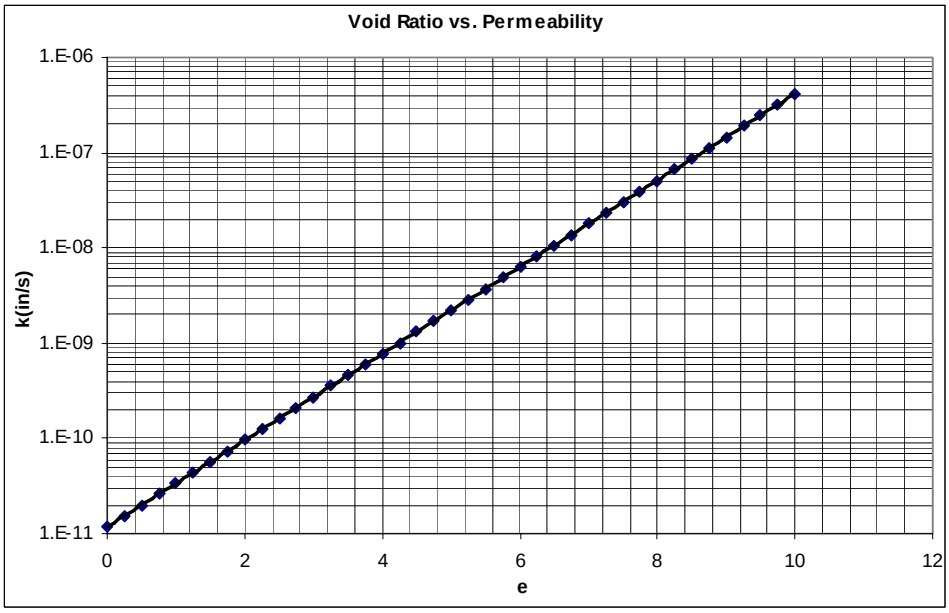

Figure 3-6. Permeability vs. Void Ratio.

3.3 SHEAR STRENGTH OF ORGANIC SOIL

The shear strength of soil is an important parameter in its behavior under various loading conditions. Practical situations in which the shear strength needs to be assessed are the stability of natural slopes and embankments, and the evaluation of bearing capacity. Organic soils generally have low shear strength and consequently a low bearing capacity in their natural condition. This low strength is undesirable from an engineering viewpoint. Before the shear characteristics of peat can be determined or improved, the mechanism of how shear strength is mobilized in organic soils should be understood.

3.3.1 Effect of Fibers

The fiber content has an important effect on the shear behavior. Soil with negligible fiber content (amorphous-granular) derives it shear strength in a similar manner to mineral soils. The shear strength is developed from cohesion between the particles and from the frictional resistance between the grains.

Fibrous soil on the other hand mobilizes its shear strength in an entirely different manner. In the natural fabric, the organic fibers tend to be somewhat oriented and overlapping – Figure 3–7. In a loose natural state, the fibers are surrounded by water, and the soil matrix has low shear strength. Most of the shear strength in this condition is from apparent cohesion due to mineral soil (clay) contamination and/or entanglement of the fibers.

During compression the fibers tend to align themselves at right angles to the direction of the applied (vertical) stress. Water is expelled and the fibers come in contact. The fibers in this condition act as reinforcement to triaxial shear and the shear strength is a function of the friction between the fibers and the tensile strength of the fibers. In this compressed state, the shear

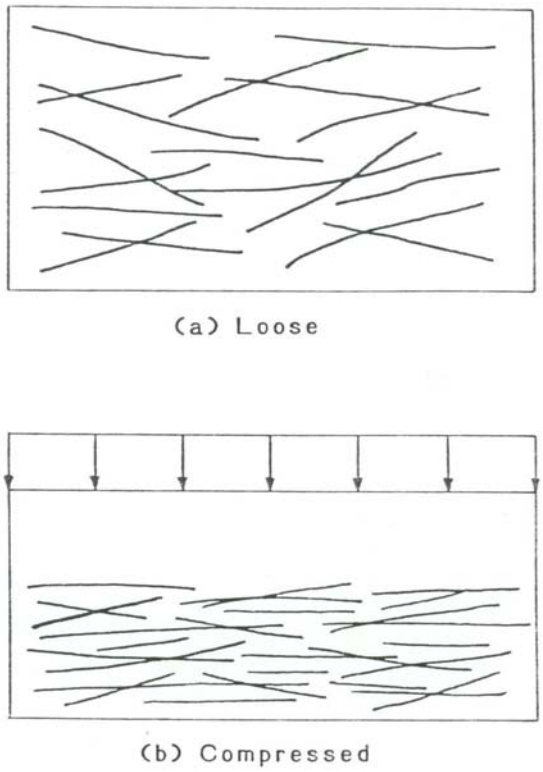

Figure 3-7. Effect of Compression on Peat Fabric.

strength is derived from the fiber resistance (frictional component), and the apparent cohesion is relatively small. Thus, as the soil is stressed, the organic fibers become more oriented and move closer together. This results in a large increase in shear strength from the fiber reinforcing effect.

This mechanism of internal resistance seems to agree with Amaryan (1972), who described the behavior of a fibrous peat under a range of loadings. According to Amaryan, the angle of friction is small for low stress increases and the shear strength is mainly due to cohesion (Figure 3–8). At higher stress levels, the shear strength develops mainly from friction, and the effective cohesion becomes negligible.

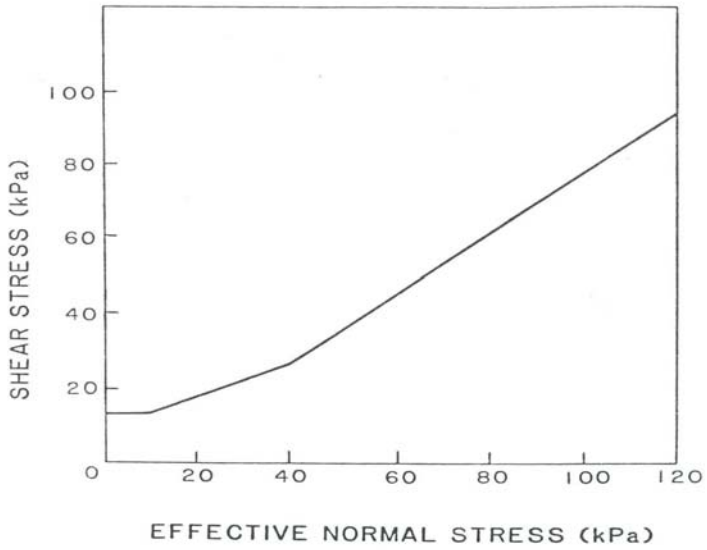

Figure 3-8. Shear Strength as Function of Effective Stress (Landva, 1980).

It has been shown by many investigators (Helenelund 1975, Landva 1980, MacFarlane 1969) that the shear strength of fibrous soil is less in the horizontal plane than in vertical planes. This is to be expected because when fibrous soil is sheared parallel to the fibers (horizontally), the reinforcement effect of the overlapping is lost, and the soil will fail with the fibers sliding over each other (Figure 3-9).

In general, a large discrepancy in shear strength is observed when direct shear results are compared with triaxial shear strengths. This is because the failure plane is forced parallel to the fibers in a direct shear test and the reinforcing effect is lost. Note, the majority of deformations in organic deposits, i.e., road embankment or other typical structures resemble the triaxial compression. However, if the soil is exposed to a horizontal load or for a portion of a slip surface is horizontal (i.e., lowest point) then the direct shear test would be the appropriate measure of the soil's shear strength. With anistropic soils, the laboratory test, as well as sample orientation is of significance.

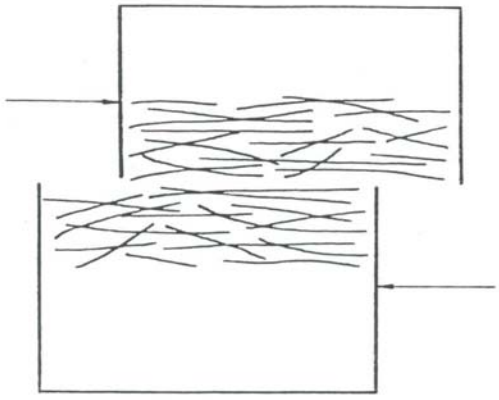

(a) Direct Shear.

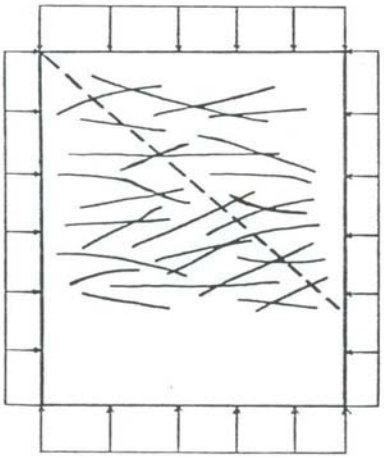

(b) Triaxial Shear.

Figure 3-9. Shear Failure Modes.

Since the mobilization of shear strength is affected significantly by fiber action, as discussed above, any variability in fiber type and content will result in variation in shear behavior. For highly fibrous peats, the effect of the fibers will be quite dominant, to the extent that failure may not be reached in triaxial compression, unless the fibers themselves fail in shear. For peats with low fiber content, the effect of fiber reinforcement will be insignificant and a shear failure may be expected to occur in the matrix, more or less independent of the fibers, in a manner similar to mineral soils.

3.3.2 Other Influences

Other factors have been found to have an influence of the shear strength of peat. According to Wyld (1956), "Qualitatively, the shear strength of peat varies inversely with its water content and directly with ash content and degree of deformation in compression." Helenelund (1975) notes, "The undrained shear strength diminishes with increasing water content and an increasing degree of humification."

Shear behavior also depends on permeability. As peat is sheared, excess pore water pressure is generated. The permeability of peat governs the rate of pore pressure dissipation. Thus, the shear strength varies directly with permeability. The lower the permeability, the lower the shear strength.

In general, the permeability decreases with increasing degree of humification. Since the degree of humification often varies both horizontally and vertically, in a somewhat erratic pattern, the permeability and shear characteristics will vary accordingly. This makes the determination of a representative shear strength for a particular deposit difficult to ascertain.

3.3.3 Determination of Shear Strength

Many researchers have tried to quantitatively relate shear strength to some physical properties, with little success. Landva (1980) stated: "In general, it must be concluded that no reliable empirical relationships have as of yet been developed with respect to the shear strength of peat." The undrained shear strength of peat has been measured by field vane tests, although other types of insitu tests, such as cone penetration and screw auger pulling have been employed (Huang, 1982). In peats, with high degrees of humification, the vane shear test can be regarded as a reliable shear test. However, the vane shear test is not recommended for fibrous peats. Landva (1980) devoted an entire paper to the topic of using the vane shear test on peat, and

concluded that the vane shear test was not a reliable method of determining the insitu shear strengths of peat. Some of the disadvantages of the vane shear test are:

- Vane tests tend to overestimate actual shear strength, thus being non-conservative.
- The value of shear resistance is a function of the vane size; larger vanes give lower values of shear resistance.
- When the vane shear is inserted into the peat, drainage occurs rapidly, resulting in a compression and an apparent high value of shear resistance. In addition, the great majority of practical situations require values for shear parameters that will reflect the change in strength with variations in stress environment and loading history. The vane shear test can not simulate either of these situations.

As stated earlier, the actual mode of deformation of a peat deposit under road embankment or other vertically loaded structure resembles that in triaxial compression. Thus, when these types of loads are applied to a peat deposit, a triaxial compression test should be used to determine the shear strength. Many investigators have successfully used both drained and undrained triaxial tests to observe the shear behavior of peat (Gautschi 1965, Adams 1961, Hanrahan et. al. 1967, Hollingshead and Raymond 1972). In most cases large strains were reached before failure occurred.

Hanrahan et al. (1967), studied the shear behavior of peat and found that the Hvorslev failure criterion was applicable in peat at water contents ranging from 250% to 350%. However, most natural peats have water contents much higher than this, so determination of the Hvorslev strength parameters would not be practical for use with peat. Hanrahan et al. (1967) did conclude however, that the Coulomb-Terzaghi failure criterion could be applied to peats with satisfactory results. The shear strength τ_f of peat may be represented as:

$$\tau_f = c' + \sigma' \tan \phi' \qquad (3.1)$$

Where: c' is the effective stress strength intercept, σ' is the effective normal stress, and ϕ' is the effective angle of internal friction.

Likewise, direct shear tests may be run if the expected failure surface is parallel to the fibers. At present, these two laboratory tests run on representative samples give the most reasonable results for stability analysis.

CHAPTER 4

ONE-DIMENSIONAL OEDOMETER TESTING OF ORGANIC SOILS

This chapter reports on the behavior of organic soils (Chapters 1 and 6) under one-dimensional compression loading. The following factors were investigated: loading time, loading rate and maximum loading pressure were investigated. Both loading and unloading were studied. Only representative data is shown, complete results are listed in Appendices A, B, C and D.

4.1 COMPRESSIBILITY

High organic soils in their natural state have high compressibility compared to non-organic soils. Organic soils' compressibility may be attributed in part to their loose structure and high water content. As a result of their loose state, they have high permeability. Consequently when load is applied, water quickly flows out causing large volumetric deformations in the near term, as well as large creep deformations. Moreover, because of their typical locations, i.e., near the surface, organic soils generally have small to medium maximum past pressures, which result in large primary settlements under small load changes. All of the latter suggests that organic soils are not recommended as a foundation material; however with deep deposits and the expense associated with removal, surcharging becomes a viable option.

Of interest is the compressibility of organic soils both short term related to the dissipation of excess pore pressure, as well as long term creep associated with either compression or rearrangement of the organic particles. The reported laboratory tests considered short and long term loading as well as unloading. All of the sample preparation, testing (loading & unloading) and data reduction was performed at the State Materials Office in Gainesville, Florida with their personnel.

4.1.1 One Dimensional Oedometer Testing of Organic Soils

One-dimensional loading of a soil results in a volume change caused by expulsion of water from the pores within the soil mass. If gas is present, it will be expelled and/or compressed. The soil particles will fill the space created by escaping water and gas, and solid constituents will continue to adjust their relative positions during compression. In fibrous peat, during compression, the fibers are reduced in size, rearranged and reoriented, with faces normal to the applied load. The expulsion of water and gas occurs relatively quickly compare to mineral soils; however, the final stages of compression may occur over long periods of time. This is because the permeability of organic soil decreases during compression, and there is creep associated with particle realignment and compression. In the case of consolidation, Dhowian and Edil (1980) have reported a reduction of 10,000 times in organic soil permeability.

Ideally, consolidation of high organic soil can be separated into four components (Figure 2-1):

1. Instantaneous strain, $\Delta\varepsilon_i$.
2. Primary strain, $\Delta\varepsilon_p$.
3. Secondary strain, $\Delta\varepsilon_s$.
4. Tertiary strain, $\Delta\varepsilon_t$.

The total strain is the sum of all components: $\varepsilon_{total} = \Delta\varepsilon_i + \Delta\varepsilon_p + \Delta\varepsilon_s + \Delta\varepsilon_t$ (4.1)

Instantaneous strain is due to elastic compression. Organic soil generally contains 5% to 10% gas, which may contribute to the immediate or initial compression and rebound if the load is totally removed (Landva and LaRochelle, 1982). Instantaneous strain usually is a result of step loading which is not the case under field conditions. Generally, the total strain is considered the sum of just three components:

$$\varepsilon_{total} = \Delta\varepsilon_p + \Delta\varepsilon_s + \Delta\varepsilon_t \quad (4.2)$$

Following the immediate initial compression, there follows primary strain, associated with significant excess pore water pressure dissipation. This component occurs relatively quickly and generally accounts for 50% of the total settlement. Secondary settlement occurs under small to negligible excess pore water pressures. This portion of strain normally causes deformations, which occur linearly with the logarithm of time. Secondary strain can be considered a creep phenomenon, which occurs under constant effective stress. Tertiary strain refers to a substantial increase in the rate of creep over that in the secondary phase. Tertiary creep has been observed both in laboratory and field condition as mentioned in Chapter 2 for organic soils.

Figure 4-1 can be used to illustrate the relationship between the height of the sample and the components of strain. At the current height H_t, the total strain accumulated from the original height H_0 is:

$$\varepsilon_{total} = \frac{H_0 - H_t}{H_0} \quad (4.3)$$

or:
$$\varepsilon_{total} = \frac{\left(H_0 - H_p\right) + \left(H_p - H_s\right) + \left(H_s - H_t\right)}{H_0} = \frac{\Delta H_p}{H_0} + \frac{\Delta H_s}{H_0} + \frac{\Delta H_t}{H_0} \quad (4.4)$$

Where: $\frac{\Delta H_p}{H_0}$, $\frac{\Delta H_s}{H_0}$, $\frac{\Delta H_t}{H_0}$ are the increments of strain due to primary, secondary and tertiary compressions, respectively.

Note Equation 4.4 is Equation 4.2 defined in terms of the change in the sample's original height. For one-dimensional analysis, the change in void ratio can be related to the change in strain using the equation:

$$\Delta\varepsilon = \frac{\Delta e}{1 + e_0} \quad (4.5)$$

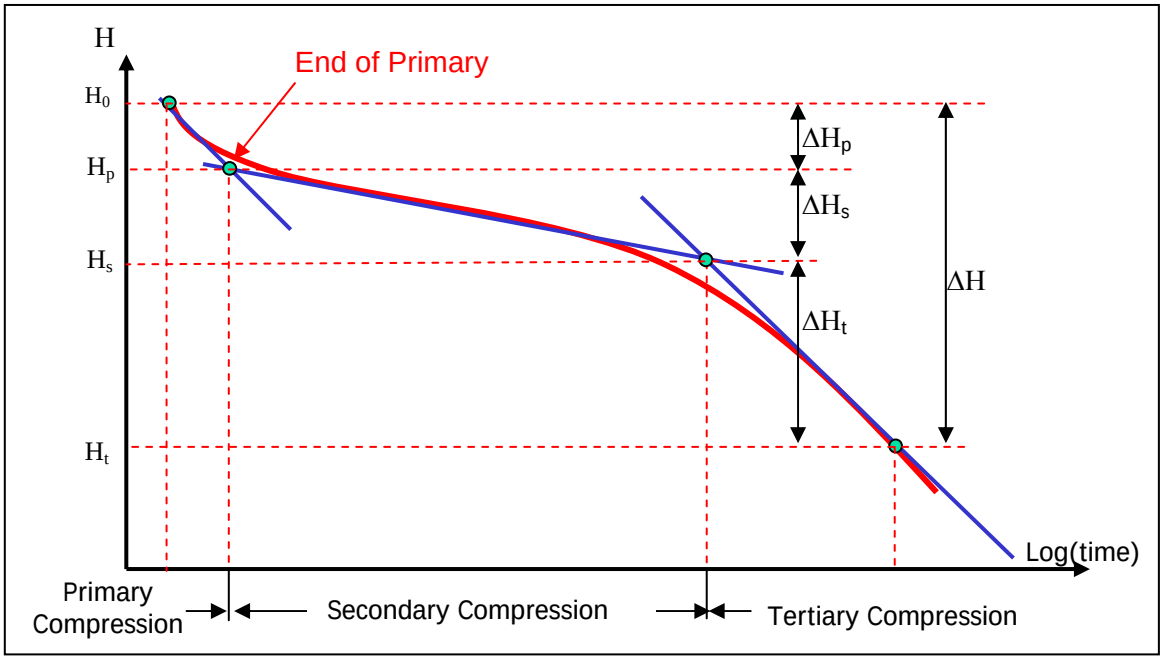

Figure 4-1. Deformation versus Time.

Where: e_0 is the initial void ratio and is associated with the original volume of sample.

Mesri and Godlewski (1971) characterized the slope after primary consolidation by defining the *compression index*:

$$C_\alpha = \frac{\Delta e}{\Delta \log(t)} \tag{4.6}$$

Ladd (1977) defined the *compression ratio* based on strain:

$$C_{\alpha\varepsilon} = \frac{\Delta \varepsilon}{\Delta \log(t)} \qquad \text{or } C_{\alpha\varepsilon} = \frac{C_\alpha}{1+e_0} \tag{4.7\&8}$$

If the creep includes both secondary and tertiary compressions, each equation (4.6, 4.8) gives us two slopes, one for the secondary and one for tertiary.

Settlement curves for embankment built over organic deposits resemble that shown in Figure 4-2. The latter suggests that all components of strain are occurring simultaneously in the field. Landva and LaRochelle (1982) observed that the secondary compression is of such a large

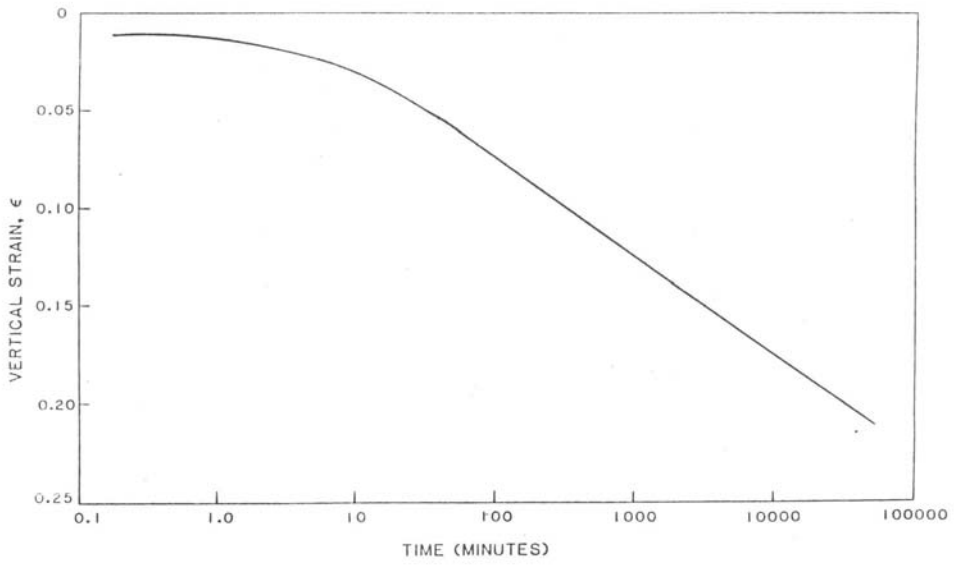

Figure 4-2. Typical Field Settlement Curve.

magnitude, that it masks the primary portion. After the excess pore water pressure has dissipated, primary consolidation has stopped and the secondary creep continues linearly with the logarithm of time. This masking effect makes it difficult to demarcate the end of primary consolidation, which leads to difficulties in analyzing the settlements. In general, the shape of the settlement versus logarithm time relationship is a function of permeability and the rate of creep (Adams, 1963).

4.1.2 Factors Affecting Compressibility

The settlement behavior of organic soil is influenced by many factors. The texture (amorphous-granular, fibrous) has a major effect on the compressibility. Amorphous-granular compresses in a different manner than fibrous soil. As a rule, fibrous peat has higher void ratio

and permeability, and consolidation proceeds more rapidly than that for humified amorphous-granular soil (Karesniomi, 1972). To illustrate this difference, Adams (1965) introduced a separated mechanism of compressibility for fibrous peat. According to him, fibrous peat may be regarded as a system of coarse channels (macro-pores), with the organic material contains a system of compressible very fine fibers with micro-pores. Primary consolidation involves the dissipation of pore-water pressure in the macro-pores. As stress is transferred to the fibers, water drains from the micro-pore to the macro-pore system; this process of compression is designated as the secondary compression stage. Both stages initially occur simultaneously with the micro-pores taking much longer to compress. Dhowian and Edil (1980) suggested this might be a valid concept for fibrous peats. Berry and Poskitt (1972) also realized a difference in compressibility between amorphous-granular and fibrous peat. In developing a theory of consolidation for peat, they found it necessary to derive two separate models; one theory for amorphous-granular and a different one for fibrous peat. Mathematically, both water content and void ratio are directly proportional to compressibility. As discussed earlier, permeability is strongly influenced by compressibility, with permeability dictating the rate at which water can be expelled from the peat (Wilson, 1964).

It has been found that mineral soil content is inversely proportional to compressibility (Anderson and Hemstock, 1959). In addition, Rutledge and Johnson (1958) found the rate of creep decreased with increasing mineral content.

Gas content affects the compressibility by reducing the area through which water can flow. Thus, gas content varies inversely with compressibility. Most peats have about 5% to 10% gas (Moran et al. 1958, Lea and Brawner, 1963). This gas is a combination of entrapped air and gas generated by organic decomposition.

4.1.3 Compressibility of Natural Organic Deposits

The depositional and physical characteristics of an organic deposit can make the estimation of settlement very difficult. A prediction of the magnitude of settlement in peat presents difficulties, mainly because of the variability with organic. This variability can be traced partly to variations in porosity or water content, and partly as suggested by Gautschi (1965), to the fabric and structure of organic soil. In addition, compressibility decreases with increasing degree of humification. Since the degree of humification often varies both horizontally and vertically, the compressibility will vary in a similar manner (Karesniomi, 1972). Due to this large and erratic variability, it is sometimes best to predict an upper bound of the compressibility and use this value in design.

In many organic deposits, the underlying soils may be more dangerous from the standpoint of stability and settlement than the organic soil. Seldom is the compressible soil layer only peat. Generally it also contains organic clay and/or marl, which may not drain as quickly as peat. These materials may develop high excess pore pressures, resulting in loss of effective stress and instability. If the soft layers are significantly thicker than the organic layer, they may contribute a larger portion to the total settlement. In general, organic deposits consist of layers of peat, organic clays and soft normally consolidated materials with different consolidation characteristics. Consequently, correct estimation of time vs. settlement behavior necessitates simultaneous estimates of consolidation and creep of two or more layers.

4.2 LABORATORY TESTING PROGRAM

4.2.1 Long-Term Deformation Testing Program

In this section, samples recovered from the Seminole Expressway and SR-20 were tested and the results are summarized below. Chapter 6 covers the site conditions, and boring locations for each project.

Table 4-1 summaries the boring number, organic content, as well as physical properties of the specimens. The first 19 samples were collected from the Seminole Expressway project

Table 4-1. Samples and Their Properties.

No.	Sample ID	Moisture Content (%)	Organic Content (%)	Specific Gravity	Void Ratio	Unit Weight (pcf)	Cc
1	SP6(2) – 1	80.50	14.70	2.40	1.78	97.2951	0.4595
2	SP16(2) – 1	25.02	4.80	2.55	0.73	114.8308	0.7500
3	SP17(2) – 1	70.40	9.80	1.88	1.16	92.4869	0.4746
4	SP20(1) – 1	50.87	12.64	2.06	0.94	100.1446	0.7688
5	SP16(3) – 1	91.69	18.93	1.90	1.67	85.0625	--
6	SP16(2) – 2	39.85	6.45	2.54	1.04	108.7286	--
7	SP20(3) – 1	183.15	34.50	2.10	3.98	74.5976	0.7842
8	SP22(3) – 1	145.00	47.10	1.43	1.95	73.8845	0.7303
9	SP6(3) – 1	105.50	24.70	2.21	2.18	89.1664	1.3295
10	SP6(3) – 2	105.25	22.70	2.20	2.58	78.6659	1.7342
11	SP22(2) – 1	118.90	22.30	2.29	2.78	82.7706	1.4307
12	SP22(2) – 2	160.27	29.40	2.13	3.32	80.0907	2.5306
13	SP22(2) – 3	105.29	27.80	1.97	2.42	73.9176	0.2829
14	SP16(1) – C	420.07	80.10	1.32	5.51	65.9358	2.6599
15	SP16(1) – S	445.11	82.50	1.28	5.94	62.5535	3.5399
16	SP17(1) – 1	582.00	85.60	1.28	7.70	62.4711	3.4586
17	SP22(1) – 1	562.35	81.90	1.22	6.93	63.3903	3.7114
18	SP22(1) – 2	474.00	82.50	1.10	5.35	61.8700	3.9444
19	SP17(1) – 2	582.00	91.50	1.39	8.68	61.1453	6.1443
20	SR20(15)	300.00	67.60	1.551	5.20	72.0000	---
21	SR20(16)	233.68	44.70	1.774	4.13	67.0000	---

while the last two from the SR-20 project. The samples were grouped into three different categories based on organic content: Low (0% < OC < 20%), medium (20% < OC < 50%), and high (OC > 50%). There were total of 21 samples: 6 with low OC, 8 with medium OC and the last 7 are high OC.

All samples, except SP22 (3)-1 and SP16 (1)-S, were extruded directly from their thin-walled tubes into over sized (71 mm) consolidation rings to minimize disturbance from trimming.

All of the Oedometer tests were conducted in accordance with a Multiple Stage Loading (MSL) procedure with a Load Increment Ratio (LIR) of one. The Oedometer tests were designed to duplicate field stress conditions, i.e., consolidation under surcharge pressure, then rebound and creep under final pressure, i.e., after surcharge was removed.

The Oedometer test program was design and carried out to investigate loading scenarios and their possible effect on the long-term behavior of organic soils. Consequently, three design scenarios were considered:

1. The embankment was built directly on organic foundation without any soil improvement methods.
2. The site was surcharged to an OCR = 2, i.e., the surcharge load is twice as high as the final embankment load, and
3. The surcharge load was increased, OCR = 4, to potentially accelerate settlement (consolidation & creep) and minimize surcharging time.

Tables 4-2, 4-3 and 4-4 show the testing schedule that was applied to the samples. A description of the laboratory test program for each group follows.

Table 4-2. Low OC Samples Testing Schedule (days).

Low Organic Samples						
Stress (tsf)	**SP6(2)-1**	**SP16(2)-1**	**SP17(2)-1**	**SP20(1)-1**	**SP16(3)-1**	**SP16(2)-2**
0.05	1	1	5	1	1	1
0.1	1	1	1	1	1	3
0.2	3	1	1	1	1	1
0.4	42	38	3	1	1	3
0.8	115	15	1	150	1	40
0.4	255	181				
.8						
1.2			1			
1.6			28		30	
3.2						
0.4			180	36	261	
1.6						
0.8						
0.2						

Table 4-3. Medium OC Samples Testing Schedule (days).

Medium Organic Samples								
Stress (tsf)	**SP6(3)-1**	**SP6(3)-2**	**SP20(3)-1**	**SP22(2)-1**	**SP22(2)-2**	**SP22(2)-3**	**SP22(3)-1**	**SR20(16)**
0.05	1	1	1	1		1	1	3
0.1	1	3	3	2		1	1	1
0.2	3	1	2	1		1	1	1
0.4	1	1	46	1		4	1	1
0.8	2	32	14	150		1	1	192
0.4		379	185	253				57
0.8								
1.6	32					31	4	
3.2							1	
0.4	376					274		
1.6							1	
0.8							11	
0.2							15	

Table 4-4. High OC Samples Testing Schedule (days).

High Organic Samples							
Stress (tsf)	**SP16(1)-S**	**SP16(1)-C**	**SP17(1)-1**	**SP17(1)-2**	**SP22(1)-1**	**SP22(1)-2**	**SR20(15)**
0.05	1	1	1	1	1	1	1
0.1	1	1	1	1	3	1	1
0.2	1	1	3	1	2	1	1
0.4	1	1	48	1	57	3	1
0.8	1	63	12	150	176	1	274
0.4	1	196	187	99			56
0.8	1						
1.6	1					29	29
3.2	1						
0.4	179					309	309

4.2.1.1 Low OC:

Six samples of the low OC were tested (Table 4-2) in which 5 of them were unloaded at different OCRs and after different loading times. Only sample SP16(2)-2 was tested without an unloading phase. The test on sample SP20(1)-1 was discarded due to a power interruption. All of the samples experienced rebound with none of the samples exhibiting downward settlement, i.e., creep after unloading. The latter confirmed the use of pre-compression, i.e., surcharging, as a potential solution to minimize settlement and creep of low OC samples. As shown in the next section, even low OC samples suffer from significant secondary settlement if surcharging is not utilized. All data is provided in Appendix A.

4.2.1.2 Medium OC:

Eight samples of medium OC were tested (Table 4-3) in which all of the specimens were unloaded at different over consolidation ratios (OCRs) after different loading times. Sample SP22(2)-2 was discarded due to disturbance introduced during the preparation process.

All samples experienced rebound after unloading. The amount of rebound was directly related to the OC and compressive strain from the previous load step. Some samples did exhibit a little creep after rebound. All test results are provided in Appendix B.

4.2.1.3 High OC:

Seven samples of high OC soils were tested (Table 4-4), in which six specimens were loaded to different OCR levels, and subsequently unloaded at different times. Sample SP22 (1)-1 was maintained at its maximum load without unloading. All six samples which were unloaded, did exhibit rebound. The amount of rebound was directly related to the OC and compressive strain from the previous load step. Three of them showed *noticeable* creep downward after initial rebound. In general, only the high OC samples exhibited downward creep after rebound when unloaded. All of the data for the high OC soil tests are listed in Appendix C.

The next two sections are devoted to in-depth discussion of *load/unload* behavior of organic soils.

4.2.2 Loading Behavior

Each sample's 1-D settlement vs. time curve had distinct shapes depending on their OC level. Figures 4-3, 4-4 and 4-5 show typical consolidation curves for each level of organic content (OC): $20 < OC$, $20 < OC < 50$ and $OC > 50$. The low organic samples, $20 < OC$, had the typical S-shaped curve, while the medium and high organic samples showed significant creep effects. Moreover, the low OC samples had a clearly delineated breaking point at the end of primary (EOP) consolidation, as well as a constant coefficient of secondary compression index.

The medium and high organic content soils, $OC>20$ (Figures. 4-3, 4-4) had no well-defined end of primary consolidation (EOP) or constant C_α value. To determine the EOP, Taylor's method (plotting deformation vs. square root of time) was used, ASTM D 2435-90, as suggested by Mesri (1997).

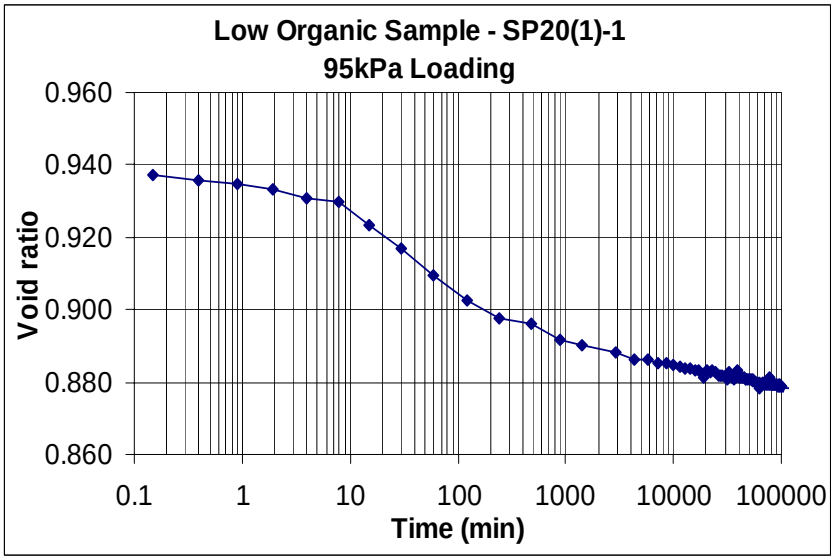

Figure 4-3. Low OC Consolidation Curve.

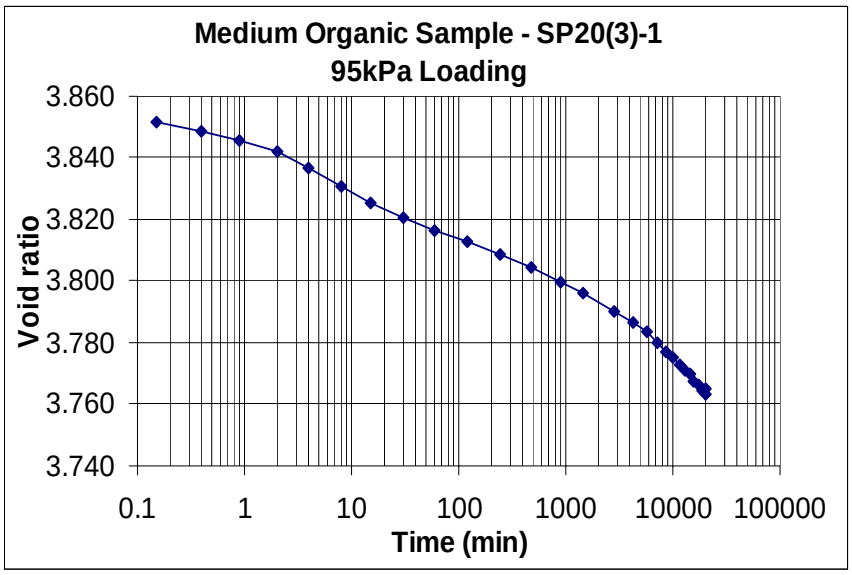

Figure 4-4. Medium OC Consolidation Curve.

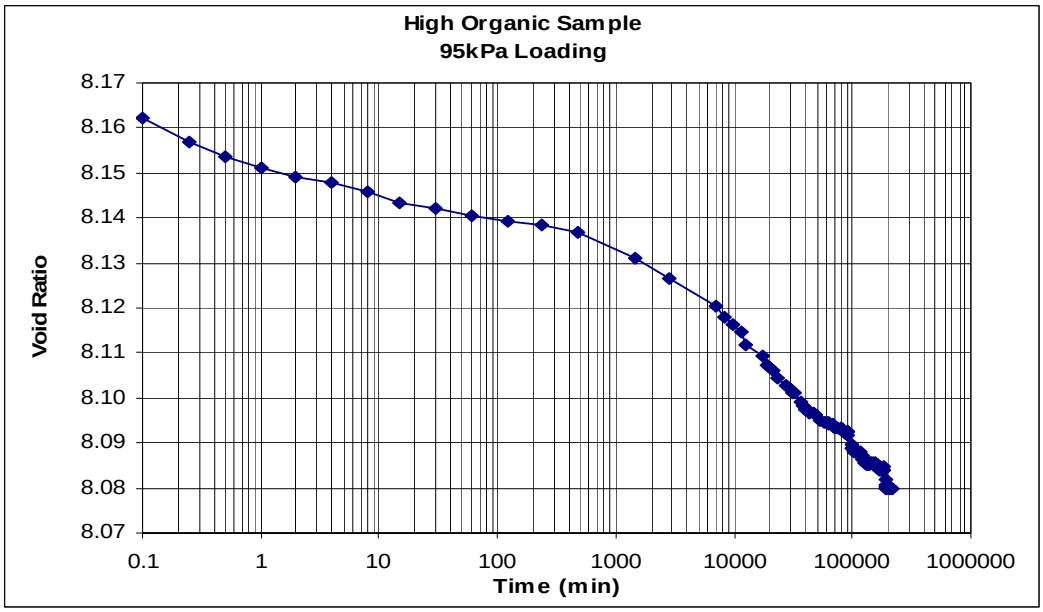

Figure 4-5. High OC Consolidation Curve.

Evident from the settlements (Figures 4-4 and 4-5), the soils are experiencing secondary, as well as tertiary compression (Dhowian and Edil, 1980). Lefebvre et al., (1984); Litus-Lan, (1992); and Fox, (1992) have observed similar results.

Mesri et al. (1997) suggested three reasons why high organic soils exhibit significant creep:

1. Organic soils are generally formed at high water and void ratio contents;
2. Duration of primary consolidation is relatively short as a result of their high initial permeability; and
3. Organic soils in general have one of the highest C_α / C_c ratios for soils. Based on the results from this study, the EOP typically occurred between ten and thirty minutes after initial load application in the laboratory.

For each sample, $e - \log \sigma'$ plots were constructed using the EOP consolidation data. Subsequently, the maximum past effective stress for each test was obtained using Casagrande's method. All of the samples had maximum past effective stresses equal to their effective stress in the ground,

i.e., the samples were normally consolidated. Appendix D presents the $e - \log \sigma'$ plots for the tests. A typical curve is shown in Figure 4-6. The field compression index, C_c was computed:

$$C_c = \frac{\Delta e}{\Delta \log(\sigma')} \tag{4.9}$$

The field compression index, C_c, was compared to initial void ratio, Figure 4-7, and water content, Figure 4-8, for all of the tests. Das (1998) and Mesri (1997) have reported similar correlations.

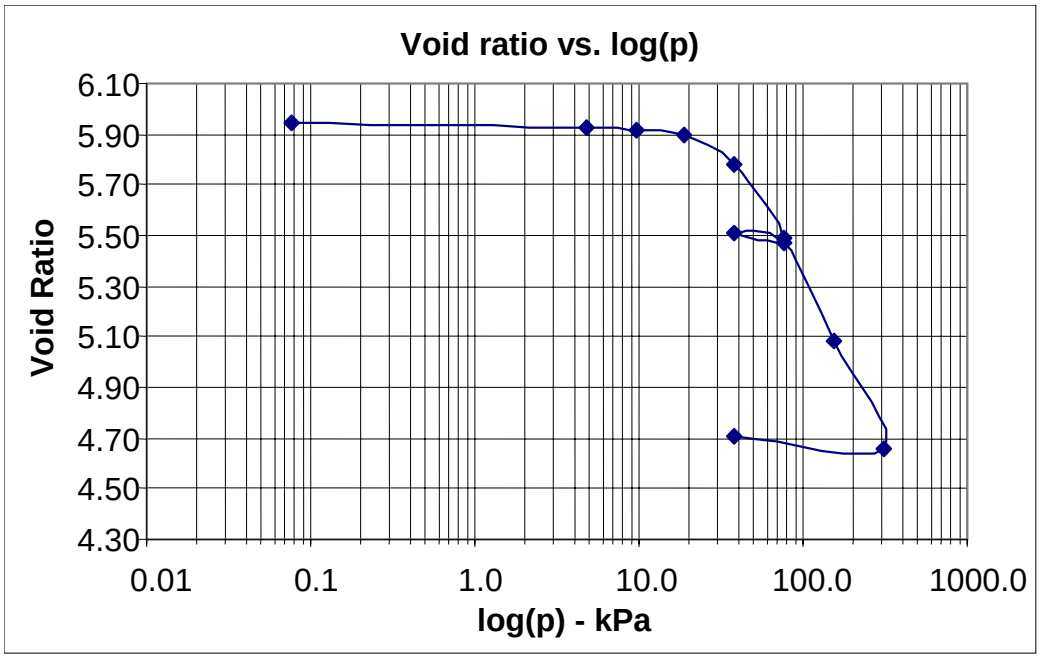

Figure 4-6. Typical EOP e-log(σ) Curve, TH16(1)-S.

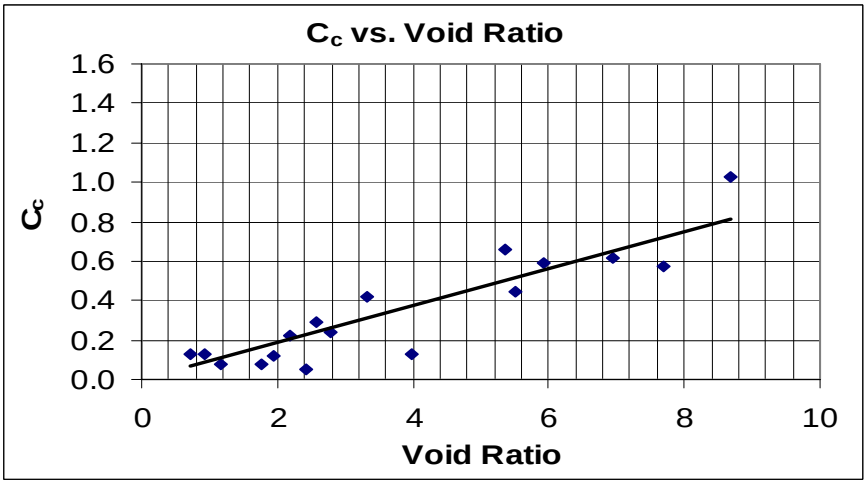

Figure 4-7. C_c versus Void Ratio.

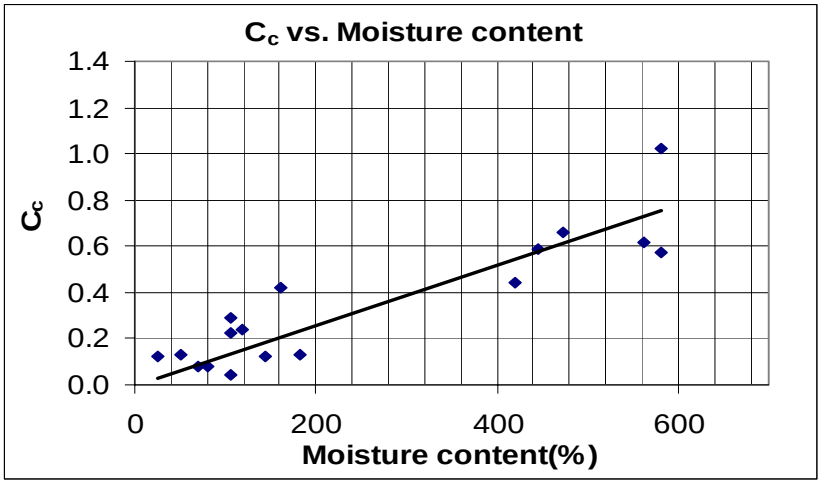

Figure 4-8. Cc versus Moisture Content.

The creep response of the medium and high organic soils was characterized through tangent secondary and tertiary compression ratios, $C_{\alpha\varepsilon}$. The values of C_α (Eq. 4.6) were determined from the tangents of secondary and tertiary creep slopes for each individual void ratio versus log (time) plot for each applied load increment. Subsequently, the C_α (Eq. 4.6) values were divided by $(1+e_0)$ to obtain the *creep compression ratio,* $C_{\alpha\varepsilon}$, Eq. 4.8. In addition, the tangent secondary and tertiary compression ratios, $C_{\alpha\varepsilon}$ (Eq. 4.8), were normalized with the sample's organic content (OC). Figures 4-9 and 4-10 present $C_{\alpha\varepsilon}$ /OC as a function of the applied load (stress) for both the medium and high organic soils. Evident from these figures, the tertiary compression ratio is approximately twice the secondary value. Also, it should be noted that Ladd's compression ratio, $C_{\alpha\varepsilon}$, greatly diminished the variability in creep index, C_α.

The dependency of $C_{\alpha\varepsilon}$ on OC is well indicated in Figures 4-9 and 4-10, that is $C_{\alpha\varepsilon}$ is directly proportioned to OC. Samples with higher OC have higher values of $C_{\alpha\varepsilon}$. The correlation between $C_{\alpha\varepsilon}$ and effective stress σ' offers an interesting idea on how to design the surcharge. If the purpose of the surcharge is to reach a certain level of compression, an engineer

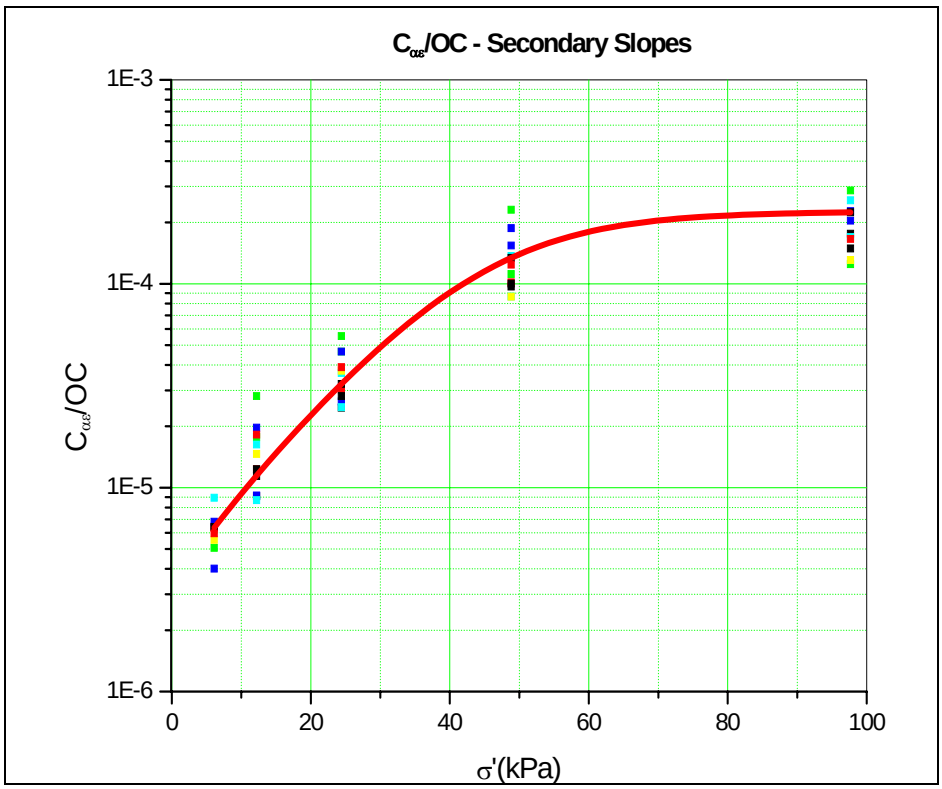

Figure 4-9. $C_{\alpha\varepsilon}$ versus σ'- Secondary Slope.

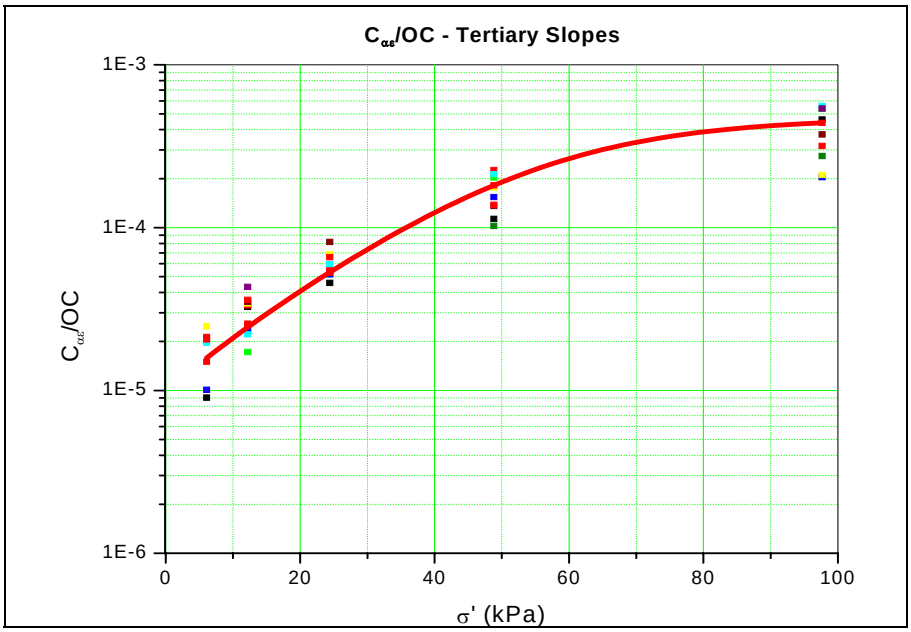

Figure 4-10. $C_{\alpha\varepsilon}$ versus σ'- Tertiary Slope.

can reduce the surcharge time by increasing the surcharge stress to aim for a higher value of $C_{\alpha\varepsilon}$. The associated risk with this practice is the potential for slope instability when a higher embankment is needed for higher surcharge stress.

4.2.3 Unloading Behavior

The unloading behavior of organic soils plays a very important role in a surcharge design. The post construction settlement is directly related to the amount of creep that the soil experiences after surcharge removal. The general behavior of organic soils subjected to unloading has been described by Mesri, Ullrich and Choi (1978). For this study, samples from all three groups (i.e., organic categories) were subjected to unloading.

Since unloading is the reverse process of loading, the soil will first experience negative pore-water pressure, and heave from surcharge removal which will last a short period of time (high permeability). The latter is generally referred to as *primary rebound*. Next, the organic soils will undergo more heave without any change in the effective stress or pore-water pressure. Finally, depending on the samples OC level, a downward creep process may reoccur for the high OC samples. The low OC samples did not exhibit any creep after rebound i.e., remained flat after reaching the maximum rebound. Some of the medium OC sample showed a slight or insignificant amount of downward creep after rebound. Figure 4-11 displays the unloading behavior of the low, medium and high organic soil specimens. Evident from the figure, the phenomenon of creep after rebound is attributed to the presence of organic matter.

Characterizing the phenomenon of creep after surcharge removal and using it in design was an important task for this research. Consequently, the oedometer tests were designed to investigate the effect of surcharge removal at different stress levels and surcharging times so that the influence of OCR and *prior* compressive strains could be studied. The normalized unload

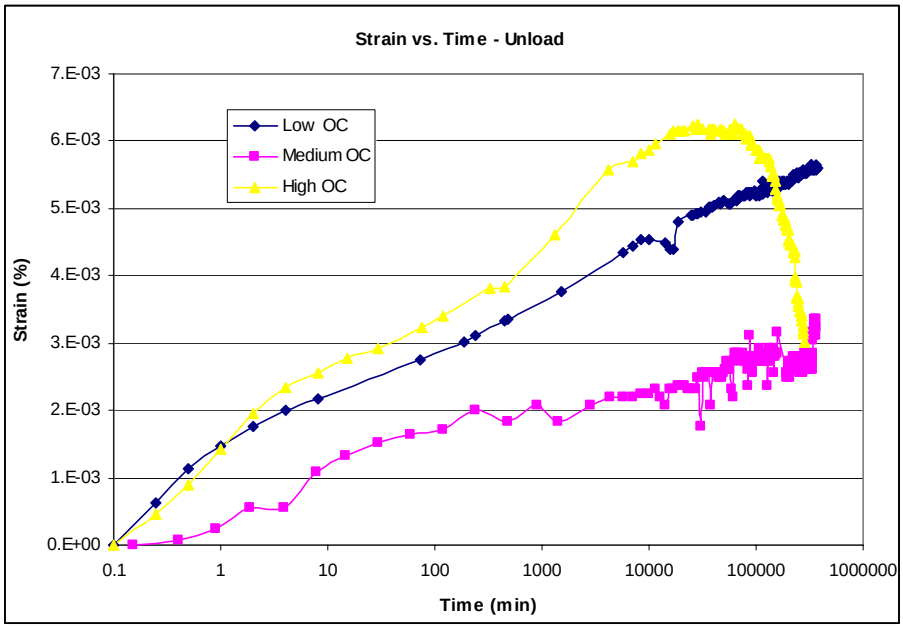

Figure 4-11. Unload Strain vs. Time.

behavior of low, medium and high OC groups are illustrated in Figures 4-12, 4-13 and 4-14. One important aspect of surcharge design involves the determination of time for creep to reoccur if the phenomenon is observed. Based on the organic content, Figure 4-15 depicts the onset of downward creep, $T_{cr,}$ for high organic soils. The onset time, T_{cr}, was correlated to OC^{-1} because the OC is the decisive factor determining whether creep reoccurs after surcharge removal.

From the design point of view, engineers can construct an unload curve for peat based on the OCR, OC and past compressive strain. And in a simple design, this unload curve can be used to estimate the field behavior of a surcharge construction, especially the post-construction settlement of roadway embankments. For a more complicated design such as multiple layers, or high variation of organic content with depth, a computer program is required. The theory to predict such settlement is described in Chapter 5.

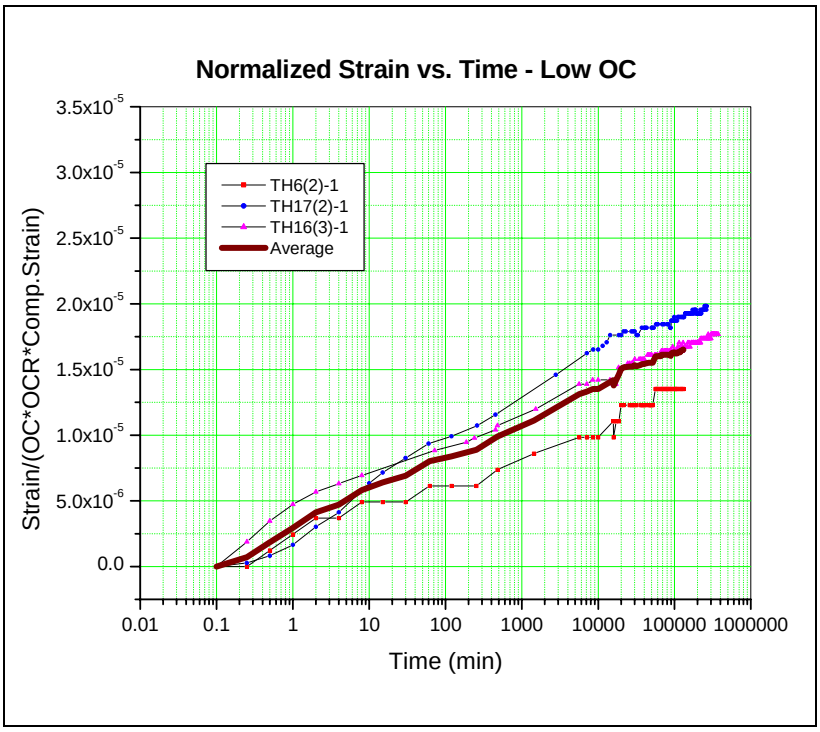

Figure 4-12. Unload Behavior - Low OC.

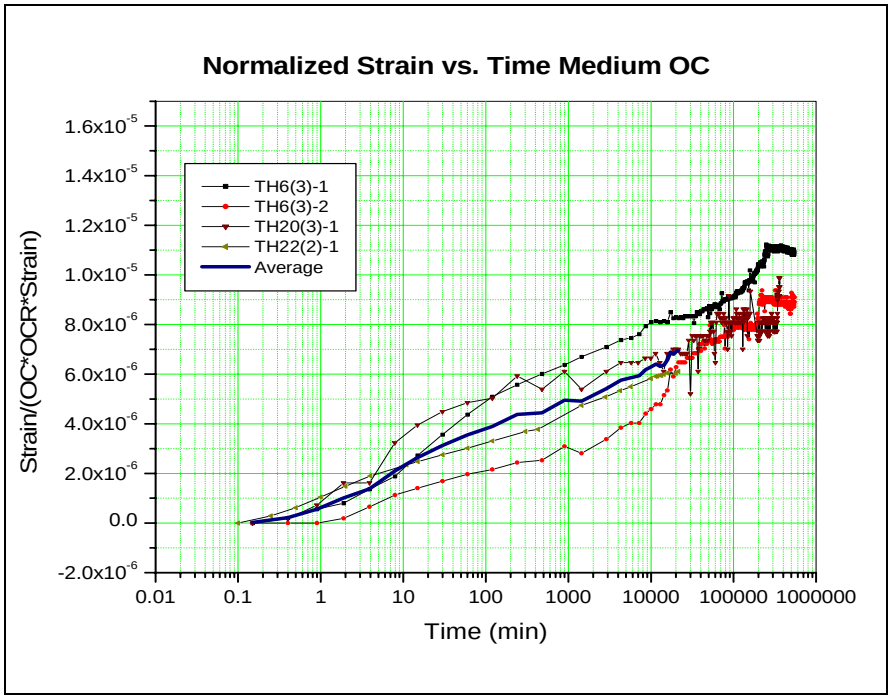

Figure 4-13. Unload Behavior - Medium OC.

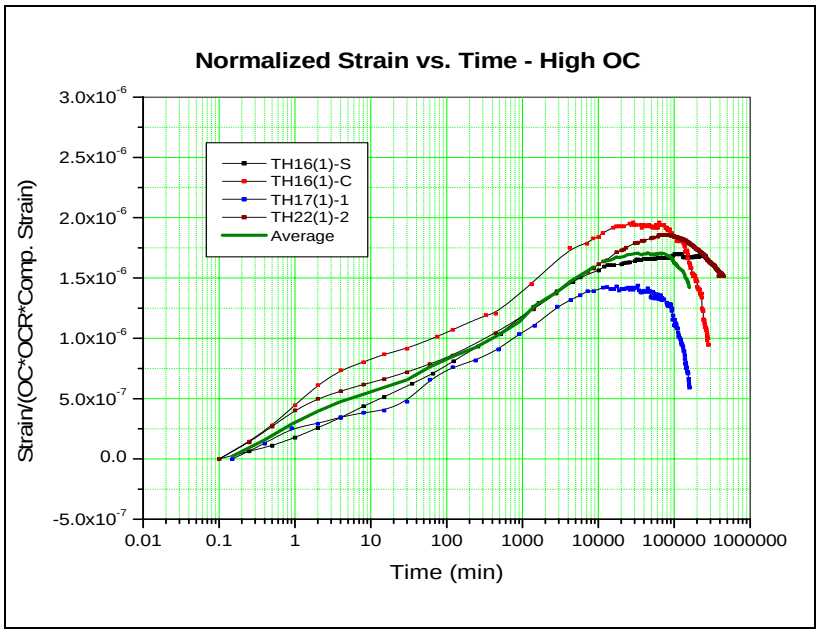

Figure 4-14. Unload Behavior - High OC.

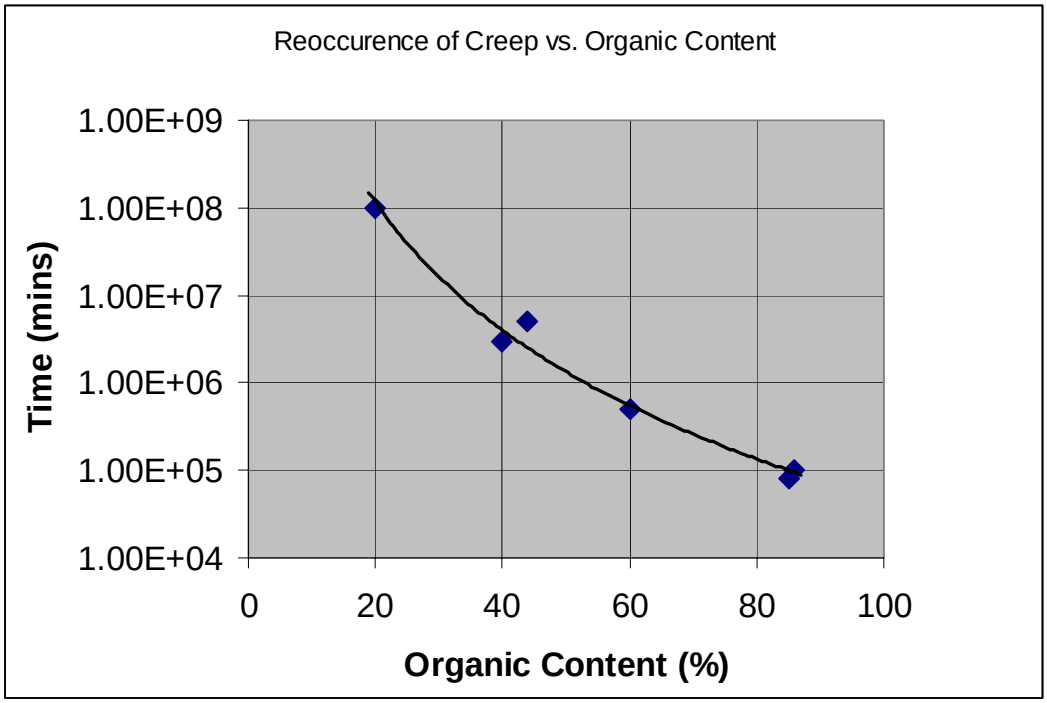

.

Figure 4-15. Time Required for Creep to Reoccur, Surcharge 2x Final Stress.

CHAPTER 5

COMPUTATIONAL MODEL

A computational model for organic soil deformation is derived and implemented using the Finite Difference Approach. The model considers nonlinear, large deformation consolidation in conjunction with nonlinear visco-elastic creep. Both load/unload behavior as well as multiple layers may be simulated with the model. Detailed descriptions of the parameters used in the model are also presented.

5.1 FINITE NONLINEAR CONSOLIDATION FORMULATION

5.1.1 The Balance Laws

Three balance laws are required, the conservation of linear momentum of the mixture (Darcy-Gersevanov) and the conservation of mass of each of the phases: water and solids, respectively. A discussion of each follows.

5.1.1.1 Particle Motion

We consider a segment of a layer, which occupies position – P'Q'R'S' – at time zero (t = 0) as shown in Figure 5-1. Height of specimen, particle position, etc. is described in terms of X and is generally referred to as a material position, i.e., particle which occupied position X at time t = 0. With the application of load, the particles compress or move together. At some time, t, the particle that was located at X is now at position $\xi(X, t)$ (Figure 5-1). The height of the segment: δX changes to $\delta\xi$ with time, t. The new height, $\delta\xi$, may be described in terms of the original height, δX through the volume of segment:

$$\delta\xi = \Delta V_s \left(1 + e\right); \quad \delta X = \Delta V_s \left(1 + e_0\right) \tag{5.1}$$

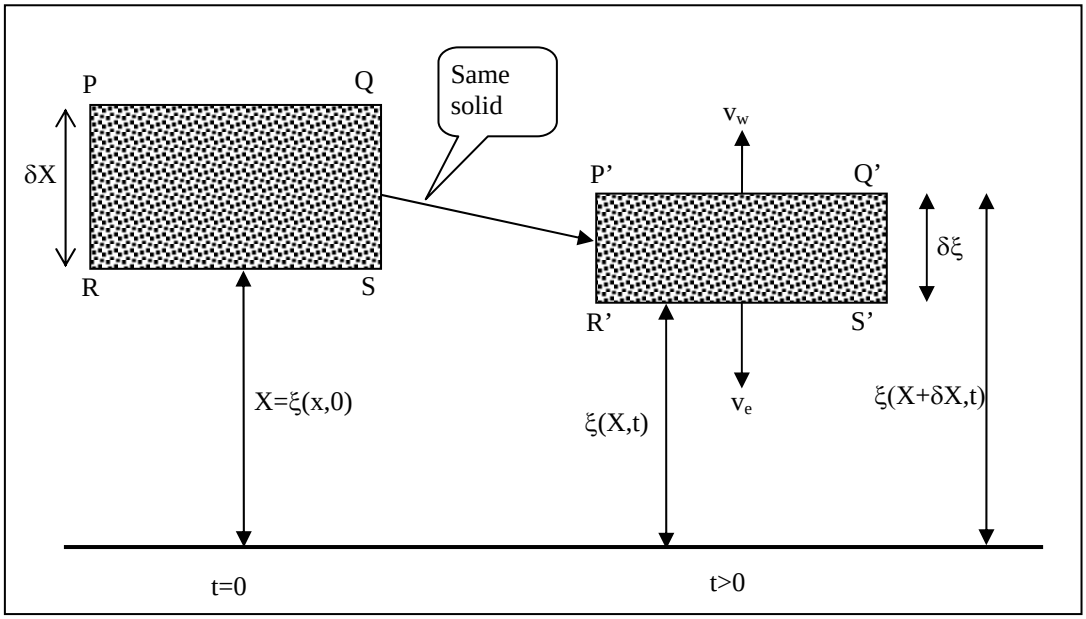

Figure 5-1. Lagrangian Configuration.

Noting that the volume of solids, ΔVs, within the segment has not changed, the ratio of the heights of the segments may be obtained:

$$\frac{\delta\xi}{\Delta X} = \frac{\partial\xi}{\partial X} = \frac{(1+e)}{(1+e_0)} \tag{5.2}$$

The velocity of particle P relative to R (Figure 5-1) may then obtained from Eq. 5.2 by differentiating:

$$\frac{\Delta\delta\xi}{\Delta t} = \frac{\Delta X}{(1+e_0)}\,\frac{\Delta e}{\Delta t} \tag{5.3}$$

Then the change in spatial positions (δξ) between particles R and P with increment of time, Δt, may be obtained:

$$\Delta\delta\xi = \frac{\Delta X}{(1+e_0)}\Delta e \tag{5.4}$$

The above equation will be used to update the geometry of the deposit, i.e., the change in position of particle P relative to R, $\Delta\ \delta\xi(X,t,)$, as a function of time. It requires the original spacing between particles (i.e., ΔX) and initial void ratio (e_0), as well as the change in void ratio, Δe, between the two particles with time increment, Δt.

5.1.1.2 The Conservation of Mass of the Pore-Water

The representative element volume (P'Q'R'S') is shown in Figure 5-2. The pore-water is flowing into the element with an mass *influx $J_w(\xi,t)$-mass/unit area/unit time,* across the face (R'S') and is flowing out of the element, across (P'Q') with an *efflux $J_w(\xi+\delta\xi,t)$-mass/unit area/unit time*. The mass flux, J_w, may be described by

$$J_w(\xi,t) = \rho_w q(\xi,t) \tag{5.5}$$

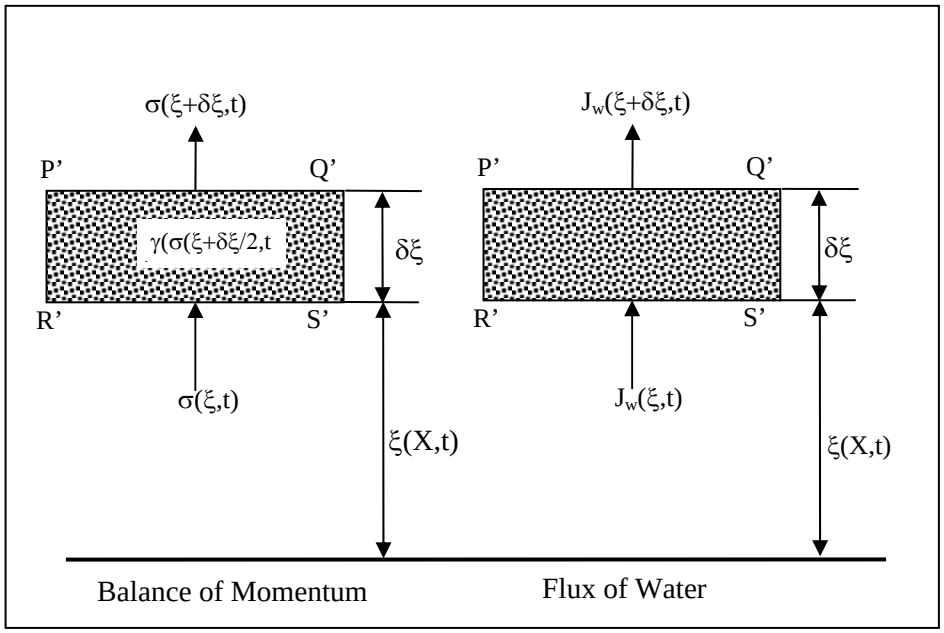

Figure 5-2. Balance Laws.

Where:

ρ_w ≡ density of water

$q(\xi,t)$ ≡ volume of water flowing per unit time through a unit cross-sectional area (i.e., velocity)

The mass of water within the volume (Figure 5-2) is given as:

$$M_w = \frac{M_w}{V_w} \frac{V_w}{V} \delta V = \rho_w n \delta V \tag{5.6}$$

Where:

$n \equiv$ porosity of soil

Subsequently, the change of mass within the volume, δV, over increment in time Δt is:

$$\left|M_w\right|_{t+\Delta t} - \left|M_w\right|_t = \left\{\left|\rho_w n\right|_{t+\Delta t} - \left|\rho_w n\right|_t\right\} \delta V \tag{5.7}$$

Next, relating the mass outflow minus the mass inflow to the change of mass within the control volume:

$$-\left\{J_w(\xi+\delta\xi, t) - J_w(\xi, t)\right\} \delta A \Delta t = \left|M_w\right|_{t+\Delta t} - \left|M_w\right|_t = \left\{\left|\rho_w n\right|_{t+\Delta t} - \left|\rho_w n\right|_t\right\} \delta V \tag{5.8}$$

Dividing both sides of Eq. 5.8 by $\delta V \Delta t$:

$$- \frac{\left\{J_w(\xi+\delta\xi, t) - J_w(\xi, t)\right\}}{\Delta \xi} = \frac{\left\{\left|\rho_w n\right|_{t+\Delta t} - \left|\rho_w n\right|_t\right\}}{\Delta t} \tag{5.9}$$

and simplifying gives:

$$- \frac{\partial J_w}{\partial \xi} = \frac{\partial}{\partial t}\{\rho_w n\} \tag{5.10}$$

The mass flux, J_w, may be replaced by the water density and volume flow rate (Eq. 5.5) to give:

$$\frac{\partial\left(\rho_w q(\xi, t)\right)}{\partial \xi} + \frac{\partial}{\partial t}\{\rho_w n\} = 0 \tag{5.11}$$

Recognizing that the volume flow rate of the fluid may be characterized through its interstitial pore fluid velocity, v_w, and porosity, i.e.,

$$q(\xi, t) = n v_w(\xi, t) \tag{5.12}$$

Then the conservation of fluid mass, Eq. 5.11, becomes:

$$\frac{\partial\left(\rho_w\, n\, v_w\left(\xi,\, t\right)\right)}{\partial \xi} + \frac{\partial}{\partial t}\left\{\rho_w\, n\right\} = 0 \tag{5.13}$$

If the fluid is assumed to be incompressible, i.e., does not vary with location or with time, then ρ_w may be dropped from the equation.

5.1.1.3 The Conservation of Mass of the Solids

The continuity of solids can be developed in the same manner as the pore-water by replacing n with (1-n), and v_w by v_s:

$$\frac{\partial\left(\rho_s\left(1-n\right) v_s\left(\xi, t\right)\right)}{\partial \xi} + \frac{\partial}{\partial t}\left\{\rho_s\left(1-n\right)\right\} = 0 \tag{5.14}$$

Since, the mass flux of the solids, J_s, is expressed as:

$$J_s = q_s\, \rho_s \tag{5.15}$$

and the volume flow rate of the solids, q_s, may be represented by the solid particle velocities, v_s, and porosity as:

$$q_s\left(\xi, t\right) = \left(1 - n\right) v_s\left(\xi, t\right) \ . \tag{5.16}$$

5.1.1.4 The Continuity of the Mixture

Assuming that both the fluid and solid particles are incompressible, and that the relative velocity of the fluid respect to the solid particles may be expressed by the Darcy-Gersevanov relationship:

$$n\left(v_w - v_s\right) = -k\left(e\right)\frac{\partial h_{total}}{\partial \xi}\,. \tag{5.17}$$

Equations 5.13, 5.14, and 5.17 may be combined to give (McVay 1986):

$$\frac{\partial}{\partial \xi}\left(\frac{k}{\gamma_w}\frac{\partial u}{\partial \xi}\right) = \frac{1}{(1-n)}\frac{Dn}{Dt} = \frac{1}{(1+e)}\frac{De}{Dt} \tag{5.18}$$

Where D/Dt represents the change in porosity or void ratio as one follows the particles. Equation 5.18 requires the need to update the current coordinate system, $\xi(X,t)$, since it changes with time. To simplify the evaluation, Eq. 5.18 may be converted to Lagrangian coordinates (i.e., X, t) with (McVay, 1988):

$$\frac{\partial F}{\partial \xi} = +\left[\frac{\partial F}{\partial X}\right] \Big/ \left[\frac{\partial \xi}{\partial X}\right] \tag{5.19}$$

Using Eq. 5.2, in Eq. 5.19, substituted into Eq. 5.18:

$$\frac{(1+e_0)}{(1+e)}\frac{\partial}{\partial X}\left\{\frac{k(e)}{\gamma_w}\frac{(1+e_0)}{(1+e)}\frac{\partial u}{\partial X}\right\} = \frac{1}{(1+e)}\frac{De}{Dt} \tag{5.20}$$

Simplifying the above equation, gives:

$$\frac{\partial}{\partial X}\left\{\frac{k(e)}{\gamma_w}\frac{(1+e_0)}{(1+e)}\frac{\partial u}{\partial X}\right\} = \frac{1}{(1+e_0)}\frac{De}{Dt} \tag{5.21}$$

Next, one recognizing that $\frac{De}{Dt}\frac{1}{1+e_0} = \frac{D\varepsilon}{Dt}$ is the *strain rate*, or Eq. 5.21 becomes:

$$\frac{\partial}{\partial X}\left\{\frac{k(e)}{\gamma_w}\frac{(1+e_0)}{(1+e)}\frac{\partial u}{\partial X}\right\} = \frac{D\varepsilon}{Dt} \tag{5.22}$$

In the above expression, the dependent variable is the excess pore water pressure, u. Of interest is the change in vertical effective stress vs. void ratio or vertical strain. In the case of surcharge loading, the change in excess pore pressure is directly proportional to the change in vertical effective stress, or

$$\frac{\partial \sigma'}{\partial X} = \frac{\partial u}{\partial X} \tag{5.23}$$

Substituting Eq. 5.23 into Eq. 5.22, results in

$$\frac{\partial}{\partial X}\left\{\frac{k(e)}{\gamma_w}\frac{(1+e_0)}{(1+e)}\left(\frac{\partial \sigma'}{\partial X}\right)\right\} = \frac{D\varepsilon}{Dt} \tag{5.24}$$

This equation is the *governing* equation of *nonlinear, finite strain* consolidation and creep expressed in terms of effective stress and strain rate. In the following section the right hand side (RHS) for both consolidation and creep phases will be developed.

5.1.2 The Gibson-Lo Model of Creep

Gibson and Lo (1961) proposed a model that represents the deformation of soil skeleton with respect to change in load and time. This *one-dimensional* model suggests that soil skeleton can be replaced by a combination of three simple rheological components as originally recommended by Tan (1957).

5.1.2.1 Schematic Representation of the Consolidation Process

The proposed model of the soil skeleton undergoing one-dimensional compression consists of a *Hookean spring* connected in series with a *Kelvin or Voigt element* as shown in Figure 5-3. The latter may be explained as follows.

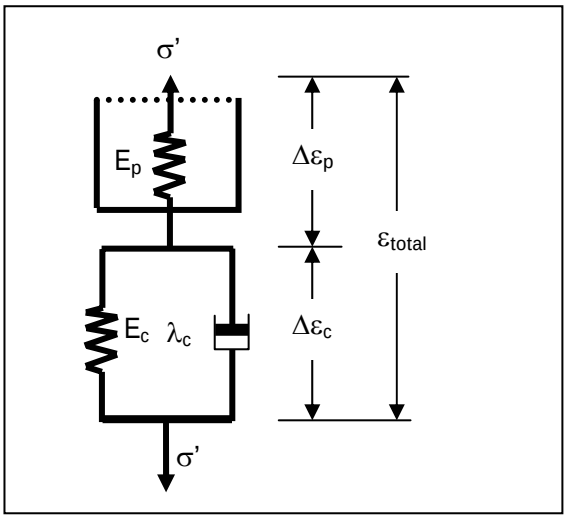

Figure 5-3. Model Representation of Soil Skeleton.

When a time dependent stress $\sigma'(t)$ acts on an element of soil at depth ξ, where the response of the soil skeleton is schematically represented by Figure 5-3, the spring E_p is compressed gradually due to the consolidation of soil skeleton. Since the transference of stress from pore-water to soil skeleton is delayed due to the permeability of the soil, the effective stress $\sigma'(t)$ increases gradually from zero to the full value of the applied stress. Hence, the compression of the spring E_p is gradual and is fully accomplished only when the applied stress has become fully effective. The period during which the settlement and rate of settlement is dominated by compression of the spring E_p is often called the *hydrodynamic* period and the settlements referred to as consolidation strains.

Under the gradually increasing effective stress, the *Kelvin* body (spring and dashpot in parallel) commences to compress. Initially the full load is taken by the *Newtonian dashpot* -λ_c, and no creep strain occurs. However, with time, load/stress is transferred to the spring – E_c – and creep occurs. This phenomenon of transference corresponds to the process of secondary consolidation, which arises under sustained effective stress. After a very appreciable time has elapsed, the full effective stress is taken through springs $E_{p \text{ and }} E_{c;}$ then the dashpot λ_c will then carry none of the load.

5.1.2.2 Formulation of the Model

At any time, the total strain, ε_t, will be the sum of the consolidation, $\Delta\varepsilon_{p,}$ and creep, $\Delta\varepsilon_{c,}$ increments:

$$\varepsilon = \Delta\varepsilon_p + \Delta\varepsilon_c \tag{5.25}$$

Where the consolidation portion of the strain increment:

$$\Delta\varepsilon_p = \frac{\sigma'}{E_p} \tag{5.26}$$

is obtained from the e or ε vs. log σ' curve. The compressive strains associated with the creep, $\Delta\varepsilon_c$, may be derived by noting that the sum of the stresses in the creep spring and dashpot, must be equal to the applied stress, σ', or:

$$\Delta\varepsilon_c E_c + \lambda_c \frac{\Delta\varepsilon_c}{\Delta t} = \sigma'(t) \tag{5.27}$$

In the above equation both $\Delta\varepsilon_c$ and σ'(t) are a function of the depth, ξ. The solution of this equation, satisfying the initial condition $\varepsilon_c(0) = 0$, is:

$$\Delta\varepsilon_c = \frac{e^{-\frac{E_c t}{\lambda_c}}}{\lambda_c} \int_0^t \sigma'(\tau) e^{\frac{E_c \tau}{\lambda_c}} d\tau \tag{5.28}$$

The total strain, Eq. 5.26 is then:

$$\varepsilon = \Delta\varepsilon_p + \Delta\varepsilon_c = \frac{\sigma'}{E_p} + \frac{e^{-\frac{E_c t}{\lambda_c}}}{\lambda_c} \int_0^t \sigma'(\tau) e^{\frac{E_c \tau}{\lambda_c}} d\tau \tag{5.29}$$

The *strain rate* (derivative of Eq. 5.29) is:

$$\dot{\varepsilon} = \frac{d\varepsilon}{dt} = \frac{1}{E_p}\frac{\partial\sigma'(t)}{\partial t} + \frac{\sigma'(t)}{\lambda_c} - \frac{Ec}{\lambda_c^2} e^{-\frac{E_c t}{\lambda_c}} \int_0^t \sigma'(\tau) e^{\frac{E_c \tau}{\lambda_c}} d\tau \tag{5.30}$$

This equation is the RHS of Eq. 5.24. The governing equation using Gibson-Lo model is now:

$$\boxed{\frac{\partial}{\partial X}\left\{\frac{k(e)}{\gamma_w}\frac{(1+e_0)}{(1+e)}\left(\frac{\partial\sigma'}{\partial X}\right)\right\} = \frac{1}{E_p}\frac{\partial\sigma'(t)}{\partial t} + \frac{\sigma'(t)}{\lambda_c} - \frac{Ec}{\lambda_c^2} e^{-\frac{E_c t}{\lambda_c}} \int_0^t \sigma'(\tau) e^{\frac{E_c \tau}{\lambda_c}} d\tau} \tag{5.31}$$

5.1.3 Surcharge Problem

Of interest is the effective stress distribution vs. settlement or strain for some given time for the boundary conditions shown in Figures 5-4 and 5-5.

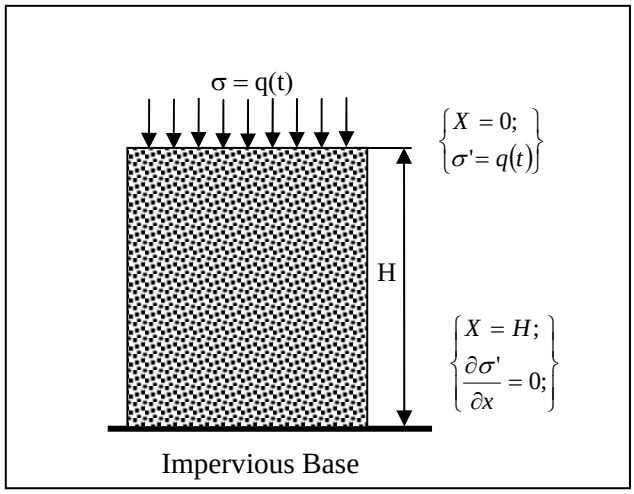

Figure 5-4. Case 1 - Impervious Base.

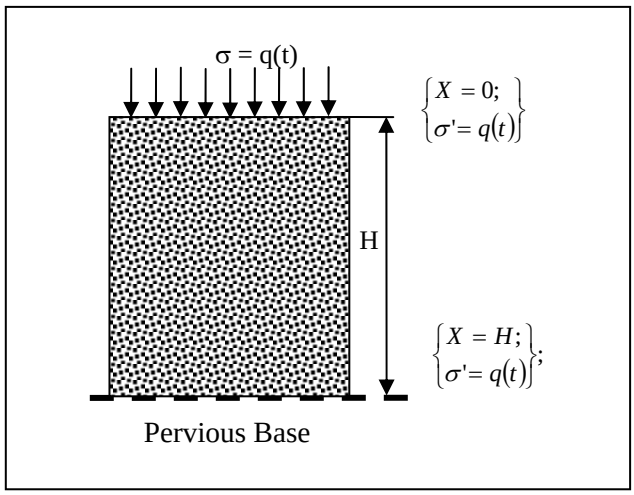

Figure 5-5. Case 2 - Pervious Base.

One should assume that the soil is *non-homogeneous,* i.e., soil properties (unit weight, void ratio, permeability) vary with depth. The applied stress, *q(t),* will vary with time for either the load or unload condition.

5.2 FINITE DIFFERENCE SOLUTION

A *Finite Difference Solution* (FDS) for solving Equation 5.31 with the boundary condition as shown in Figures 5-4 and 5-5 is derived next. The developed FDS is based on an *explicit*

time marching scheme. The discretization of the LHS and RHS of Eq. 5.32 are handled separately.

5.2.1 The LHS

The LHS of Eq. 5.31 is:

$$\frac{\partial}{\partial X}\left\{\frac{k(e)}{\gamma_w}\ \frac{(1+e_0)}{(1+e)}\left(\frac{\partial \sigma'}{\partial X}\right)\right\} \tag{5.32}$$

Because the initial void ratio, e_0, and unit weight are assumed independent of time and position, the following constant, A, is assigned:

$$A = \frac{(1+e_0)}{\gamma_w} \tag{5.33}$$

which comes out of the derivative, Eq. 5.32. However, since the permeability and void ratio, e, varies with space and stress, the coefficient, B,

$$B = \frac{k(e)}{(1+e)} \tag{5.34}$$

remains within the derivative, and Equation 5.32 becomes:

$$A\ \frac{\partial}{\partial X}\left\{B\frac{\partial \sigma'}{\partial X}\right\} \tag{5.35}$$

Consider the soil layers are divided into N elements and nodes as shown in Figure 5-6. Equation 5.32 must be satisfied at every node from 1 to N + 1 in which N + 2 is the virtual node needed for the boundary condition, if necessary.

5.2.1.1 At Node i^{th}, Time Step j^{th} (Figure 5-7)

Similar to $\frac{\partial^2 \sigma'}{\partial X^2} = \frac{\sigma_{i+1} - 2\sigma_i + \sigma_{i-1}}{\Delta X^2}$ - *Central Scheme* (5.36)

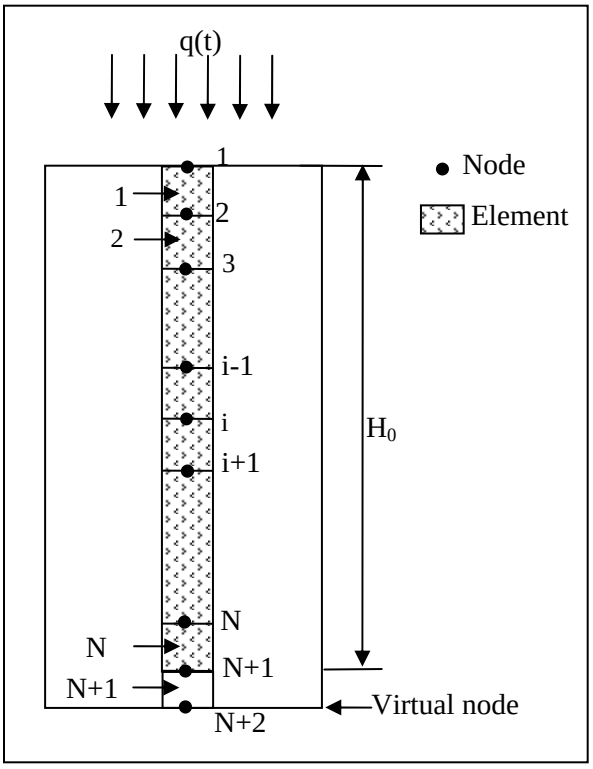

Figure 5-6. Finite Difference Scheme.

Eq. 5.35 may be expressed as,

$$\frac{\partial}{\partial X}\left[B\frac{\partial \sigma'}{\partial X}\right]_i^j = \left(\frac{\left(B\frac{\partial \sigma'}{\partial X}\right)_{i+1} - \left(B\frac{\partial \sigma'}{\partial X}\right)_{i-1}}{\Delta X}\right)^j \tag{5.37}$$

For 1st order derivatives:

$$\left(\frac{\partial \sigma'}{\partial X}\right)_{i+1}^j = \left(\frac{\sigma'_{i+1} - \sigma'_i}{\Delta X}\right)^j \text{ - } \textit{Backward Scheme} \tag{5.38}$$

$$\left(\frac{\partial \sigma'}{\partial X}\right)_{i-1}^j = \left(\frac{\sigma'_i - \sigma'_{i-1}}{\Delta X}\right)^j \text{ - } \textit{Forward Scheme} \tag{5.39}$$

Substituting into Eq. 5.37,

$$\frac{\partial}{\partial X}\left[B\frac{\partial \sigma'}{\partial X}\right]_i^j = \left(\frac{B_{i+1}\frac{\sigma'_{i+1}-\sigma'_i}{\Delta X} - B_{i-1}\frac{\sigma'_i-\sigma'_{i-1}}{\Delta X}}{\Delta X}\right)^j \tag{5.40}$$

Simplifying,

$$\frac{\partial}{\partial X}\left[B\frac{\partial \sigma'}{\partial X}\right]_i^j = \frac{1}{\Delta X^2}\left(B_{i+1}\sigma'_{i+1} - \sigma'_i\left(B_{i+1}+B_{i-1}\right) + B_{i-1}\sigma'_{i-1}\right)^j \quad (5.41)$$

Note if B were constant, then Eq. 5.41 would be the same as Eq. 5.36. The LHS of Eq. 5.32 may now be approximated as:

$$\frac{A_i}{\Delta X^2}\left(B_{i+1}\sigma'_{i+1} - \sigma'_i\left(B_{i+1}+B_{i-1}\right) + B_{i-1}\sigma'_{i-1}\right)^j \quad (5.42)$$

Or if it was set equal to D_i^j:

$$D_i^j = \frac{A_i}{\Delta X^2}\left(B_{i+1}\sigma'_{i+1} - \sigma'_i\left(B_{i+1}+B_{i-1}\right) + B_{i-1}\sigma'_{i-1}\right)^j \quad (5.43)$$

Note, the D_i^j term contains only the current time step j^{th} (Figure 5-7) in its evaluation.

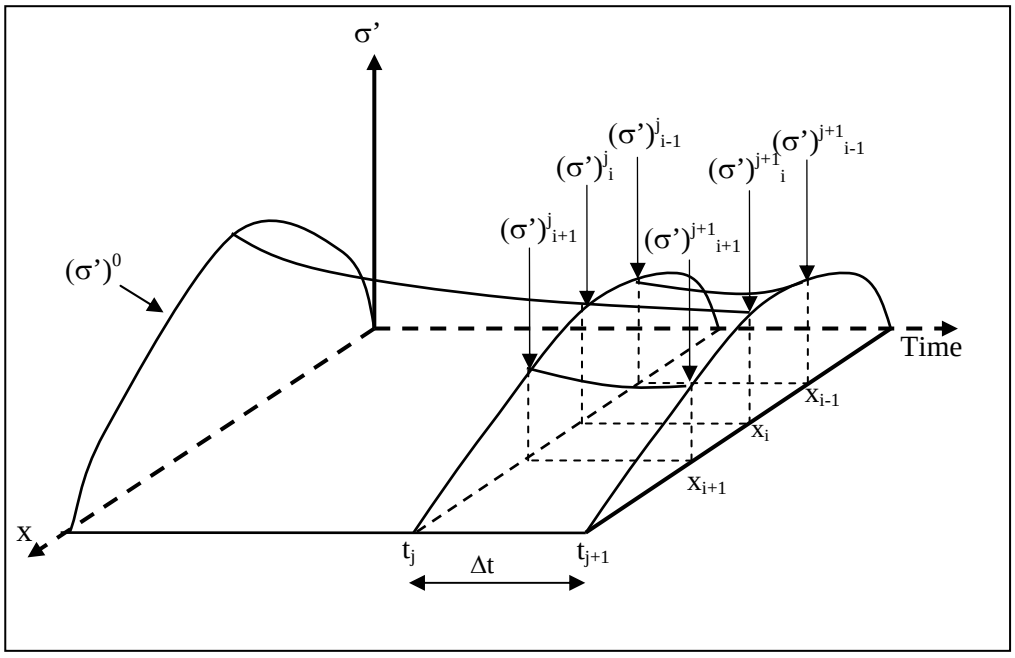

Figure 5-7. Finite Difference Approximation.

5.2.2 The RHS

The RHS of (5.31) is:

$$\boxed{\frac{1}{E_p}\frac{\partial \sigma'(t)}{\partial t}+\frac{\sigma'(t)}{\lambda_c}-\frac{Ec}{\lambda_c^2}e^{-\frac{E_c t}{\lambda_c}}\int_0^t \sigma'(\tau)e^{\frac{E_c \tau}{\lambda_c}}\,d\tau} \tag{5.44}$$

The RHS contains a time derivative in the first term. This time derivative will relate the values of current time step, j, to the next one, j+1, using the explicit time-marching scheme as described in the next section.

5.2.2.1 At Node i^{th}, Time Step j^{th} (Figure 5-7)

The first term in Eq. 5.44 may be approximated as

$$\left(\frac{1}{E_p}\frac{\partial \sigma'(t)}{\partial t}\right)_i^j=\left(\frac{1}{E_p}\right)^j\frac{\sigma'^{j+1}_i-\sigma'^{j}_i}{\Delta t} \tag{5.45}$$

This equation relates the *unknown* effective stress σ'^{j+1}_i at time step j + 1 to the *known* effective stress σ'^{j}_i at time step j where i is its spatial position (Figure 5-7).

The second term of Eq. 5.44 is simply:

$$\left(\frac{\sigma'(t)}{\lambda_c}\right)_i^j=\frac{\sigma'^{j}_i}{\lambda_{c\,i}^{\,j}} \tag{5.46}$$

The integral: $\int_0^t \sigma'(\tau)e^{\frac{E_c\tau}{\lambda_c}}\,d\tau$ in Eq. 5.44 can be expressed as:

$$\int_0^{t_j}\sigma'(\tau)e^{\frac{E_c\tau}{\lambda_c}}d\tau=\left[\int_0^{t_{j-1}}\sigma'(\tau)e^{\frac{E_c\tau}{\lambda_c}}\,d\tau+\int_{t_{j-1}}^{t_j}\sigma'(\tau)e^{\frac{E_c\tau}{\lambda_c}}d\tau\right] \tag{5.47}$$

If, one allows:

$$\boxed{\begin{aligned} I_i^j &= \int_0^{t_j} \sigma'(\tau) e^{\frac{E_c \tau}{\lambda_c}} d\tau; \\ I_i^{j-1} &= \int_0^{t_{j-1}} \sigma'(\tau) e^{\frac{E_c \tau}{\lambda_c}} d\tau; \\ \Delta I_i^j &= \int_{t_{j-1}}^{t_j} \sigma'(\tau) e^{\frac{E_c \tau}{\lambda_c}} d\tau; \end{aligned}} \tag{5.48}$$

One can approximate the value of $\Delta I_i^j = \int_{t_{j-1}}^{t_j} \sigma'(\tau) e^{\frac{E_c \tau}{\lambda_c}} d\tau$ as:

$$\Delta I_i^j = \int_{t_{j-1}}^{t_j} \sigma'(\tau) e^{\frac{E_c \tau}{\lambda_c}} d\tau = \frac{1}{2} \left(\sigma'^{j-1}_i e^{\frac{E_c t_{j-1}}{\lambda_c}} + \sigma'^{j}_i e^{\frac{E_c t_j}{\lambda_c}} \right) \Delta t \tag{5.49}$$

Then the integral $\int_0^t \sigma'(\tau) e^{\frac{E_c \tau}{\lambda_c}} d\tau$ in Eq. 5.44 may be obtained as:

$$I_i^j = I_i^{j-1} + \Delta I_i^j \tag{5.50}$$

In which I_i^{j-1} is I_i^j of the previous step. Next, the exponential in the integral in Eq. 5.45 may be expressed as

$$g^j = \frac{E c}{\lambda_c^2} e^{-\frac{E_c t}{\lambda_c}} \tag{5.51}$$

and the exponential integral term in Eq. 5.44 may be expressed as

$$\frac{E c}{\lambda_c^2} e^{-\frac{E_c t}{\lambda_c}} \int_0^t \sigma'(\tau) e^{\frac{E_c \tau}{\lambda_c}} d\tau = g^j I_i^j \tag{5.52}$$

The RHS of Eq. 5.44 now becomes:

$$\frac{1}{(E_p)^j} \frac{\sigma'^{j+1}_i - \sigma'^{j}_i}{\Delta t} + \frac{\sigma'^{j}_i}{\lambda_{ci}^j} - g^j I_i^j \tag{5.53}$$

In this expression the *only unknown* is σ'^{j+1}_i.

Now, if the LHS (Eq. 5.32) is set equal to the RHS (Eq. 5.44), then the consolidation-creep relationship, Eq. 5.31, becomes:

$$D_i^j = \frac{1}{\left(E_p\right)^j}\frac{\sigma_i'^{j+1} - \sigma_i'^{j}}{\Delta t} + \frac{\sigma_i'^{j}}{\lambda_{ci}^j} - g^j I_i^j \tag{5.54}$$

The above equation may be solved for the unknown stress, σ^{j+1}. This gives the general recurrence formula for determining the change in stress with time at a specific location, i, within the deposit:

$$\sigma'^{j+1}_i = \left(E_p\right)^j \Delta t \left\{ D_i^j - \frac{\sigma'^{j}_i}{\lambda_{ci}^j} + g^j I_i^j \right\} + \sigma'^{j}_i \tag{5.55}$$

The new stress σ'^{j+1}_i is determined from the known values of $\left\{\left(E_p\right)^j, D_i^j, \sigma_i'^{j}, g^j, I_i^j\right\}$ at time step t_j.

5.2.3 The Strain - ε_{total}

Equation 5.29 gives the total strain:

$$\varepsilon = \Delta\varepsilon_p + \Delta\varepsilon_c = \frac{\sigma'}{E_p} + \frac{e^{-\frac{E_c t}{\lambda_c}}}{\lambda_c}\int_0^t \sigma'(\tau) e^{\frac{E_c \tau}{\lambda_c}}\, d\tau \tag{5.56}$$

and will be estimated step by step as follows.

5.2.3.1 The Consolidation Strain

The consolidation strain component, $\Delta\varepsilon_p$, is estimated by using a nonlinear stress-strain curve shown in Figure 5-8. The value of E_{pi} is calculated from the EOP e-log(σ') curve. The next section of this chapter deals in detail on how to obtain E_p from C_c, and C_r of the e-log(σ') curve.

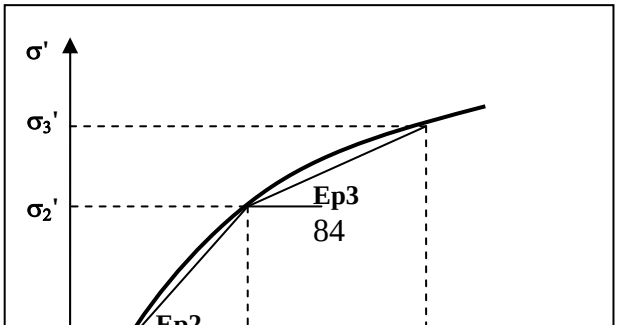

Figure 5-8. Illustration of Stress-Strain Curve and E_p.

The total primary strain is $\Delta\varepsilon_p$:

$$\left(\Delta\varepsilon_p\right)_i^{j+1} = \sum_{k=1}^{j+1} \frac{\sigma'^{k}_i - \sigma'^{k-1}_i}{\left(E_{pi}\right)_k} \tag{5.57}$$

or

$$\left(\Delta\varepsilon_p\right)_i^{j+1} = \sum_{k=1}^{j} \frac{\sigma'^{k}_i - \sigma'^{k-1}_i}{\left(E_{pi}\right)_k} + \frac{\sigma'^{j+1}_i - \sigma'^{j}_i}{\left(E_{pi}\right)_j} \tag{5.58}$$

If set

$$\boxed{\begin{aligned}\left(S_p\right)_i^j &= \sum_{k=1}^{j} \frac{\sigma'^{k}_i - \sigma'^{k-1}_i}{\left(E_{pi}\right)_k} \\ \left(\Delta S_p\right)_i^{j+1} &= \frac{\sigma'^{j+1}_i - \sigma'^{j}_i}{\left(E_{pi}\right)_j}\end{aligned}} \tag{5.59}$$

Then:

$$\left(\Delta\varepsilon_p\right)_i^{j+1} = \left(S_p\right)_i^j + \left(\Delta S_p\right)_i^{j+1} \tag{5.60}$$

Note, the consolidation strain, $\Delta\varepsilon_p$, is found (updated) after the new stress σ'^{j+1}_i (Eq. 5.55) is determined.

5.2.3.2 The Creep Strain

The creep strain, $\Delta\varepsilon_c$, at time j+1, may be computed from Eq. 5.28,

$$\left(\Delta\varepsilon_c\right)_i^{j+1} = \frac{e^{-\frac{E_c t_{j+1}}{\lambda_c}}}{\lambda_c}\int_0^{t_{j+1}}\sigma'(\tau)e^{\frac{E_c\tau}{\lambda_c}}\,d\tau \tag{5.61}$$

Again, the integral $\int_0^{t_{j+1}}\sigma'(\tau)e^{\frac{E_c\tau}{\lambda_c}}d\tau$, or I_i^{j+1} may be calculated based on Eqs. 5.48 to 5.50 or

$$I_i^{j+1} = I_i^j + \Delta I_i^{j+1} \tag{5.62}$$

In which I_i^{j+1} is approximated by:

$$\Delta I_i^{j+1} = \frac{1}{2}\left(\sigma_i^{j+1}e^{\frac{E_c t_{j+1}}{\lambda_c}} + \sigma_i^j e^{\frac{E_c t_j}{\lambda_c}}\right)\Delta t \tag{5.63}$$

and I_i^j is I_i^{j+1} from the previous step. The creep strain, obtained from Eq. 5.51 and Eq. 5.62 is then:

$$\left(\varepsilon_c\right)_i^{j+1} = \frac{e^{-\frac{E_c t_{j+1}}{\lambda_c}}}{\lambda_c}\int_0^{t_{j+1}}\sigma'(\tau)e^{\frac{E_c\tau}{\lambda_c}}\,d\tau = \frac{\lambda_c}{E_c}g^{j+1}I_i^{j+1} \tag{5.64}$$

5.2.4 The Computational Procedure

The *computational procedure* is to compute the new value of effective stress, σ'^{j+1}_i, at time t+Δt, j+1, based on Eq. 5.55, which is a function of $\left(E_p\right)^j$, D_i^j, σ'^j_i, I_i^j at time t. Once the new value of stress, σ'^{j+1}_i is known, the consolidation strain (Eq. 5.60), and creep strain (Eq. 5.64) are computed, followed by void ratio, and finally the permeability. After the stress, strain, void ratio, and permeability are updated, then $\left(E_p\right)^{j+1}$, D_i^{j+1}, and I_i^{j+1} are computed for the next time step and the whole process is repeated. The consolidation process will continue until there is no more change with effective stress with depth and time. The creep consolidation will continue with time, but at diminishing values.

5.3 SOIL PARAMETERS

There are 3 soil compressibility parameters required for the proposed model: E_p, E_c, λ_c , Figure 5-3. This section covers the method of determining the compressibility properties from a 1-D consolidation test. The primary consolidation parameter, E_p, is obtained from the traditional Coefficient of Consolidation Index, Cc. The creep parameters E_c and λ_c are obtained from a void ratio vs. log time plot for a specific stress increment (i.e., embankment, surcharge, etc.). If the shape of the void ratio vs. log time plot is the traditional S shape, i.e., low organics (Figure 4-3) then the conventional 24 hr time period of holding the load is acceptable. However, if the void ratio vs. lot time plot shows significant creep (Figure 4-5), then it is recommended that the load be held for approximately 2 weeks (20,160 mins.) to differentiate both secondary $(E_c, \lambda_c)_{secondary}$ and tertiary creep $(E_c, \lambda_c)_{tertiary}$ parameters. An example showing the calculation of each follows.

The *consolidation* stiffness, E_p is obtained from the traditional e-log(σ') curve. The slope of the loading portion of this curve is identified as the compression index, C_c, and the unloading portion of the curve is the recompression index, C_r.

E_p may be derived from C_c as follows. Starting from the definition of C_c:

$$C_c = \frac{\Delta e_p}{\Delta\left(\log\left(\sigma'\right)\right)} = \frac{d e_p}{d\left(\log\left(\sigma'\right)\right)} \tag{5.65}$$

Or

$$\frac{d}{de_p}\left(\log\left(\sigma'\right)\right) = \frac{1}{C_c} \tag{5.66}$$

Differentiating the left side:

$$\frac{d}{de_p}\left(\log\left(\sigma'\right)\right) = \frac{1}{\sigma' \ln(10)} \frac{d\sigma'}{de_p} = \frac{1}{C_c} \tag{5.67}$$

Recognizing that E_p is the derivative of effective stress with respect to strain. Using the chain rule,

$$E_p = \frac{d\sigma'}{d\varepsilon_p} = \frac{d\sigma'}{de_p}\frac{de_p}{d\varepsilon} \tag{5.68}$$

Noting that the vertical strain is equal to volumetric strain for 1-D compression, i.e.

$$\Delta\varepsilon_p = \Delta\varepsilon_{vol} \equiv \frac{\Delta V}{V_0} \equiv \frac{(\Delta e_p)V_s}{(1+e_0)V_s} \tag{5.69}$$

Using the relationship between void ratio and vertical strain, the derivative of void ratio to vertical strain is then

$$\frac{de}{d\varepsilon} = \frac{\Delta e}{\Delta\varepsilon} = (1 + e_0) \tag{5.70}$$

Substituting Eqs. 5.67, and 5.70 into Eq. 5.68 gives E_p as

$$E_p = \frac{\sigma' \ln(10)}{C_c}(1+e_0) = \frac{2.3\sigma'}{C_c}(1+e_0) \tag{5.71}$$

Evident from Eq. 5.71, the consolidation modulus, $E_{p,}$ is a function of both vertical effective stress and the soil's compression index. Typical values for Cc range from 0.1 to 0.8 (Table 4-1, Figure 4-8) and are a function of the soil's initial void ratio and organic content. In the case of secondary and tertiary creep where the vertical effective stress is constant, E_p is also a constant.

After the consolidation time has elapsed, the effective stress becomes constant and the soil skeleton carries the load. However, significant creep that is characterized by the spring and dashpot, Figure 5-3 (parameters E_c and λ_c), is still ongoing. Settlements with constant effective stress may be obtained by directly integrating Equation 5.31, or

$$S(t) = \Delta\sigma gh\left[\frac{1}{E_p} + \frac{1}{E_c}\left(1 - e^{-\frac{E_c}{\lambda_c}t}\right)\right] \tag{5.72}$$

In the above equation, E_p is the average consolidation modulus, which gives the consolidation settlement, whereas the second term is the creep settlement. For significantly, long periods of time, e.g., $t = \infty$, Eq. 5.72 reduces to

$$S(\infty) = \Delta\sigma gh\left[\frac{1}{E_p} + \frac{1}{E_c}\right] \tag{5.73}$$

And is identical to Eq. 5.25, if h is brought to the other side of Eq. 5.73.

Equation 5.73 may be used to estimate the creep compression modulus, E_c, for a soil. Solving Eq. 5.73 for E_c gives,

$$E_c = \left(\frac{\Delta\sigma}{\frac{S(\infty)}{h} - \frac{\Delta\sigma}{E_p}}\right) = \left(\frac{\Delta\sigma}{\varepsilon_t - \Delta\varepsilon_p}\right) \tag{5.74}$$

Evident, from Eq. 5.74, the creep compression modulus, E_c, is the applied stress increment divided by the creep strain (i.e., total strain minus consolidation strain).

The rate of creep strain accumulation is controlled by the parameter λ_c. For constant effective stresses, i.e., post consolidation, the creep strain, $\Delta\varepsilon_c$, may be obtained from Eq. 5.72 as

$$\Delta\varepsilon_c = \frac{\Delta\sigma}{E_c}\left[1 - e^{\frac{-E_c t}{\lambda_c}}\right] \tag{5.75}$$

Knowing both the stress increment, $\Delta\sigma$, and creep modulus, E_c, the rate of creep consolidation, λ_c, may be solved from Eq. 5.75 as

$$\lambda_c = \frac{-E_c(t_2 - t_1)}{\ln\left(1 - \Delta\varepsilon_c \frac{E_c}{\Delta\sigma}\right)} \tag{5.76}$$

For soils exhibiting both secondary and tertiary creep, there will be two sets of creep parameters (E_c and λ_c), obtained from Eqs. 5.74 and 5.76. The latter is accomplished by separating the creep

strain ($\Delta\varepsilon_c$) into two increments (secondary, $\Delta\varepsilon_{cs}$, and tertiary, $\Delta\varepsilon_{ct}$) corresponding to the two creep slopes. The value of t_1 and t_2 correspond to the beginning and ending of each slope. An example of parameter estimation is given in the next section.

5.4 WORKED EXAMPLE FOR CREEP PARAMETER ESTIMATION

Consider the void ratio vs. log time response of the highly organic sample, SP 17(1) from the Florida Turnpike at the ½ tsf load increment (final embankment conditions). Based on Taylor's void ratio vs. square root of time, the void ratio at the end of consolidation was 7.16. Using an initial void ratio, e_0, of 7.3, the consolidation strain, $\Delta\varepsilon_p$, is calculated from Eqs. 4.4 and 4.5 as

$$\Delta\varepsilon_p = \frac{\Delta e}{1+e_0} = \frac{e_0 - e_p}{1+e_0} = \frac{7.3-7.16}{1+7.3} = 0.0168 \tag{5.77}$$

Next since the sample exhibits both secondary and tertiary creep, i.e., two distinct creep slopes, two different creep compression modulus, E_c, and compression rate, λ_c parameters will be determined.

From laboratory curve, Figure 5-9, secondary compression is estimated to end at void ratio of 6.9, and tertiary at 6.2. Consequently, the secondary creep compression modulus, E_{cs} is estimated by first estimating the total secondary creep strain (denominator of Eq. 5.74),

$$\Delta\varepsilon_{cs} = \varepsilon_t - \Delta\varepsilon_p = \frac{\Delta e_t}{1+e_0} - \frac{\Delta e_p}{1+e_0} = \frac{(e_0 - e_f) - (e_0 - e_p)}{1+e_0} = \frac{7.16-6.9}{1+7.3} = 0.032 \tag{5.78}$$

where e_p represents the void ratio at the end of consolidation and e_f is the void ratio at the end of secondary settlement. Subsequently, the secondary creep modulus as computed from Eq. 5.74 is

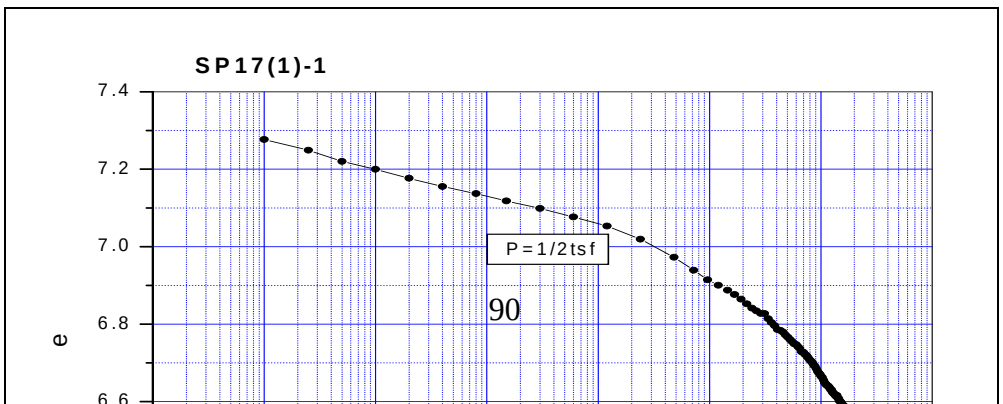

Figure 5-9. Laboratory Void Ratio vs. Log Time Plot for Sample SP 17 (1) at ½ tsf Load.

$$E_{cs} = \left(\frac{\Delta\sigma}{\varepsilon_t - \Delta\varepsilon_p} \right) = \frac{500\,\text{psf}}{0.032} \approx 15,500\,\text{psf} \tag{5.79}$$

where $\Delta\sigma$ = 500 psf, is the change in stress from previous load increment (1/4 tsf). Next, the total tertiary creep, $\Delta\varepsilon_{cs}$, is calculated using the void ratio at the end of secondary creep, 6.9, and the ending void ratio for tertiary creep, i.e., 6.2,

$$\Delta\varepsilon_{ct} = \varepsilon_t - \Delta\varepsilon_p - \Delta\varepsilon_{cs} = \frac{\Delta e_t}{1+e_0} - \frac{\Delta e_p}{1+e_0} - \frac{\Delta e_{cs}}{1+e_0} = \frac{\left(e_0 - e_f\right) - \left(e_0 - e_p\right) - \left(e_p - e_s\right)}{1+e_0} = \frac{6.9 - 6.2}{1+7.3} = 0.084 \tag{5.80}$$

then the tertiary creep modulus (Eq. 5.74) is computed as,

$$E_{ct} = \left(\frac{\Delta\sigma}{\varepsilon_t - \Delta\varepsilon_p} \right) = \frac{500\,\text{psf}}{0.084} \approx 6,000\,\text{psf} \tag{5.81}$$

Next, the secondary compression rate, λ_{cs}, is computed from Eq. 5.76 using a time and void ratio of interest. For instance, at time of 300 minutes (Figure 5-9), the void ratio, e, is 7.0. To match the void ratio, the creep strain is first computed,

$$\Delta\varepsilon_{cs} = \frac{7.16 - 7.0}{1+7.3} = 0.0193 \tag{5.82}$$

then, the secondary compression rate, λ_{cs}, may be computed from Eq. 5.76 with the secondary compression modulus given in Eq. 5.79.

$$\lambda_c = \frac{-E_c\left(t_2 - t_1\right)}{\ln\left(1 - \Delta\varepsilon_c \frac{E_c}{\Delta\sigma}\right)} = \frac{-15{,}500\,\text{psf}\left(300\,\text{min s} - 2\,\text{min s}\right)}{\ln\left(1 - 0.0193\frac{15{,}500\text{psf}}{500\text{psf}}\right)} = 5.1\text{x}10^6\ \text{psf} - \text{min s} \qquad (5.83)$$

Similarly, the tertiary compression rate, λ_{ct}, may be computed, by first selecting a void ratio and time of interest, i.e., e = 6.4, time = 40,000 min., Figure 5-9. Next, the tertiary creep for the latter time and void ratio is found,

$$\Delta\varepsilon_{ct} = \frac{6.9 - 6.4}{1 + 7.3} = 0.060 \qquad (5.84)$$

then, the tertiary compression rate, λ_{ct}, may be computed from Eq. 5.76 with the secondary compression modulus given in Eq. 5.81

$$\lambda_c = \frac{-E_c\left(t_2 - t_1\right)}{\ln\left(1 - \Delta\varepsilon_c \frac{E_c}{\Delta\sigma}\right)} = \frac{-6{,}000\,\text{psf}\left(40{,}000\,\text{min s} - 1{,}000\,\text{min s}\right)}{\ln\left(1 - 0.06\frac{6{,}000\text{psf}}{500\text{psf}}\right)} = 1.8\text{x}10^8\ \text{psf} - \text{min s} \qquad (5.85)$$

The back computed parameters are used in the model verification found in section 5.6.

5.5 COMPUTER PROGRAM

A Nonlinear Large Deformation program was developed to predict both consolidation and creep strains/deformations. The program is based on the Finite Difference Solution outlined in the previous sections. The flow chart for the program is shown in Figure 5-10. The required input data are listed in Table 5-1.

After the data is read in, the program will prepare the initial values for all the internal variables. At each time step, the program loops through all the nodal points to calculate the value

of stress, followed by strain and then void ratio. After the calculation of void ratio, the permeability and geometry are updated. The size of each time step is estimated based on the value:

$$dt = \alpha \frac{dx^2 \gamma_w}{E_p k} \tag{5.86}$$

where E_p is consolidation compression modulus, Eq. 5.71, k is the permeability and dx is the incremental distance between the nodes. For stable solutions, α varies between ¼ to ½, depending on how fast the permeability varies with the change in void ratio.

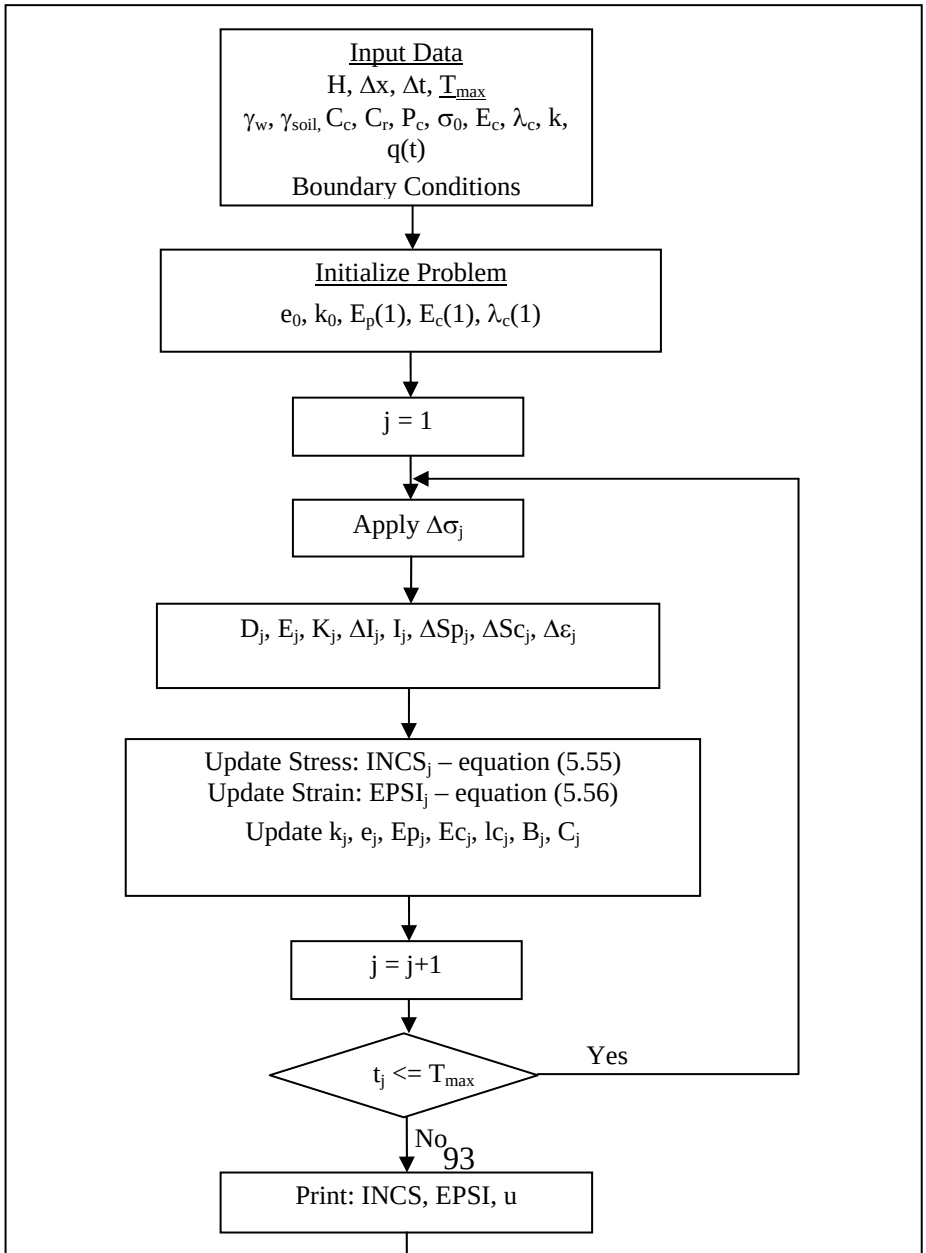

Figure 5-10. Software Flow Chart.

Table 5-1. Input Data for NLD.

Description	Input data	Note
General	Problem Description	Text Line
Geometry	H_{top}, H_{bottom} N_{node}, N_{elem}	Top and bottom elevation Number of nodes, elements
Soil Properties	γ_w γ_{soil} e_0 C_c C_r P_c S_c E_c λ_c k	Unit weight of water Unit weight of soil Initial void ratio Compression index Recompression index Maximum effective stress Insitu effective stress Creep modulus Creep viscosity Permeability
Load	q_{max} t_{load} t_{consol} t_{unload} UL_{dt} q_{min}	Maximum surcharge load Time required to build surcharge Maximum time of interest Time to start unload Time required to remove surcharge Final load
Boundary condition	BC1 BC2	Top boundary condition Bottom boundary condition

5.6 MODEL VERIFICATION

The model was verified using four examples. The first two are laboratory compressive test results in which the samples were loaded and allowed to creep for prolonged period of time. The laboratory samples were then subjected to unload in which the samples were allowed to rebound and then creep afterward.

Samples SP17 (1)-1 and TH 22(2)-1 represent both the high and medium OC class of samples. They were loaded in a geometric progression up to 1 tsf using the procedures described in Chapter 4. The maximum compressive stress of 1 tsf was maintained for a period of 12 days. The samples were subsequently unloaded to 0.5 tsf and allowed to rebound.

Figure 5-11 present the measured and predicted response for Sample TH 17 (1)-1 at 1/2tsf vertical stress. The model parameters used in the prediction are given in section 5.4. Evident, the prediction slightly under estimates the deformation in the first part, i.e., consolidation phase. This phenomenon was consistently observed for the high OC samples. One explanation for this may be the smaller value of E_p derived from the EOP e-log(σ') curves. The latter were obtained at a void ratio estimated at EOP from the $e - \sqrt{t}$ curves by Taylor's method; suggesting that Taylor may slightly under predict EOP. The predicted creep response, i.e., secondary and tertiary settlement matches the measured behavior quite well.

For the medium OC sample, TH22(2)-1, the prediction, Figure 5-12, matches the measured response for both the primary as well as the creep portions of the curves. The latter illustrates the ability of Taylor's method in predicting EOP consolidation in less than high OC samples, as defined in this study.

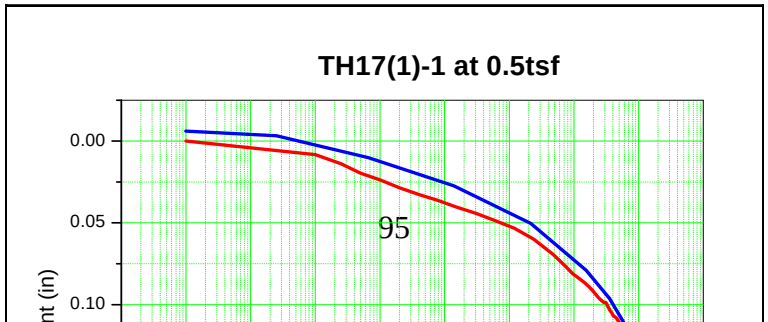

Figure 5-11. Compressive Deformation at 1 tsf of High OC.

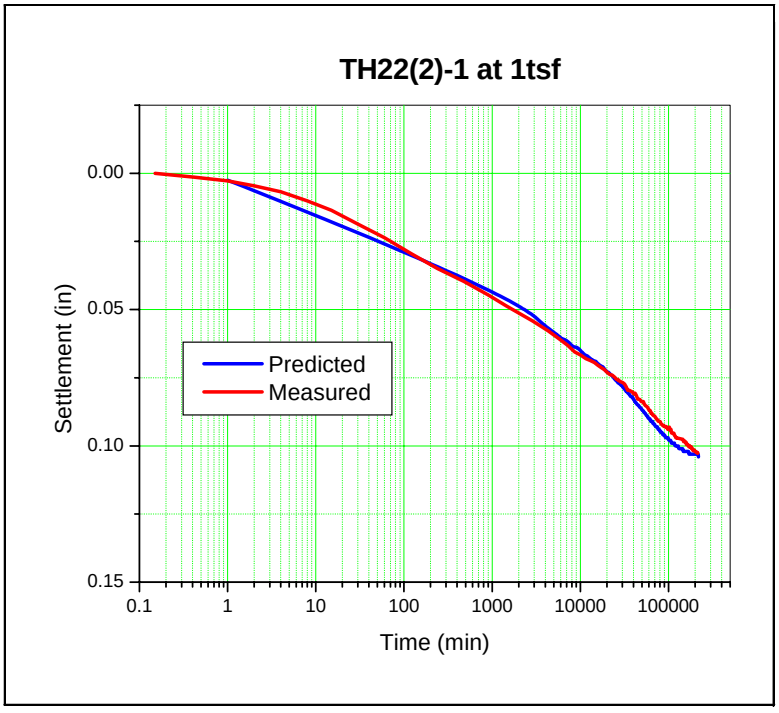

Figure 5-12. Compressive Deformation at 1 tsf of Medium OC.

CHAPTER 6

FIELD MONITORING PROGRAM AND MODEL VALIDATION

This chapter covers two topics: the field study program and model validation. The first part describes the site investigation, geotechnical design, construction plan, field instrumentation, data collection and reduction. Subsequently, the field settlements are compared to the computational model predictions described in the previous chapter using the laboratory data from Chapter 4.

6.1 TEST SITES

As presented in Chapters 2 through 4, laboratory samples from two projects, SR-20 over Sanders Creek in northwestern Florida constructed in 1974 and Seminole Expressway (SR-417) in central Florida were monitored. Both projects have significant organic zones near the ground surface. In the case of Sanders Creek the underlying organic soil was left untreated (without excavation or surcharge improvement). However, for Seminole Expressway, surcharging was employed to reduce the expected settlements due to the thick organic deposits (up to 22 m). The field settlements for SR-20 were obtained from the asphalt paving history on the bridge approach embankments, and for Seminole expressway, settlements were measured from instrumentation including conventional settlement plates and vibrating wire settlement sensors installed underneath the roadway.

6.2 SEMINOLE EXPRESSWAY

6.2.1 Site Condition

Toll 417/Seminole Expressway Project is located near Sanford, Florida. As part of the design, two new ramps were constructed at both Lake Mary Boulevard and U.S. 17, as well as new interchanges at County Road 46A, Rinehart Road and I-4 (Figure 6-1). Of interest was the

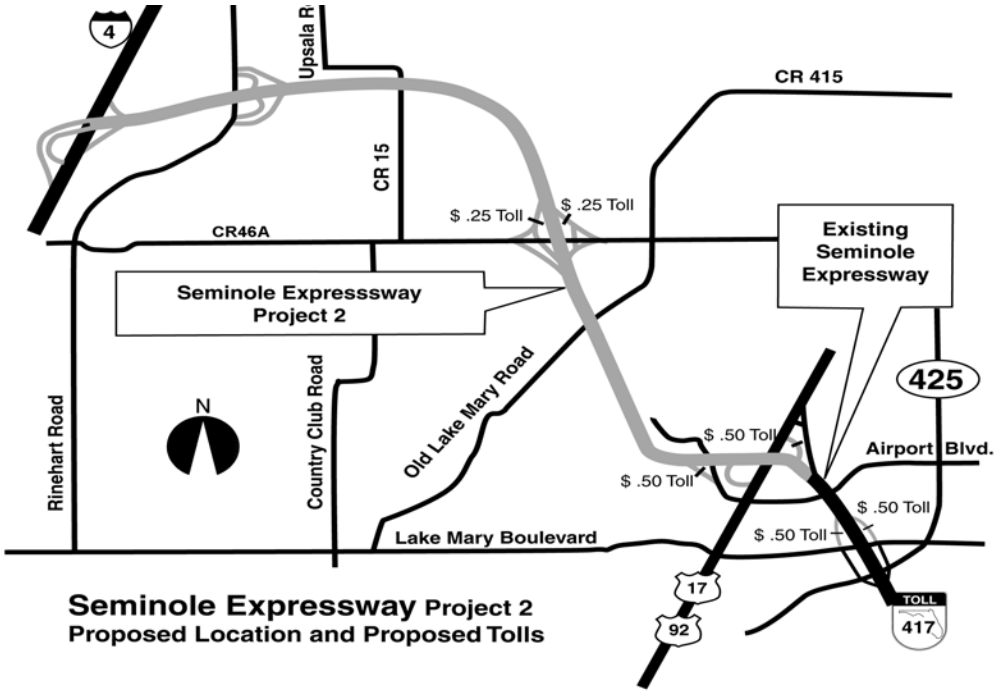

Figure 6-1. Toll 417/Seminole Project.

CR46A exit, which had significant organic deposits with a planned toll plaza. Shown in Figure 6-2 is the location of five SPT borings and 4 CPT soundings within the surcharge area. Undisturbed samples were recovered and laboratory consolidation and creep tests were performed, Chapters 2 - 4 and Appendices A-D.

The insitu data, Figures 6-3 and 6-4 was collected after 2 to 4m of free draining fill had been placed over the site. At the SPT locations, undisturbed samples were recovered as well as the placement of long-term settlement sensors. Evident from the CPT and SPT data, a significant zone (12 m to 18 m) of soft organic soil (Peat) was present at the site. Laboratory analysis of samples showed organic contents varying from 4.8% to 88.6% and unit weights ranging from 9.8 kN/m^3 to 23.4 kN/m^3. The spatial variability of the site was high, but in general, the lighter material (high organic content) was located at the shallower depths versus the heavier material beneath. A summary of the soil strata is presented in Table 6-1. Preliminary

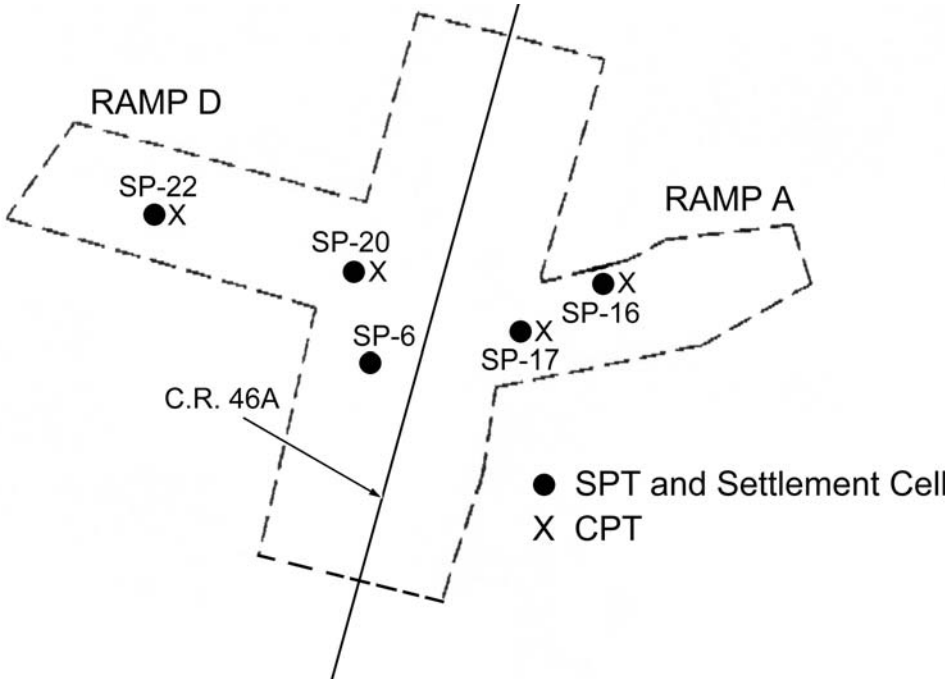

Figure 6-2. Test Site Location.

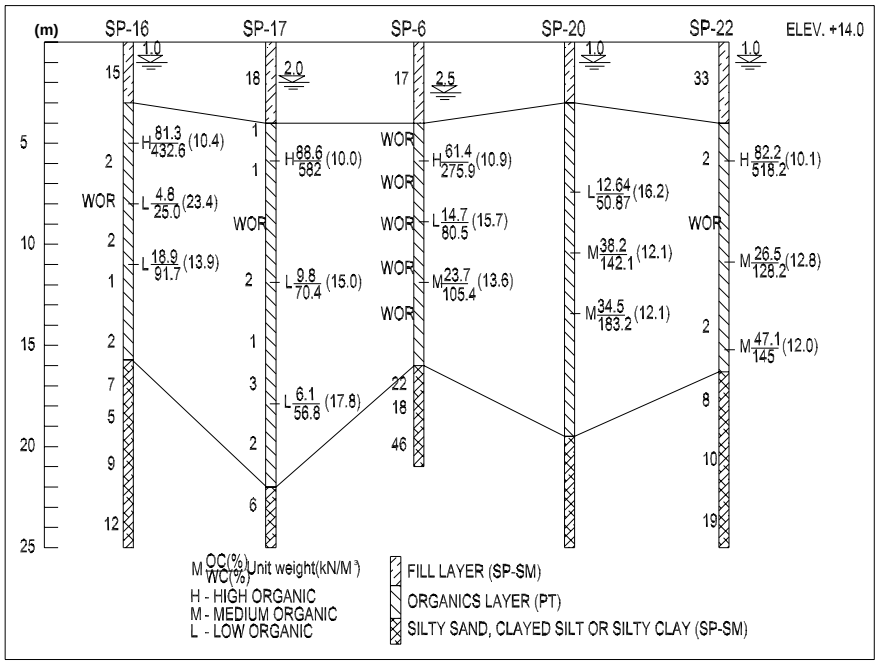

Figure 6-3. Boreholes at Test Site.

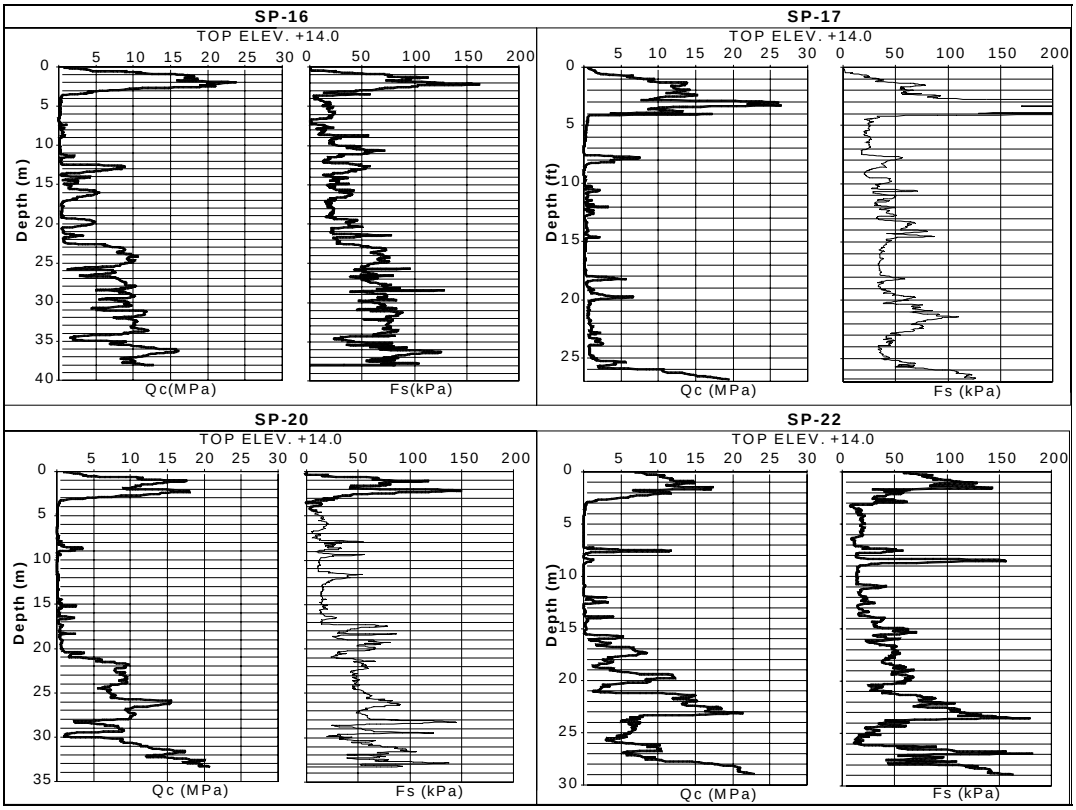

Figure 6-4. CPT Soundings.

Table 6-1. Soil Layering.

1st layer	Consists of 2.7 m to 3.6 m of fill material (SP-SM). N-values: 20 to 40.
2nd layer	12 m to 18 m of organic material (Pt); Initial void ratio: 3.5-7.7. **Water Content ~ 500%; Organics Content 30%-80%** *This layer is the main source of deformation.*
3rd layer	7 m to 9 m mixture of silty sand and clayey silt or silty clay. N-values: 10 to 30.
4th layer	Consists of intermediate layers of sand and soft limestone. N-values: > 40.

analyses suggest large consolidation and creep settlements would occur if the ramp embankments (Figure 6-1) were constructed directly on the existing soil. To reduce the settlements, it was decided to surcharge the site. The average height of the final embankment was 1.68 m with the height of the surcharge of about 3.6 m. To estimate settlements with and without the surcharge, eighteen (18) 1-D oedometer consolidation/creep tests were conducted.

6.2.2 Design and Construction

Preliminary analyses suggest large consolidation and creep settlements would occur if the ramp embankments were constructed directly on the existing soil. To reduce the settlements, it was decided to preload the site. Figure 6-5 shows a typical cross-section of the surcharge and final grade at the ramps. The surcharge embankment (Figure 6-6) was designed for approximately 1.0 tsf or twice the final vertical effective stress in the organic layer (i.e., after road construction). The design specified wick drains, as a mean of shortening consolidation time in order to reduce surcharging time, as well as lower the risk of pore water pressure buildup and potential for slope instability.

The surcharge embankment was approximately 15’ high and was constructed in lifts with a loading rate of about 1.5”/day to ensure the stability of the side slopes. It took approximately 150 days to complete the construction of the surcharge embankment. The surcharge was maintained for another 100 days, after which it was removed within 30 days. At every phase, the site was instrumented to monitor pore water pressure and vertical and lateral movements. Figures 6-7 to 6-10 are some images of the construction process.

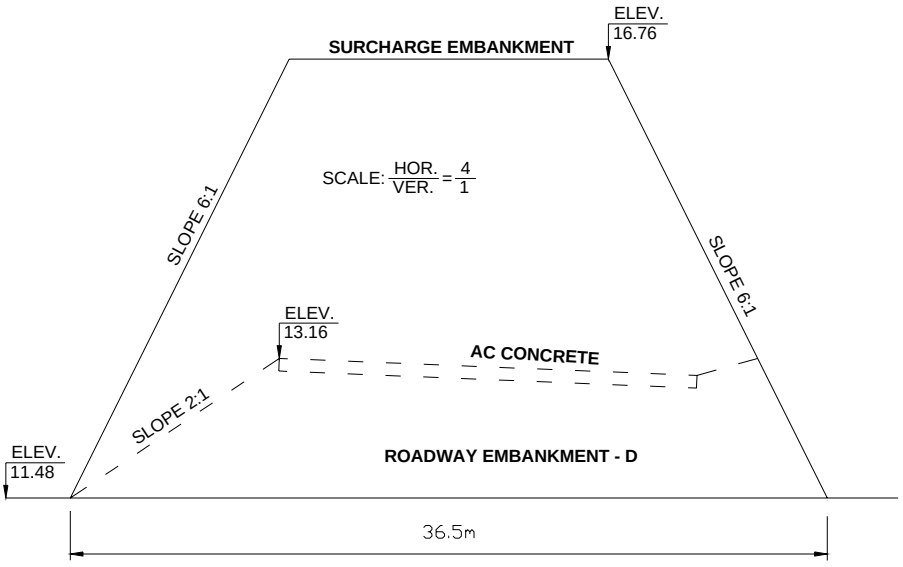

Figure 6-5. Surcharge Cross-Section.

Figure 6-6. Surcharge Embankment.

Figure 6-7. Exposure of Peat Layer.

Figure 6-8. Wick-Drain Installation.

Figure 6-9. Wick-Drain Layout.

Figure 6-10. Instrumented Surcharge Embankment.

6.2.3 Field Instrumentation

After reviewing the soil stratigraphy, Table 6-1, it was decided that a series of sensors in four of the five boring locations (SP-6, SP-16, SP-20, & SP-22), Figure 6-2, was warranted. This arrangement allowed the determination of the settlement of multiple layers (i.e., organic, silt, etc.), as well as minimizing the influence of horizontal soil variability on deformation measurements. Since such a system did not exist, a commercially available sensor was modified to allow multiple sensors to be strung together in the same borehole as shown in Figure 6-11. Each sensor in the "string" consists of vibrating wire pressure sensors located in a "closed" column of de-aired antifreeze solution connected to a reservoir. Each reservoir was equipped with a vent line, which was connected to a desiccant chamber to prevent moisture from entering the vent line from the reservoir. This arrangement ensured that the sensor readings were not influenced by temperature changes inside the reservoir, or by changes in barometric pressure. The cell monitored only the change in hydraulic head in the "closed" column of de-aired antifreeze as a result of the change in vertical distance between the reservoir and the pressure sensor.

Since the long-term creep settlement was sought, the signal cable for each sensor in a borehole was brought out through the embankment side slope in a PVC pipe to one of two multiplexers. From each multiplexer, the signals were sent to a data logger, which recorded the data. For monitoring slope stability, as well as rate of consolidation, the site instrumentation was augmented with inclinometers, piezometers, and conventional settlement plates. All the sensors were read on a daily basis.

6.2.4 Measured Field Settlements

Shown in Figures 6-12 to 6-15 are the settlements for all of the layers at the four locations (Figure 6-1) along with fill height history. To obtain the total settlement of the deposit

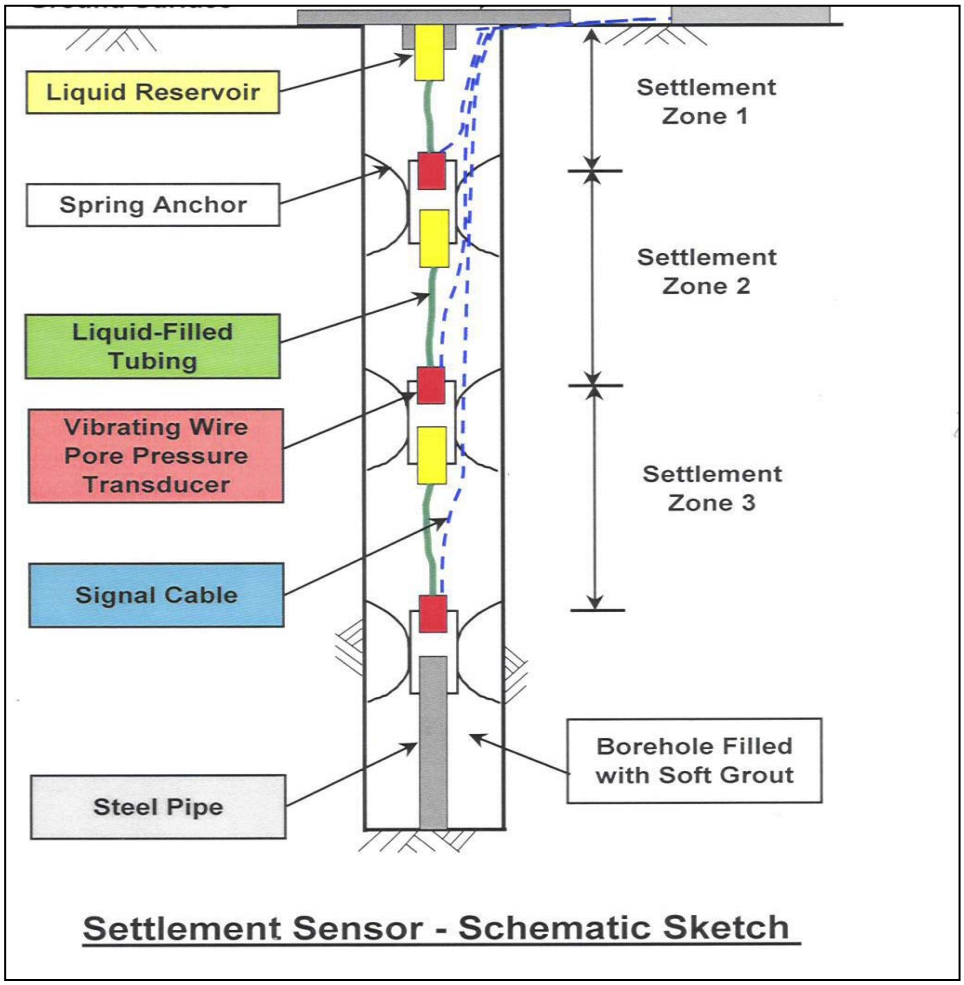

Figure 6-11. Schematic Sketch of Multiple Cell Settlement Sensors.

from each "string" of borehole sensors (Figure 6-11), the settlement from each layer was summed. The latter was compared with the values obtained from mechanical settlement plates (i.e., steel plate with steel rod attached) located on top of the original insitu deposit. The agreement between the settlement plates and the sum of the sensors was excellent with the exception of SP-16. In the latter case, the settlement plate was located closer to the edge of the embankment than the SP-16 borehole, which may have resulted in less settlement for the plate vs. the borehole sensors.

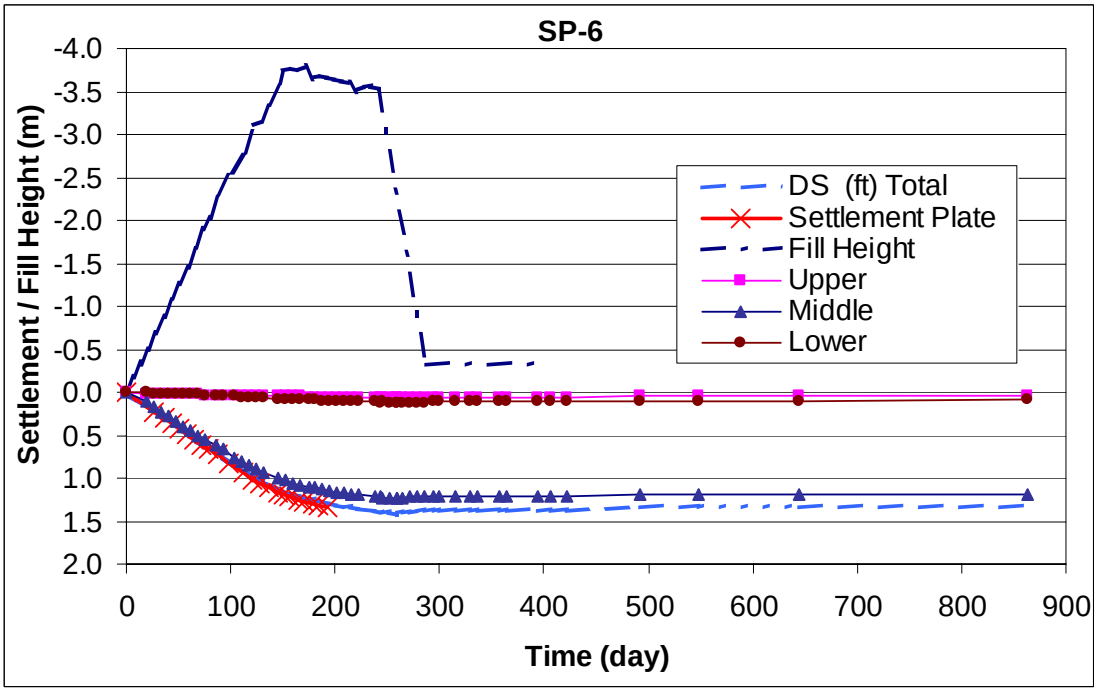

Figure 6-12. Settlement Data at SP-6.

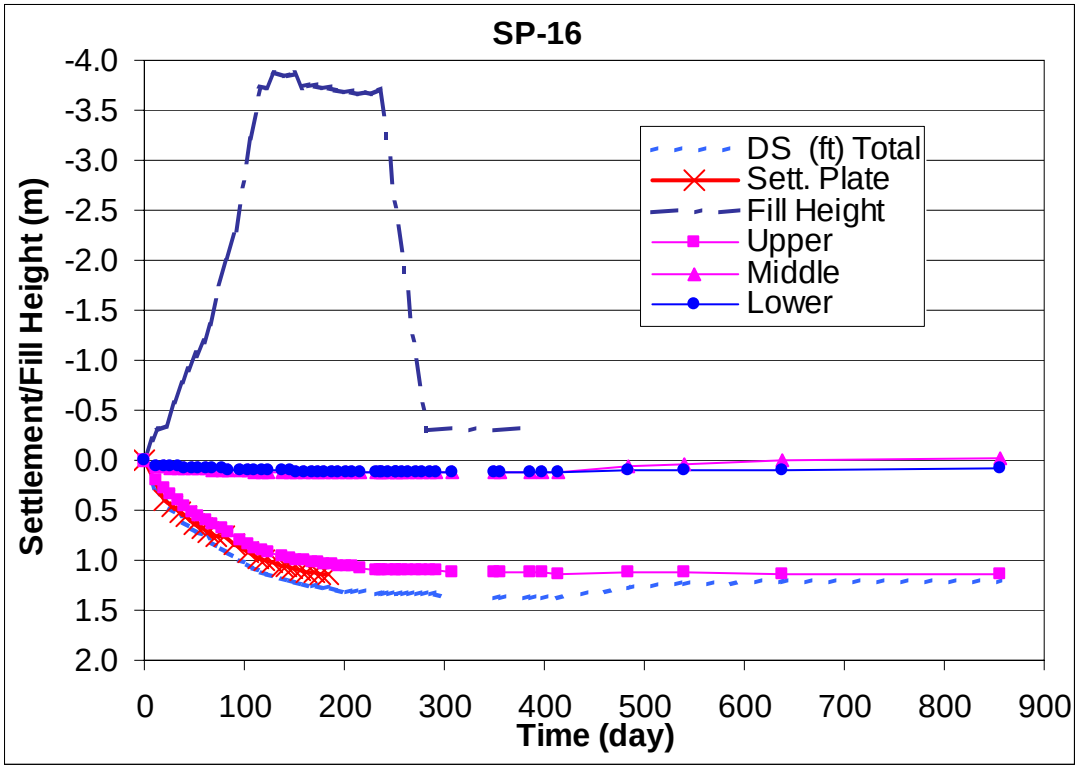

Figure 6-13. Settlement Data at SP-16.

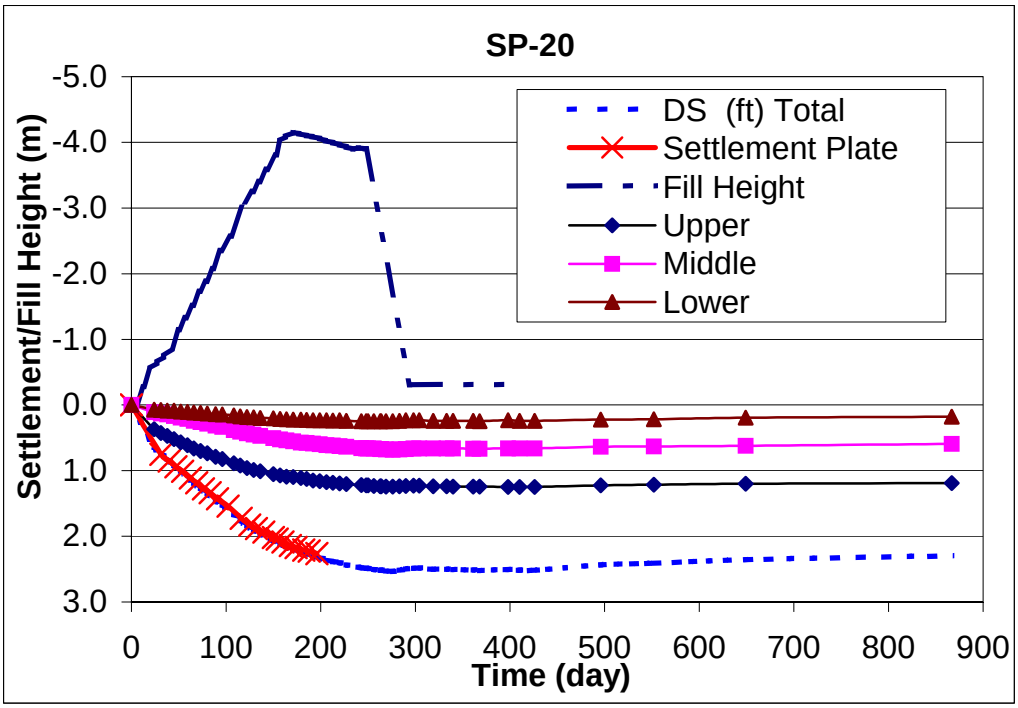

Figure 6-14. Settlement Data at SP-20.

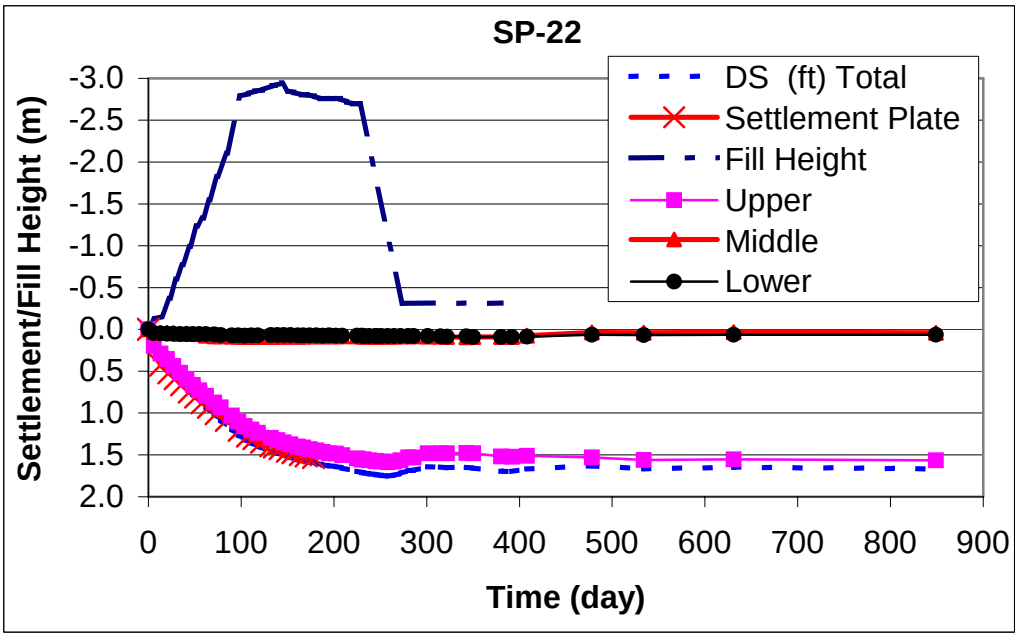

Figure 6-15. Settlement Data at SP-22.

Table 6-2 summaries the settlement of each layer as well as the total settlement of the original ground surface at the end of the surcharge phase. As expected, the upper 12 to 18m layer of organic soil (Layer 2: Table 6.1) gave the largest settlements due to its high compressibility and void ratio. However some of the lower sandy-silt layers (Layer 3: Table 6.1), did exhibit some compression (i.e., SP-20 produced 0.66m of settlement). A possible cause of the settlement was the presence of organic matter (10%) in the layer, which was not detected in the other boreholes.

Table 6-2. Summary of Settlement Data at The End of Surcharge.

Borehole	**1st cell 2nd Layer Table 1 (m)**	**2nd cell 3rd Layer Table 1 (m)**	**3rd cell 4th Layer Table 1 (m)**	**Total (m)**
SP-6	1.221	0.057	0.119	1.396
SP-16	1.104	0.124	0.121	1.349
SP-20	1.222	0.661	0.245	2.127
SP-22	1.555	0.081	0.068	1.710

Considering the organic layers alone (Figures 6-16 and 6-17), SP-22 had the highest deformation (1.56 m), but the lowest surcharge load. The latter was attributed to the high concentration of organic matter at the SP-22 location. Laboratory tests on SP-22 revealed its organic contents on average were approximately 10% higher than the other borehole samples. These figures also show the heave of the organic layers after the surcharge was removed; approximately nine months after surcharging began. The figures suggest that the amount of rebound is proportional to the magnitude of settlement.

Of interest during the surcharging process is the amount of consolidation versus creep settlement, which is typically delineated through pore water pressure changes. Insitu pore water

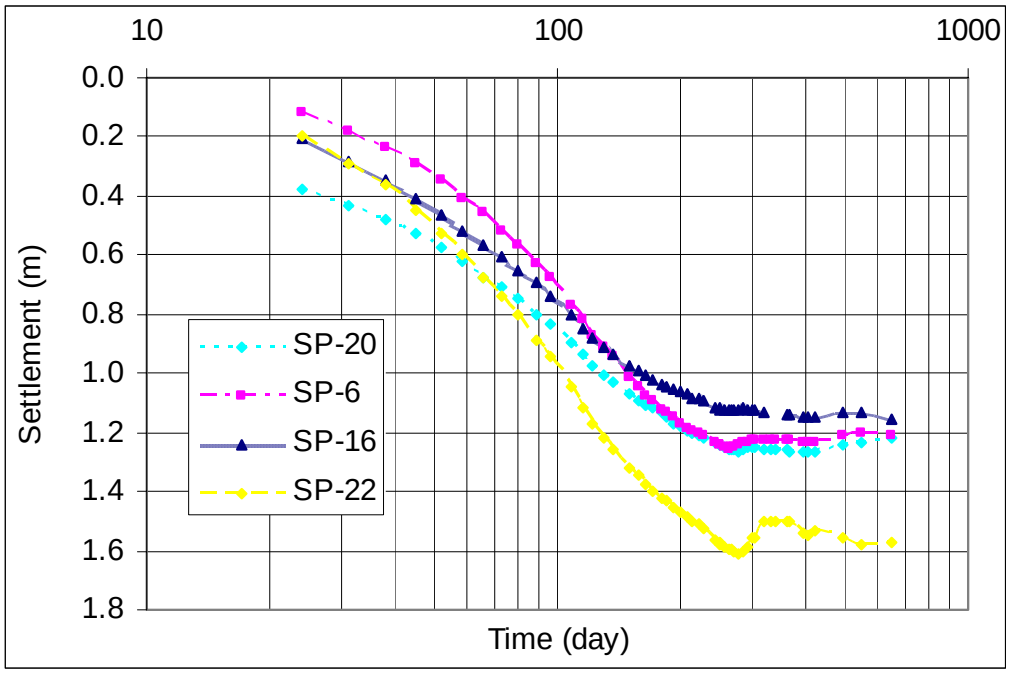

Figure 6-16. Settlement Data of Organic Layer.

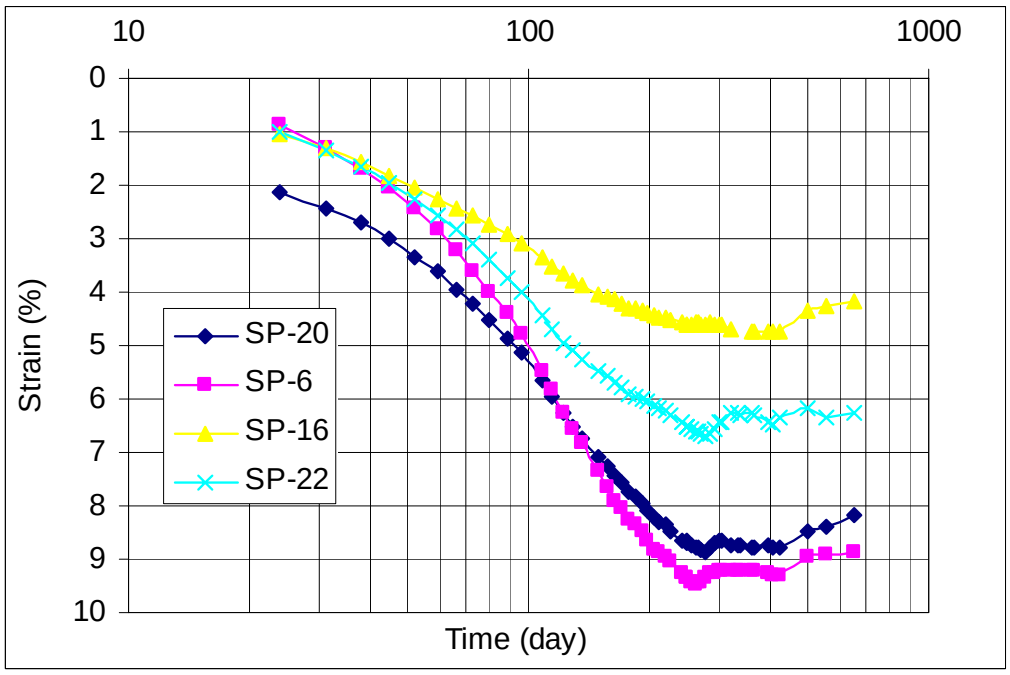

Figure 6-17. Strain Data of Organic Layer.

pressures were monitored at several locations in the field in close proximity to the settlement sensors. A typical pore water pressure record during the embankment construction is shown in Figure 6-18. Based on the relatively constant pore water pressure readings during construction, consolidation (dissipation of excess pore pressure) occurred very rapidly (i.e., prior to the end of the surcharge phase). Similar studies indicating short primary consolidation times for organic soils have been reported by Dhowian et al. (1980) in the laboratory and by Samson et al. (1985) in the field.

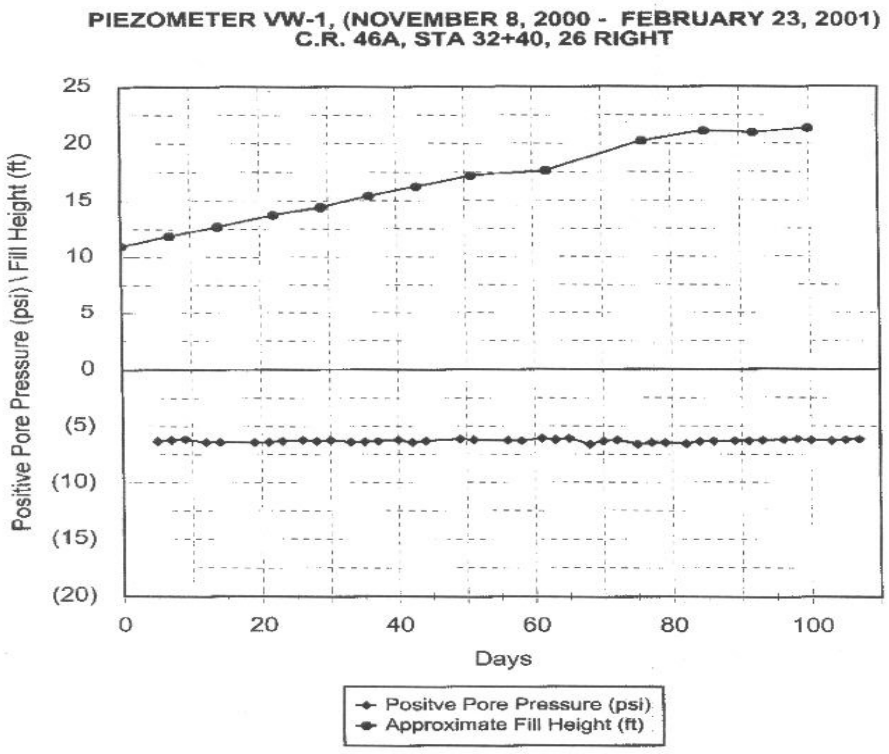

Figure 6-18. Pore Water Pressure vs. Surcharge.

6.2.5 Predicted Field Settlement

Using the consolidation-creep theory of Chapter 5, both the consolidation and creep response of the site was predicted. The input data required for the analysis was obtained from

the soil stratification (Figures 6-3 and 6-4) and laboratory consolidation and creep parameters given in Chapter 4, 5 and Appendix C. Due to the high variability of organic content and hence the soil properties, two simulations were run for every soil profile, i.e., SP-6, SP-16, SP-20 and SP-22. The first simulation provided an *upper* bound prediction or maximum possible ground movement. The latter was accomplished by assuming a conservatively high organic content for the peat layer, Table 6.1, from the Boring Logs, Figure 6-3. The second simulation, provided a lower bound prediction, or less settlement based on the lower organic contents in the Boring Logs, Figure 6-3.

A comparison of the predicted vs. measured settlement of the original ground surface with time is shown in Figures 6-19 to 6-22. Evident, the simulations provided excellent results in the compression parts of the curves i.e., the surcharging period. The simulations also provided reasonable projections of upward ground movements when the surcharges were removed as well as long-term (30 years) creep settlements predictions of future roadway embankment settlements.

The following observations based on field and simulated ground movements were recorded:

- The magnitude of predicted settlements were in good agreement with the field data for both the surcharge loading and unloading.
- At every location, the high organic profile had both the largest settlement and the largest rebound vs. the low organic soil profile.
- For two of the locations, SP-6 and SP-22, the sites have reached their maximum rebound and have started to creep downward. At the other two locations, SP-16 and SP-20, the embankment is still in the rebound phase. The differences between these two sets of locations may be explained by the higher concentration of organic materials in the top layers of SP-6 and SP-22. This is confirmed by laboratory results as shown in Figure 4-14. Note, the time required for creep to reoccur is shorter for the high organic samples.

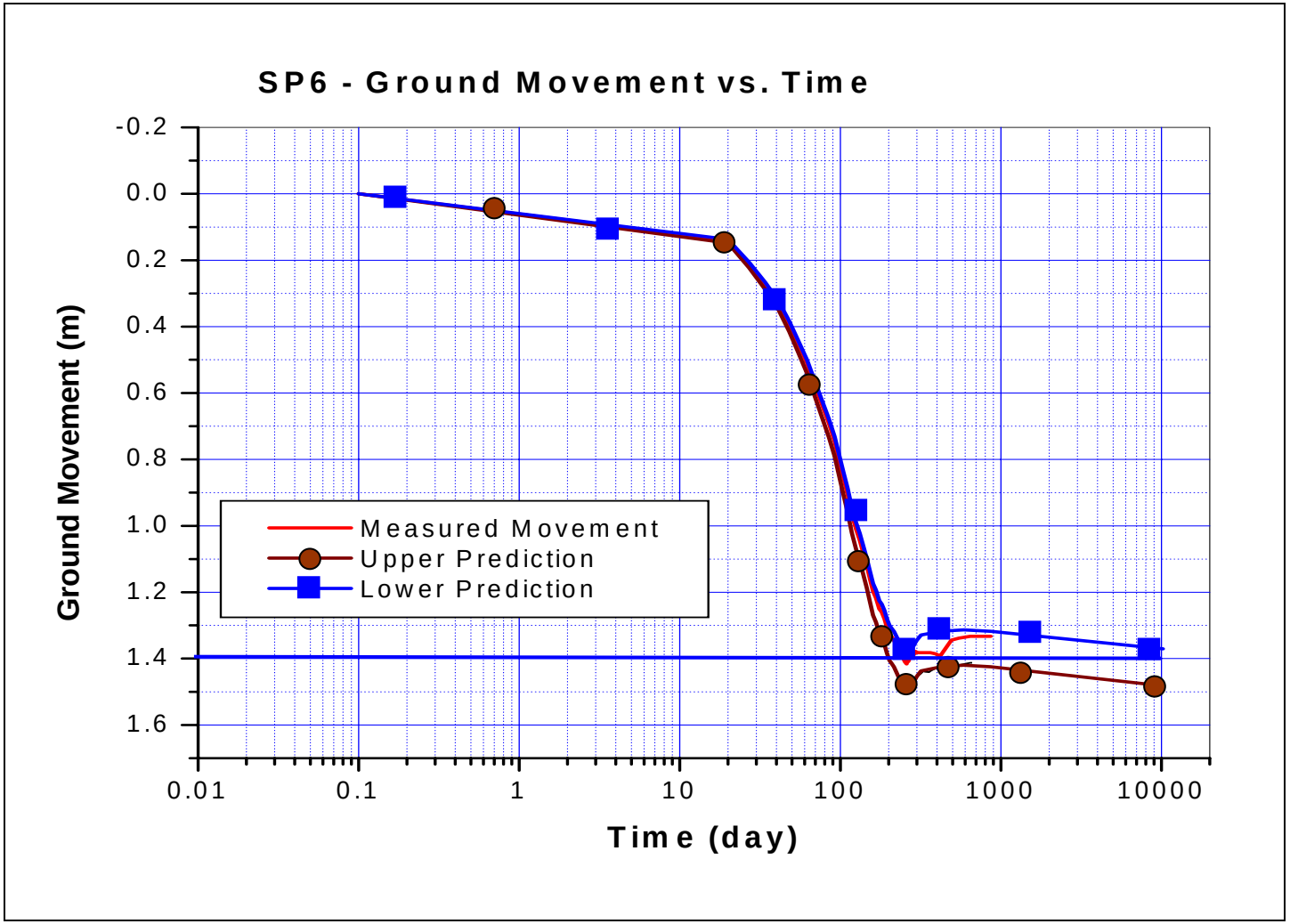

Figure 6-19. Measured and Predicted Ground Movement, SP-6.

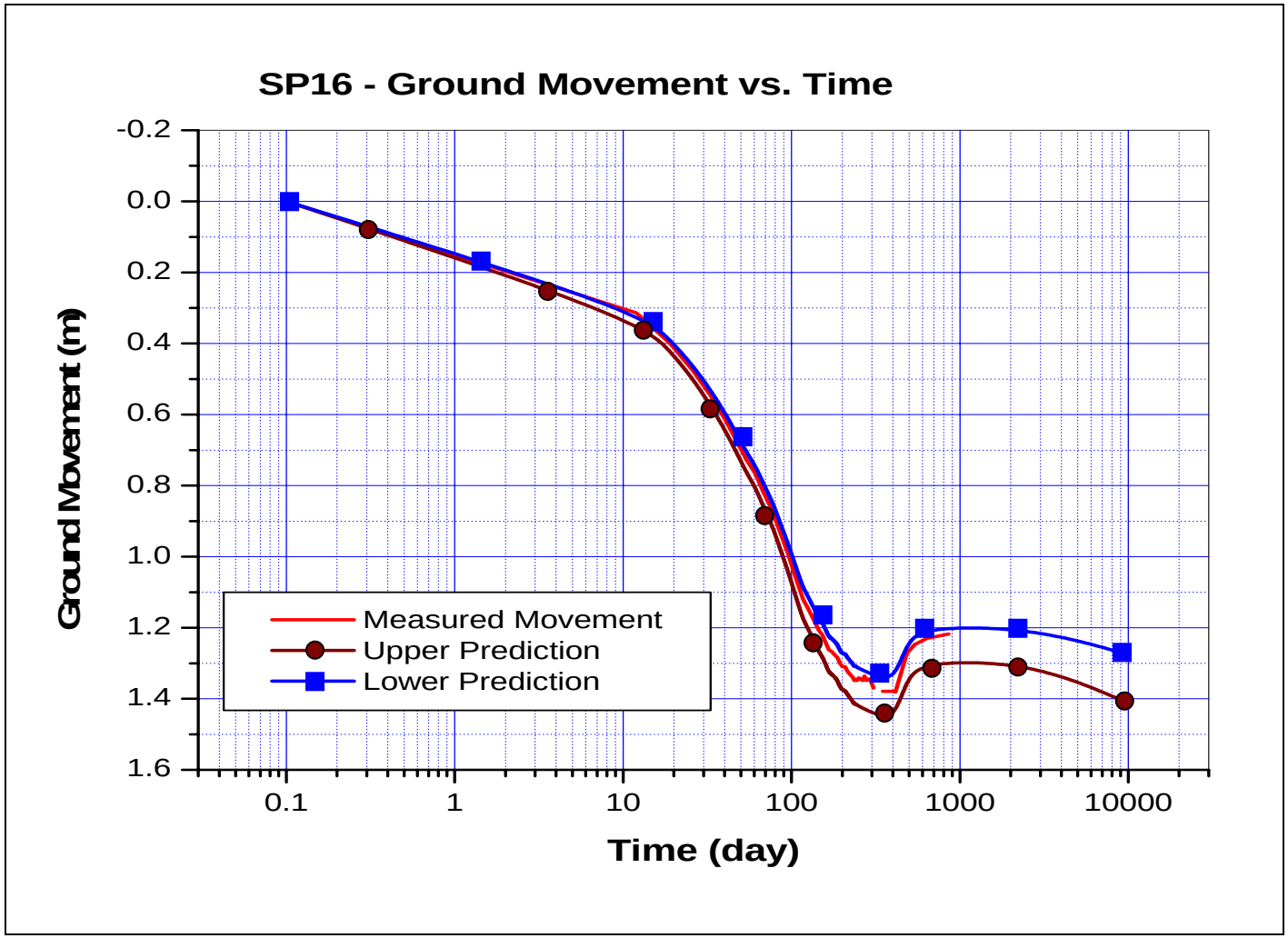

Figure 6-20. Measured and Predicted Ground Movement, SP-16.

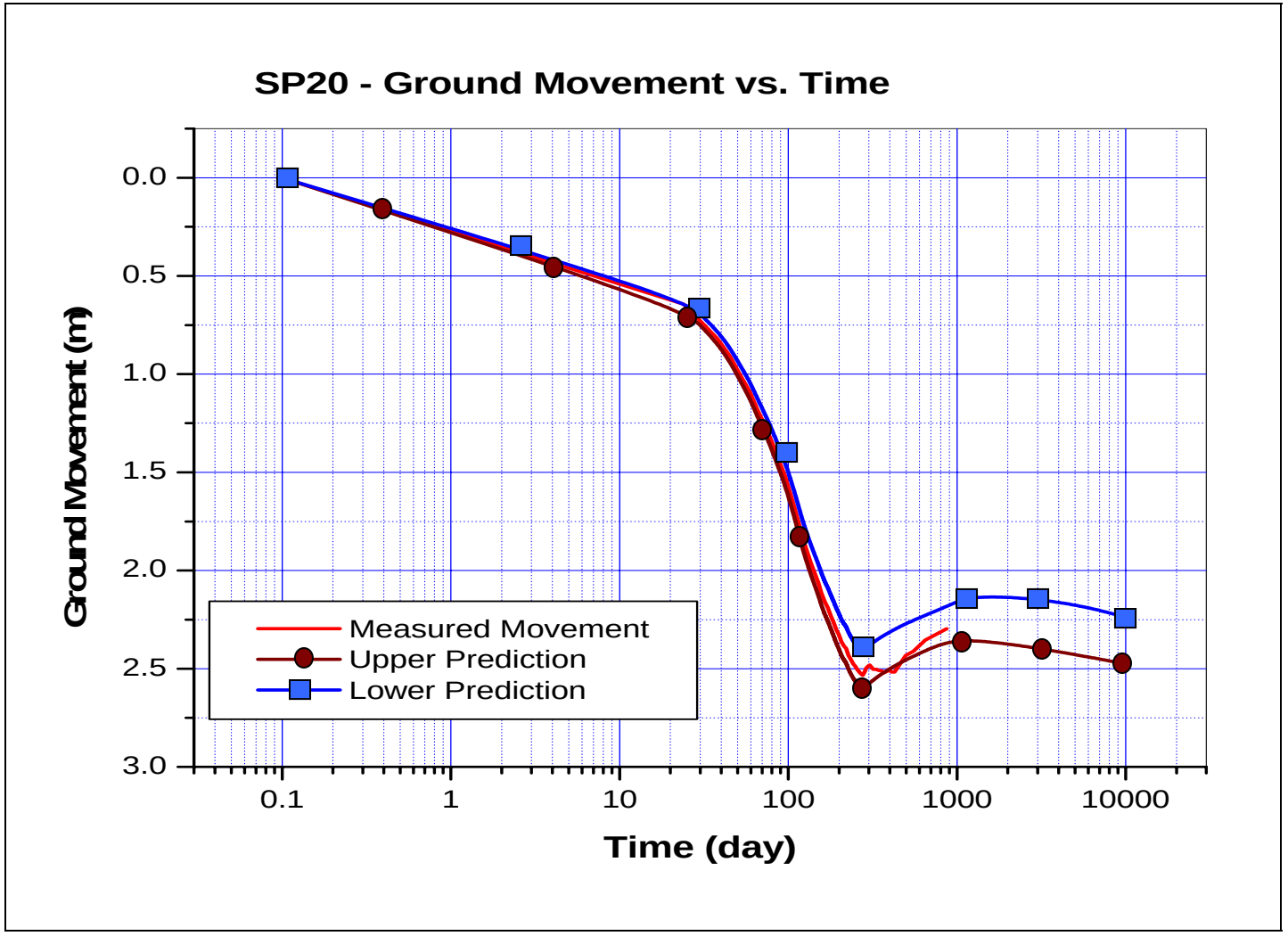

Figure 6-21. Measured and Predicted Ground Movement, SP-20.

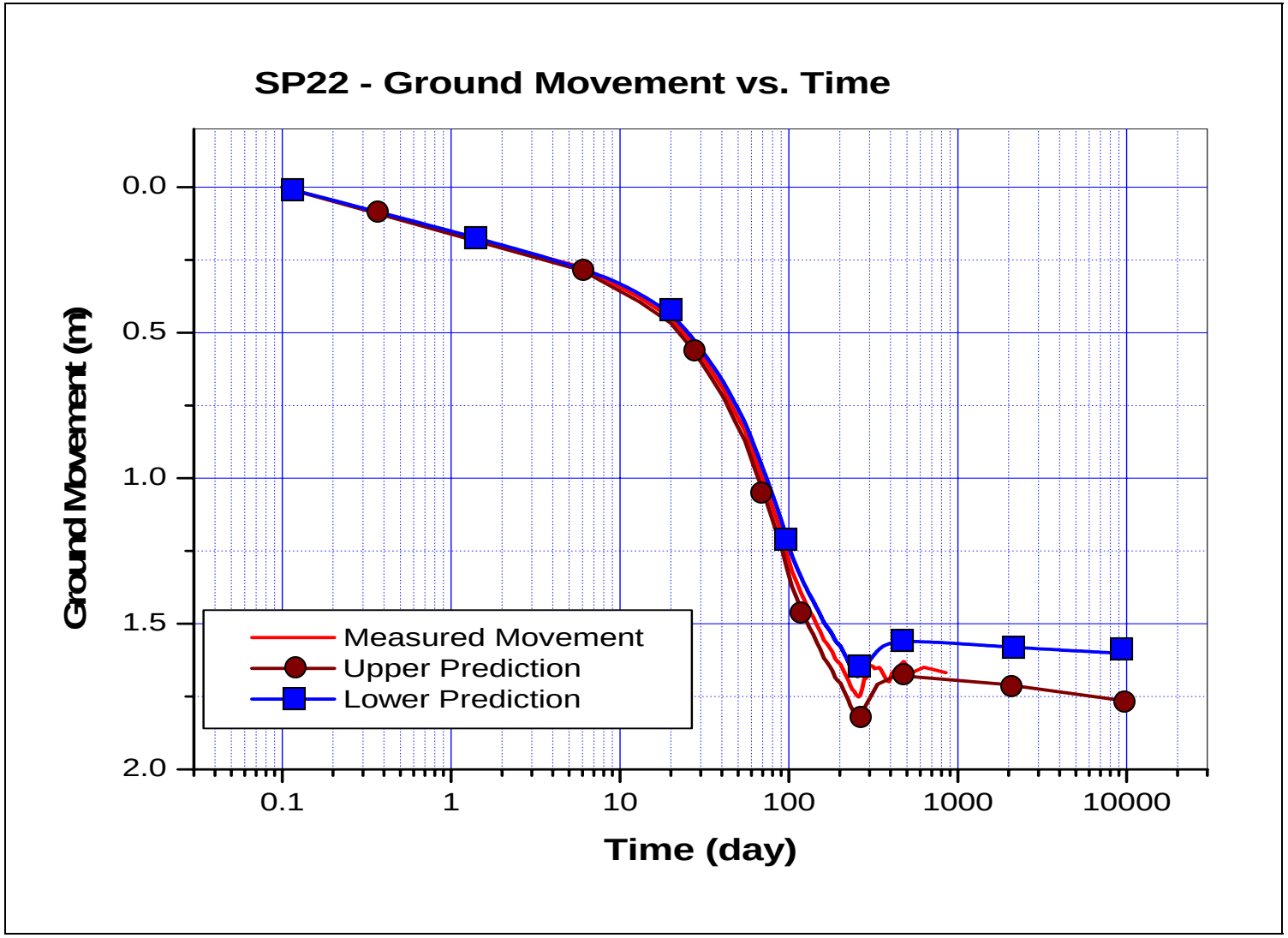

Figure 6-22. Measured and Predicted Ground Movement, SP-22.

- The predicted amount of long-term creep settlement after surcharge removal ranges from 4” to 6” over a period of 30 years. Both the amount and rate of settlement is within tolerable limits for flexible pavement highways. Note that the survey locations are located where the embankment has the greatest expected settlements. On average, the ground movements will be smaller than the predicted amounts.
- The use of surcharge of twice the final vertical stress reduces the expected long-term creep by a factor of two to three depending on organic content.

6.3 STATE ROAD 20 – SANDERS CREEK

6.3.1 Site Condition

Sanders Creek Bridge and embankment for State Road 20 (SR-20) are in Okaloosa County, Florida. Located in northwestern Florida on the Choctawhatchee Bay, SR-20 services Eglin Air Force Base, as well as many popular vacation areas (Destin, Fort Walton, etc.).

The bridge constructed on piles has not experienced substantial or noticeable settlement. However, the approach embankments founded on muck and organic sands have settled from 0.305 m to 0.457 m in the past twenty years. Figure 6-23 shows the multiple layers of asphalt over the roadway curb, placed at three to four year intervals, to reduce the “bump” at the start of the bridge.

Shown in Figure 6-24 is a typical cross-section and associated insitu data (SPT, and CPT) recorded in early 2000. The top one-meter is roadway, i.e., asphalt and associated base course, the next three meters are sand to silty sand embankment fill placed during the bridge construction, and the underlying material is the original insitu soils. Of interest is the eight meters of soft muck and organic sands at 4.5 m to 12.5 m below the roadway. Shelby tube samples of the material were collected and tested in the laboratory. Analysis of the muck revealed organic contents ranging from 45% to 60%. Likewise, the organic content of the underlying organic silty sand ranges between 25% and 40%.

Figure 6-23. Additional Layers of AC.

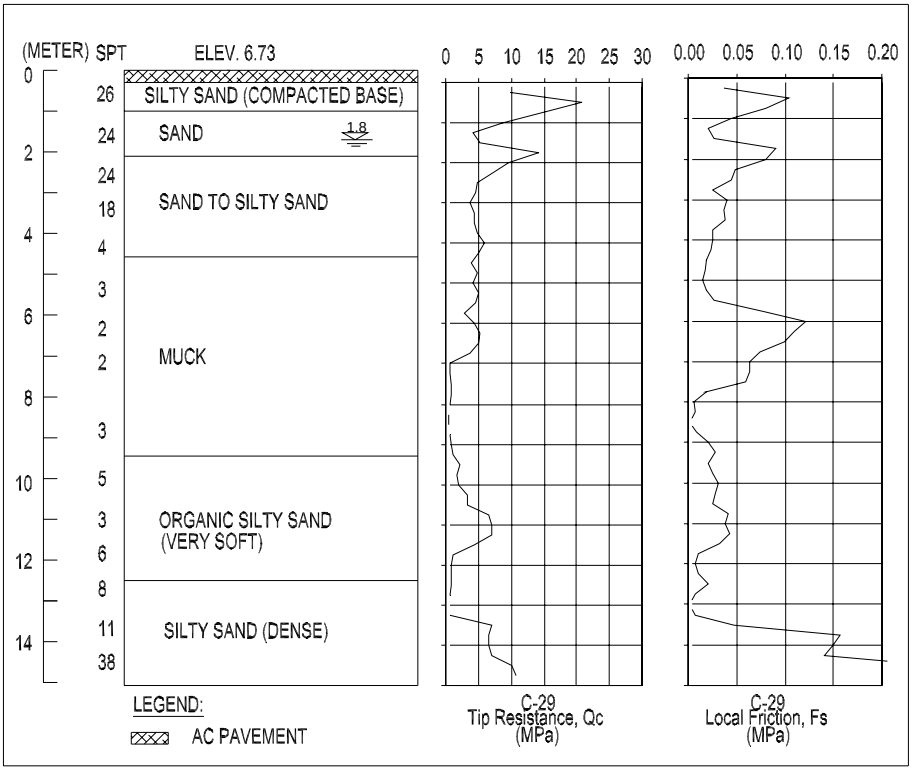

Figure 6-24. SPT and CPT Results.

Maintenance records revealed that the first overlay occurred in 1976 (2 years after construction), and subsequently on approximately four-year intervals. Field settlement records revealed 0.348 m of movement after twelve years, and 0.457 m of deformation after twenty-nine years of service.

6.3.2 Measured and Predicted Settlements

Sanders Creek is an example of continual settlement during the service life of an embankment from creep. After 30 years in service, the road is still settling, Figures 6-25 and 6-26 at a high rate, which requires constant and expensive maintenance. A major reason for the settlement is tertiary creep, which is still occurring, i.e., 30 years after the original construction. Laboratory creep tests on samples collected from the site verify this phenomenon. For instance, samples SP 16(1) and SP22 with organic contents varying from 80 to 90% (Appendix C), have tertiary creep strains varying from 5% to 15% depending on the magnitude of the load.

Using the laboratory creep data and field stratigraphy, Figure 6-24, a consolidation-creep simulation was performed over the life of the embankment. The predictions versus the measured response are plotted in Figures 6-25 and 6-26. Figure 6-25 shows the settlement history on a linear time scale. The plot clearly shows large settlements just after resurfacing, and the subsequent creep settlements, which follow. The subsequent creep settlements necessitates the addition of AC pavement which in turn adds more load and hence more settlements.

Figure 6-26 plots both the measured and predicted settlement as a function of logarithmic time scale. Troubling from the shape of the curve is that the practice of adding AC overlays will necessary for the life of the embankment. However, the plot does suggest one possible remediation scheme. Instead of putting more AC pavement, previous placed AC should be removed and replaced by lightweight fill. The removal/replacement of AC with a lightweight fill

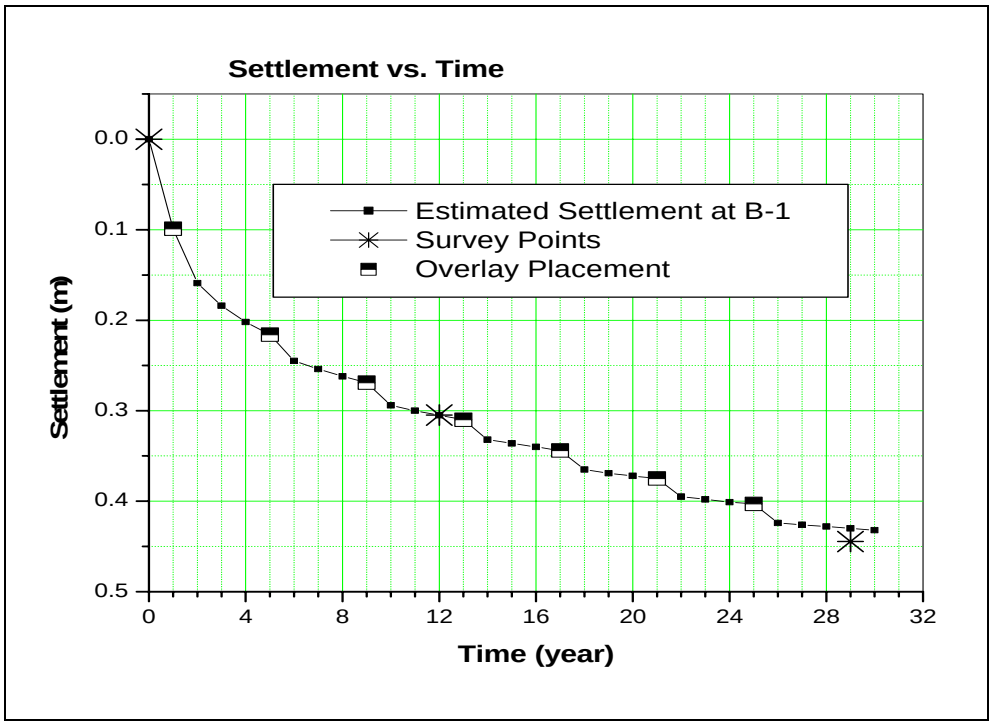

Figure 6-25. Settlement at Sanders Creek – SR 20.

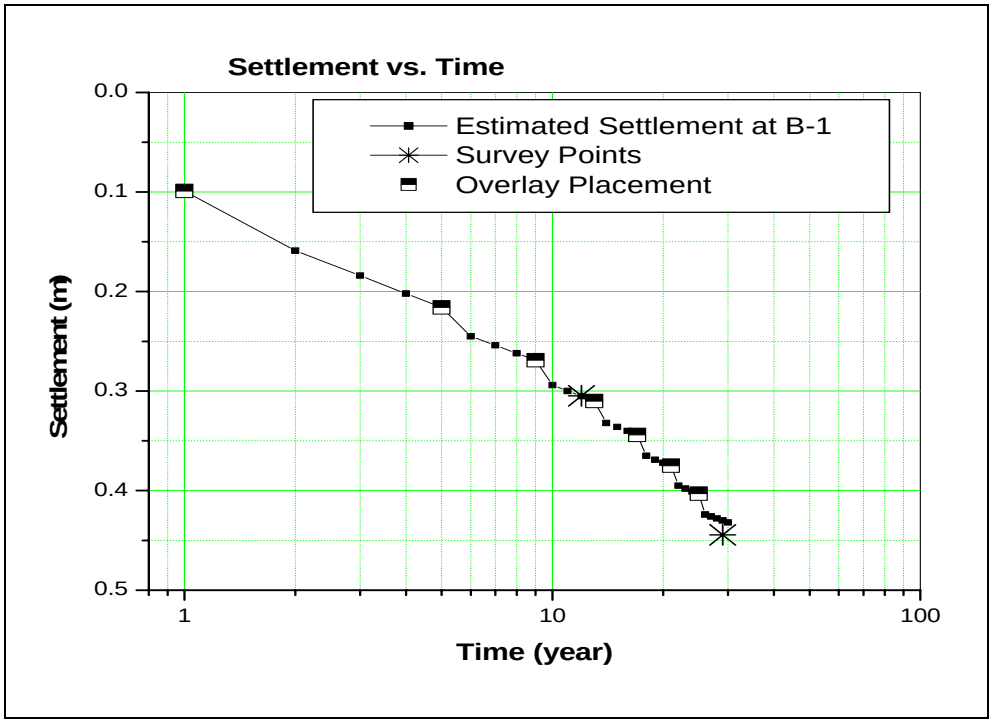

Figure 6-26. Settlement at Sanders Creek – SR 20 – Log Scale.

is equivalent to the surcharge removal technique discussed for the Turnpike (section 6.2). The ground should rebound and subsequently creep downward, but at a rate significantly smaller than current rate (i.e., see Figures 6-19 to 6-22 vs. Figure 6-26).

CHAPTER 7

CONCLUSIONS AND RECOMMENDATIONS

7.1 SUMMARY AND CONCLUSIONS

The following is the summary and conclusions from the laboratory and field investigation of the behavior of organic soils as a roadway embankment foundation material:

1. A detailed field-monitoring plan was developed and installed at the Turnpike (Toll 417) using a settlement system capable of recording deformations within multi-layer soil deposits. The multiple cell settlement system was the first to be applied in the United States. The information helped identify the main source of settlement for which later laboratory tests were performed on. The sum of the individual layer settlements from the sensors was compared to settlement plate measurements. The latter compared very favorable. The sensors, which are below the roadway, are still being monitored now, providing valuable creep data. Other aspects of field responses were also monitored: lateral movements and pore-water pressures. Field data showed minimal lateral displacement, which verified the one-dimensional compression assumption in the numerical simulations. Piezometer data showed quick dissipation of excess pore pressures due to the surcharge load. A remote data acquisition system proved to be an economical means for long-term monitoring.

2. Classification of organic soils (Chapter 3) is very important at the early stages of design. It helps identify soil characteristics so subsequent laboratory and in-situ tests can be planned. Organic soils can be grouped based on organic content and degree of humidification. Soils with organic content less than 25% have similar one-dimensional compression characteristics as inorganic soils. The influence of organic matters becomes significant if they occupy more than 25% of the soil weight. Generally, Florida soils with organic contents between 25 to 50% exhibit both secondary and tertiary creep, but upon unloading (removal of surcharge) will undergo rebound with no downward creep (see Figure 4-13). Florida soils with organic contents greater

than 50% will experience both secondary and tertiary creep under loading, and will exhibit some downward creep after surcharge removal (see Figure 4-14)

3. Organic soils usually have high permeabilities, which result in quick primary consolidation and long creep phases. For instance, laboratory consolidation tests showed dissipation of excess pore-water pressure within 10 minutes. Field monitoring (i.e., Turnpike 417) confirmed very little buildup of excess pore-water pressures, with dissipation rates faster than the field embankment construction times. Consequently, long-term settlements are mostly from creep, which can contribute up to 50% of the total settlement. Creep includes both secondary and tertiary compressions.

4. Tertiary creep was observed in all soil samples with organic contents greater than 25% under loading conditions. Generally, tertiary creep is manifested as an increased settlement rate on the semi-log time plot, which occurs after approximately one week of sustained loading in the laboratory. Tertiary compression was observed not only in the laboratory tests but also in field data (Figure 6-26). The latter resulted significant creep settlement, which required the placement of overlays, resulting in more consolidation as well as creep settlements. Again, tertiary creep should be checked in the laboratory for soils with organic content over 25%.

5. For all the medium and high organic content soils (i.e., OC > 25%), the slopes of secondary and tertiary settlement vs. log time could be normalized with respect to organic content and applied vertical effective stress (Figures 4-9 and 4-10). The latter figures are very useful, especially in preliminary embankment design without surcharging. For instance, an engineer knowing the soils' organic content and vertical effective stress for the layers beneath an embankment may estimate both secondary and tertiary creep, as well as settlements for a given stratigraphy using Eqs 4.7 and 4.8 with secondary and tertiary creep parameters, $C_{\alpha\varepsilon,}$ estimated from Figures 4-9 and 4-10.

6. Surcharging is an excellent approach to limit both consolidation and creep settlements of organic deposits over long periods of time. In the case of low and medium organic deposits (OC < 50%), surcharging to twice the final vertical effective stress will result in little if any long-term creep (Figures 4-12, 4-13, 4-15). For highly organic deposits

(OC > 50%), surcharging to twice the final vertical effective stress will result in a 30% to 50% reduction in the long-term creep due to the extended time prior to the onset of creep (Figure 4-15) when used in Eq. 4.7 with tertiary creep parameters, $C_{\alpha\varepsilon,}$ estimated from Figure 4-10. Surcharging highly organic deposits (OC > 50%) to 4 times the final vertical effective stress [TH22(1)-2] reduced the creep compression ratio, $C_{\alpha\varepsilon,}$ by a factor of 2 (Figure 4-14) which cancels the rebound after surcharge removal. Surcharging highly organic deposits (OC > 50%) to 8 times final vertical stress, [TH16(1)-S, Figure 4-14], results in no long term creep, just rebound from surcharge removal.

7. The Gibson-Lo rheological model was used to simulate both consolidation and creep behavior of Florida's organic soils. It is capable of predicting both loading and unloading events due to surcharging. The model requires simple soil compression parameters: compression index, secondary and tertiary creep moduli; as well as secondary and tertiary compression rates, λ_c. All of the parameters can be derived from non-conventional 1-D oedometer consolidation tests run for 1 to 2 weeks. Section 5.4 shows the process of back computing the parameters for a highly organic sample.

8. A computer program capable of simulating the nonlinear large deformations due to both secondary and tertiary compression from the Gibson-Lo rheological model was developed. The program updates the geometry as well as permeability as a function of void ratio. The computer program was used to predict (Chapter 6) the ground movements at the two field projects: Turnpike (417) and SR20. Both the load and unload options were tested in the above simulations. The results were in good agreement with measured ground movements.

7.2 RECOMMENDATIONS AND FUTURE RESEARCHES

The conclusions were based on data collected from two highway projects with high concentration of organic materials. Extensive laboratory and insitu tests were carried out but more case studies are needed to verify the correlations established in Chapter 4.

So far, there is no engineering classification system for organic soils used under embankments. In the near future, a unified classification system for engineers will be needed. This system will aid in the early phase of design by planning appropriate laboratory and in-situ testing programs. It will also help to identify the general behavior of the organic soils under investigation.

As for the laboratory testing, a new procedure needs to be adopted in order to detect tertiary (long-term) creep for 1-D oedometer testing of organic soils. Specifically, sufficient time needs to be allowed to properly define the tertiary slope. For instance, it is recommended that the 1-D oedometer tests be capable of monitoring long-term (over two weeks) settlements with minimal disturbance. Also it is recommended that oedometers be equipped with pore-water pressure measuring devices to differentiate the end of primary consolidation, and the start of creep deformation. The following are some general guidelines on laboratory 1-D oedometer testing:

Embankments Subject to Increased Vertical Effective Stress without Surcharging:

1) For Soils with organic contents less than 25%, the final load increment should be maintained for 24 hrs to obtain secondary creep parameters ($C_{\alpha\varepsilon}$, or Creep Modulus, $E_{c,}$ creep rate, λ_c, Chapter 5)
2) Soils with organic contents as low as 25%, but greater than 50% should exhibit tertiary creep; consequently, the final load increment should be maintained for 2 weeks to describe the slopes of both the secondary and tertiary creep.

Embankments Constructed with Surcharge Placement and Removal:

Soils loaded to twice the final vertical effective stress will under go significant reduced consolidation and creep behavior. In the case of low to medium organic soil contents (OC < 50%) no reoccurring creep is expected after surcharge removal (Figures 4-12 and 4-13).

However, for highly organic deposits (OC > 50%), surcharging to twice the final vertical effective stress will result in a 30% to 50% reduction in the long-term creep due to the extended time prior to the onset of creep (Figure 4-15) when used in Eq. 4.7 with tertiary creep parameters, $C_{\alpha\varepsilon,}$ estimated from Figure 4-10. For all soils with organic contents greater than 50% the following procedure is recommended:

1) In a standard 1-D oedometer load in one day increments up to the surcharge stress to determine both consolidation (Cc and Cv) and creep ($C_{\alpha\varepsilon}$, or Creep Modulus, $E_{c,}$ creep rate, λ_c, Chapter 5) parameters to validate field response.
2) Unload to the final vertical effective stress to obtain swell characteristics (i.e., Cs = Cr). In the case of very high organic soils (i.e., OC > 80%), the engineer may wish to maintain the load for two to three months to verify time of the onset of creep (Figures 4-14, and 4-15) for use in Eq. 4.7.

For existing embankments underlain by high organic deposits, light-weight materials such as: fly ash, geofoam, shredded tire may be good fill materials to reduce vertical effective stresses or equivalent to surcharge removal which would limit ongoing tertiary creep settlements.

REFERENCES

Adams, J.I., (1963), "A Comparison of Field and Laboratory Consolidation Measurement in Peat." 9th Muskeg Research Conference, NRC, Canada, pp. 43-56.

Adams, J.I., (1965), "The Engineering Behavior of a Canadian Muskeg." Proceedings, 6th International Conference on SMFE, Vol. 1, University of Toronto Press, pp. 3-7.

Amaryan, L.S., (1972), "Methods of Measuring Strength and Compressibility of Peat." Proceedings, 1st All Union Conference on Construction on Peaty Soils, Kalinin, Russia, Vol. 1, pp. 69-89.

Anderson, K.O., Hemstock, R.A., (1959), "Relating the Engineering Properties of Muskeg to Some Problems of Fill Construction." Proceedings, 5th Muskeg Research Conference, NRC of Canada, Technical Memorandum No. 61, pp. 16-25.

ASTM (1991), "Test Method for One-Dimensional Consolidation Properties of Soils." D 2435-90, Philadelphia, PA.

Barden, L., (1969), "Time Dependent Deformation of Normally Consolidated Clays and Peats." Journal of the Soil Mechanics and Foundations Division, ASCE, Vol. 95, No. SM1, pp. 1-31.

Berry, P.L., (1983), "Application of Consolidation Theory for Peat to the Design of a Reclamation Scheme by Preloading." Q.J. eng. Geol. London, Vol. 16, pp. 103-112.

Berry, P.L., Poskitt, T.J., (1972), "The Consolidation of Peat." Geotechnique 22, No. 1, pp. 27-52.

Buisman, A.S.K., (1936), "Results of Long Duration Settlement Tests." Proceedings, 1st International Conference on Soil Mechanics and Foundation Engineering, Cambridge, MA, Vol. 1, pp. 103-106.

Candler, Chartres, (1988), "Settlement Measurement and Analysis of Three Trial Embankments on Soft Peat Ground." Baltic Conference on Soil Mechanics and Foundation Engineering on Peats and Deformations of Structures on Highly Compressible Soils, Vol. 1, pp. 268-272.

Casagrande, A., (1938), “Notes on Soil Mechanics.” Havard University, Graduate School of Engineering.

Das, B.M., (1998), “Principles of Geotechnical Engineering,” 4th Edition, PWS publishing Company, pp. 321.

Davis, E.H., Raymond, G.P., (1965), “A Non-Linear Theory of Consolidation.” Geotechnique, 15, pp. 161-173.

De Jong, G.D.J., (1968), “Consolidation Models Consisting of an Assembly of Viscous Element on a Cavity Channel Network.” Geotechnique, Vol. 18, pp. 195-228.

Decker, M., (1982), “Peats as an Energy Source.” Internal Report Ground Engineering, No. 104, Purdue University, West Lafayette, IN.

Dhowian, A.W., Edil, T.B., (1980), “Consolidation Behavior of Peats.” Geotechnical testing journal, GTJODJ, Vol. 3, pp. 105-114.

Feustel, I.C., Byers, H.G., (1930), “The Physical and Chemical Characteristics of Certain American Peat Profiles.” USDA, Bureau of Chemistry and Soils, Technical Bulletin 214, Washington D.C.

Fox, P.J., Tuncer, E.B., Lan, L., (1992), “C_α /Cc Concept Applied to Compression of Peat.” Journal Geotechnical Engineering, Vol. 118, No. 8, pp. 1256-1263.

Fox, P.J., (1992), “An Analysis of One-Dimensional Creep Behavior of Peat.” Ph.D. thesis, University of Wisconsin-Madison, USA.

Fox, P.J., Edil, T.B., (1995), “Effects of Stress and Temperature on Secondary Compression of Peat.” Can. Geotech. J. 33, pp. 405-415.

Gaustchi, M.A., (1965), “Peat as a Foundation Soil.” Research Summary Report, Norwegian Geotechnical Institute, Oslo.

Gibson, R.E., England, G.L., Hussey, M.J.L., (1967), “The theory of One-Dimensional Consolidation of Saturated Clays, I. Finite Nonlinear Consolidation of Thin Homogeneous Layers.” Geotechnique, 17, pp. 182-198.

Gibson, R.E., Lo, K.Y., (1961), “A Theory of Consolidation of Soil Exhibiting Secondary Compression.” Norwegian Geotechnical Institute, Vol. 78, No. 5, pp. 179-215.

Goodman, L.J., Lee, C.N., (1962), “Laboratory and Field Data on Engineering Characteristics of Some Peat Soils.” Proceedings 8th Muskeg Research Conference, NRC, ACSSM, Technical Memorandum 74, pp. 107-129.

Gruen, H.A., Lovell, C.W., (1984), “Compression of Peat under Embankment Loading.” Transportation Research Record 978, pp. 56-59.

Gunaratne, M., Stinnette, P., Mullins, A.G., Kuo, C.L., Echelberger, W.F., Jr., (1998), “Compressibility Relations for Peat and Organic Soil.” Journal of Testing and Evaluation. JTEVA, Vol. 26, No.1, pp. 1-9.

Harahan, E.T., (1954), “An Investigation of Some Physical Properties of Peat.” Geotechnique, Vol. 4, No. 3, pp. 108-123.

Harahan, E.T., Dunne, J.M., Sodha, V.G., (1967), “Shear Strength of Peat.” Proceedings, Geotechnical Conference, Oslo, Vol. 1, pp. 193-198.

Helenelund, K.V., (1975), “Compressibility and Settlement of Peat Layers.” Proceedings, Istanbul Conference on SMFE, Vol. 2, pp. 1-8.

Hollingshead, G.W., Raymond, G.P., (1972), “Field Loading Test on Muskeg.” Proceedings, 4th International Peat Congress, Helsinki, Vol. II, pp. 273-282.

Holtz, R.D., Kovacs, W.D., (1981), “An Introduction to Geotechnical Engineering.” Prentice-Hall, Englewood Cliffs, NJ, USA.

Huang, A.B., (1982), “In – Situ Testing of Peat.” Internal Report Ground Engineering, No. 105, Purdue University, West Lafayette, IN.

Jackson, M., (1958), “Soil Chemical Analysis.” Prentice-Hall, NJ, 148 pp.

Jefferies, J.M., (1936), “Building Roads Through Unstable Foundations.” Civil Engineering, Vol. 6, No. 5, pp. 317-320.

Johnson, S.J., (1970), “Precompression for Improving Foundation Soils.” Journal of the Soil Mechanics and Foundation Division, ASCE, Vol. 96, No. SM1, pp. 111-144.

Jones, O.B., Maddison, J.D., Beasley, D.H., (1995), “Long-Term Performance of Clay and Peat Treated by Surcharge.” Proc. Instn. Civ. Engrs. Geotech. Engng. 113, pp. 31-37.

Juarez-Badillo, E., (1988), “Postsurcharge Secondary Compression Equation for Clays.” Can. Geotech. J. 25, pp. 594-599.

Kabbaj, M., Tavenas, F., Leroueil, S., (1988), “In Situ and Laboratory Stress-Strain Relationship.” Geotechnique, Vol. 38, pp. 378-404.

Kaderabek, T.J., Barreiro, D., Call, M.A., (1985), “In Situ Tests on a Florida Peat.” Use of In Situ Tests.

Karesniomi, K., (1972), “Dependence of Humidification Degree on Certain Properties of Peat.” Proceedings, 4th International Peat Congress, Helsinki, Vol. 2, pp. 273-282.

Katona, M.G., (1984), “Evaluation of ViscoPlastic Cap Model.” Journal of Geotechnical Engineering, Vol. 110, No. 8, pp. 1106-1125.

Ladd, C.C., Foote, R., Ishihara, K., Schlosser, F., and Poulos, H.G., (1977), “Stress – Deformation and Strength Characteristics.” State-of-the-Art Report, Proceeding of the 9th International Conference on Soil Mechanics and Foundation Engineering, Tokyo, Vol. 2, pp. 421-494.

Landva, A.O., (1980), “Geotechnical Behavior and Testing of Peat.” Ph.D. thesis, Laval University, Quebec, 576 pp.

Landva, A.O., La Rochelle, P., (1983), “Compressibility and Shear Characteristics of Radforth Peats.” Testing of Peats and Organic Soils, ASTM STP 820, pp. 157-191.

Lea, N.D., Brawner, C.O., (1963), “Highway Design and Construction over Peat Deposits in Lower British Columbia.” Hwy. Res. Record, No. 7, pp. 1-32.

Lefebvre, G., Langlois, P., Lupien, C., (1984), “Laboratory Testing and in Situ Behavior of Peat as Embankment Foundation.” Can. Geotech. J. 21, pp. 322-337.

Leonards, G.A., Ramiah, B.K., (1959), “Time Effects in the Consolidation of Clays.” Symposium on Time Rate of Loading Rate in Testing Soils, ASTM, Special Technical Publication No. 254, pp. 116-130.

Litus-Lan. (1992), “A Model for One-Dimensional Compression of Peat.” Ph.D. thesis, University of Wisconsin-Madison, USA.

Lo, K.Y., (1961), “Secondary Compression of Clays.” Journal of the Soil Mechanics and Foundations Division, ASCE, Vol. 87, No. SM4, pp. 61-87.

MacFarlane, I.C., (1958), “Guide to a Field Description of Muskeg.” NCR, ACSSM Technical Memorandum 44.

MacFarlane, I.C., (1965), “The Consolidation of Peat: A Literature Review.” NCR, Technical Paper, No. 195.

MacFarlane, I.C., (1969), “Muskeg Engineering Handbook.” Muskeg Subcommittee of the NCR Associate Committee on Geotechnical Research, University of Toronto Press.

MacFarlane, I.C., Allen, C.M., (1964), “An Examination of Some Index Test Procedure for Peat.” Proceeding, 9th Muskeg Research Conference, NRC, ACSSM, Technical Memorandum 81, pp. 171-183.

McNabb, A., (1960), “A Mathematical Treatment of One-Dimensional Soil Consolidation.” Quarterly of Applied Mathematics, 17, pp. 337-347.

McVay, M.C., Townsend, F.C., Bloomquist, D.G., (1986), “Quiescent Consolidation of Phosphatic Waste Clay.” Journal of Geotechnical Engineering, ASCE, Vol. 112, No. 11, pp. 1033-1049.

McVay, M.C., Townsend, F.C., Bloomquist, D.G., (1988), “One-Dimensional Lagrangian Consolidation.” Journal of Geotechnical Engineering, ASCE, Vol. 115, No. 6, pp. 893-898.

Mesri, G., (1973), “Coefficient of Secondary Compression.” Journal of the Soil Mechanics and Foundations Division, ASCE, 99, No. SM1, pp. 123-137.

Mesri, G., (1986), “Postconstruction Settlement of an Expressway Built on Peat by Precompression: Discussion.” Canadian Geotechnical Journal, 23, pp. 430-407.

Mesri, G., Feng, T.W., 1989, “Surcharging to Reduce Secondary Settlement.” Proceedings of International Conference on Geotechnical Engineering for Coastal Development - Theory to Practice, Vol. 1, Yokohama, Japan, pp. 359-364.

Mesri, G., Godlewski P., (1977), “Time- and Stress-Compressibility Interrelationship.” Journal of the Geotechnical Engineering Division, Vol. 103, No GT5, pp. 417-430.

Mesri, G., Stark, T.D., Ajlouni, M.A., Chen, C.S., (1997), “Secondary Compression of Peat with or without Surcharging.” Journal of Geotechnical and Geoenvironmental Engineering, Vol. 123, No. 5, pp. 411-421.

Mesri, G., Ullrich, C.R., Choi, Y.K., (1978), “The Rate of Swelling of Overconsolidated Clays Subjected to Unloading.” Geotechnique 28. No. 3, pp. 281-307.

Mitchell J.K., (1993), “Soil Behavior.” 2nd Edition, John Wiley & Sons, Inc. New York, NY.

Moran, Proctor, Mueser, Rutledge, (1958), “Study of Deep Soil Stabilization by Vertical Sand Drains.” United States Department of Navy, Bureau of Yards and Docks, Report No. y88812, Washington DC, 429 pp.

Newland, P.L., Allely, B.H., (1960), “A study of the Consolidation Characteristics of a Clay,” Geotechnique, 10, N0. 2, pp. 62-74.

Nichol, D., Farmer, I.W., (1998), “Settlement over Peat on the A5 at Pant Dedwydd Near Cerrigydrucdion, North Wales.” Engineering Geology 50, pp. 299-307.

Radforth, N.W., (1952), “Suggested Classification of Muskeg for the Engineer.” Engineering Journal, Vol. 35, No. 11, pp. 1199-1210.

Raymond, G.P., Wahls, H.E., (1976), “Estimating 1-Dimensional Consolidation, Including Secondary Compression of Clay Loaded from Overconsolidated to Normally Consolidated State.” Estimation of Consolidation Settlement, Transportation Research Board, Special Report 163, pp. 17-23.

Richart, F.E., (1957), “A Review of Theories for Sand Drains.” Journal of the Soil Mechanics and Foundations Division, ASCE, SM3, No. 1301.

Russel, J.B., Lawrence, C.A., Paddock, M.W., Ross, D., (1999), “Monitoring Preload Performance.” Field Instrumentation for Soil and Rock, ASTM STP 1358, pp. 236-249.

Rutledge, P.C., Johnson, J.J., (1958), “Review of Use of Vertical Sand Drains.” Highway Research Board, Bulletin No. 173, Washington D. C., pp. 67-79.

Samson, L., (1985), “Postconstruction Settlement of an Expressway Built on Peat by Precompression.” Canadian Geotechnical Journal, 22, pp. 308-312.

Samson, L., Rochelle, P.L., (1972), “Design and Performance of an Expressway Constructed over Peat by Preloading.” Canadian Geotechnical Journal, 9, pp. 447-466.

Schiffman, R.L., Gibson, R.E., (1964), “Consolidation of Nonhomogeneous Clay Layers.” Journal of the Soil Mechanics and Foundations Division, ASCE, 90, No. SM5, pp. 1-30.

Silburn, J.D., (1972), “Peat as the Impermeable Membrane in an Earth Dam.” Symposium on Peat Moss in Canada, University of Sherbrooke, pp. 163-196.

Soper, E.K., Osbon, C.C., (1922), “Occurrence and Uses of Peat in the United States.” United States Geological Survey Bulletin, No. 728, 207 pp.

Stamatopoulos, A.C., Kotzias, PC., Barbastathis, A.G., (1987), “Preloading for Sewage Treatment Plant – Settlement and Rebound Time Curve.” European Conference on Soil Mechanics and Foundation Engineering, pp. 741-744.

Stamatopoulos, A.C., Panaghiotis, C.K., (1985), “Soil Improvement by Preloading”. John Wiley and Sons, pp. 261.

Stinnette, P., (1998), “Prediction of Field Compressibility from Laboratory Consolidation Tests of Peats and Organic Soils.” Geotechnical Testing Journal, GTJODJ, Vol. 21, No. 4, pp. 297-306.

Tan, T.K., (1957), “Secondary Time Effects and Consolidation of Clays.” Scientia Sinica, Vol. 7, No. 11, pp. 1060-1075.

Tan, T.K., (1958), “Structural Mechanics of Clays.” Scientia Sinica, Vol. 8, No. 1, pp. 83-97.

Taylor, D.W., (1948), “Fundamentals of Soil Mechanics.” John Wiley & Sons, Inc. New York, NY.

Taylor, D.W., (1942), “Research on Consolidation of Clays.” Cambridge, MA, Department of Civil and Sanitary Engineering, Serial 82.

Terzaghi, K., (1921), “Die Physikalischen Grundlagen des Technish-Geologischen Gutachtens.” Zeitschrift des Oterreichischer Ingenieur – und Architekten – Verein, 73, Heft 36/37, pp. 237-241.

Terzaghi, K., (1923), “Die Brechnung der Durchlassigkeitsziffer des Tones aus dem Verlauf der hydrodynamischen Spannungserscheinungen.” Akademie der Wissenschaften in Wein, Sitzungberichte, Matematiseh-naturwissenschaftliche Klasse, Abteilung Iia, 132, No. ¾, pp. 125-128.

Terzaghi, K., (1924), “Die Theorie der Hydrodynamischen Spannungserscheinungen und ihr erdbautechnisches Anwendungsgebeit.” Proceedings, International Congress for Applied Mechanics, Delft, The Netherlands, pp. 288-294.

Terzaghi, K., (1941), “Undisturbed Clay Samples and Undisturbed Clays,” Journal of the Boston Society of Civil Engineers, Vol. 28, No.3, pp. 211-231.

Thompson, J.B., Palmer, L.A., (1951), “Report on Consolidation Test with Peat.” Symposium on Consolidation Testing of Soil, ASTM, Special Technical Publication 126, pp. 4-7.

Thorson, B., (2001), “Surcharging. How Much? How Long?” Proceedings of the 49th Annual Geotechnical Engineering Conference, pp. 1-14.

Tuncer, B.E., (2002), “Construction Over Soft Organic Ground: Issue and Recent Directions.” Private Conversation.

Tuncer, E.B., Fox, P.J., Lan, L., (1991), “End-of-Primary Consolidation of Peat.” Proceeding of the European Conference on Deformation of Soils and Displacements of Structures, Vol. 1, pp. 65-68.

Tveiten, A.A., (1956), “Applicability of Peat as an Impervious Material for Earth Dams.” Norwegian Geotechnical Institute, Publication No. 14.

Van der Burght, J.H., (1936), “Long Duration Consolidation Tests.” Proceedings, 1st International Conference on Soil Mechanics and Foundation Engineering, Cambridge, MA, Vol. 1, pp. 51.

Von Post, L., (1922), “Sveriges Geologiska Undersoknings Torvinventering Och Nagra Av Dess Hittills Vunna Resultat.” Sv. Mosskulturfor, Tidskrift 1, pp. 1-27.

Weber, W.G., Jr., (1969), “Performance of Embankment Constructed over Peat.” Journal of the Soil Mechanics and Foundations, Vol. 95, No. SM1, pp. 53-77.

Wilson, N.E., Radforth, N.W., MacFarlane, I.C., Lo, M.B., (1965), “The Rates of Consolidation for Peat.” Proceedings, 6th ICSMFE, Vol. 1, pp. 407-411.

Witczak, M.W., (1972), “Relationships Between Physio-Graphic Units and Highway Design Factors.” NCHRP Report 132, 166 pp.

Wyld, R.C., (1956), “A Further Investigation of the Engineering Properties of Muskeg.” Unpublished M.Sc. Thesis, Faculty of Engineering, University of Alberta, 76 pp.